PHOTODISSOCIATION SPECTROSCOPY OF THE NIOBIUM DIMER CATION

by

SHELLEY B. DEOSARAN

A dissertation submitted to the Graduate Faculty in Chemistry in partial fulfillment of the requirements for the degree of Doctor of Philosophy, The City University of New York.

1998

This manuscript has been read and accepted for the Graduate Faculty in Chemistry in satisfaction of the dissertation requirement for the degree of Doctor of Philosophy.

1/28/98
Date

Chair of Examining Committe

Jan. 29, 1998
Date

Executive Officer

Dr. Derek M. Lindsay

Dr. John R. Lombardi

Dr. Lawrence Johnson

Supervisory Committee

THE CITY UNIVERSITY OF NEW YORK

ABSTRACT

PHOTODISSOCIATION SPECTROSCOPY OF TRANSITION METAL CLUSTER IONS

by

Shelley B. Deosaran

Advisers: Professor Derek M. Lindsay

Professor John R. Lombardi

This thesis describes research done in the field of cluster chemistry. It is virtually divided into two parts, virtual part I describes experimental studies of matrix isolated neutral metal clusters while virtual part II describes the design and construction of a versatile instrument to do research on gas phase cluster (van der Waals and transition metal) cations and anions.

Metal clusters, groups of metal atoms consisting of two to several thousand metal atoms, are likened to the fifth state of matter (gas, liquid, solid and plasma). Their properties lie between the extremes of individual atoms and the bulk metal. Basic research on these exotic species will aid in deciphering the nature of the transition from atom to bulk and in understanding the contribution of d-d bonding in transition metals.

Virtual part I involves absorption and Raman and scattering depletion spectroscopy on the neutral diatomic clusters of vanadium and niobium. These cluster ions were produced by argon ion sputtering, mass selected with a Wien filter, and then neutralized and embedded in frozen argon matrices. They are interrogated with visible and infrared radiation to yield ω_e and $\omega_e x_e$.

Virtual part II consists of three chapters. Chapter III describes the design and construction of the instrument to perform spectroscopic studies on gas phase cluster ions. It includes the discussion of the choice of various components and design criteria. The source is a combined laser vaporization and seeded source, employing a laser to vaporize refractory and other metals and a pulsed supersonic valve to introduce the carrier gas or other seed species. Chapter IV highlights the data acquisition and control system with the use of LabVIEW 3.1.1 for Windows and the instruments calibration and testing. Chapter V discusses photodissociation spectroscopy on the niobium dimer cation, the successes and the reasons why the photofragmentation spectrum could not be definitively assigned.

ACKNOWLEDGEMENTS

THANK YOU TO ALL THE INDIVIDUALS LISTED HEREIN

I owe a wealth of gratitude to all these wonderful people who I am proud to number among my friends.

Professor Derek Lindsay
Professor John Lombardi
Professor Larry Johnson
Professor Daniel Akins
Dr. Ron Brown

You guys always gave me good advice: Dr. Laurent Mars, Dr. Charles Hosten Dr. Karl Kernisant, Dr. Denise Garland, Dr. George Sukenick, Dr. Zhendong Hu, Dr. Joseph G. Eaton

My lab partners: Qinwei Zhou, Bo Shen, Hannae Haourai, Robert Craig, Metin Aydin, Wumin Wang, Joseph Nelson

Electronics technician Derek Quinlan
Chemistry technicians (Joe, Miguel and Mohammed)

Machinists (Joseph Altman, Joseph Duke and Lyndon Langhorn) you guys are the greatest, thanks for your invaluable assistance and great work.

Sandra and Florence Hayward-Wright
Fellow CASI graduate students, Andrew, David, Pierre, Reggie

A special thanks to David M. Toney, Wahab Emmamdee,
Jean Bacchus Sandy and Stenol Amos Lewis.

To: Rawlins and Joseph Romaldo Nicome wherever you may be Thank you for always believing in me.

These are the people whose support and love helped me to survive the ordeal.

My darling Carlene M. Libert thank you for your "love" and "support", it meant a lot to me.

A very special thanks to my family!!!

- parents Deo and Lister
- grandmother Sheila Nicome who always
- brothers Nigel, Ken, Kash, Shastri and Robin and my darling sister Betty.

My aunt Joan and her fiancee Michael Gould thank you both for welcoming me into your home, your kindness was immeasurable. I will forever be indebted to you.

Aunts Iloane and Gemma, thank you both for always making me feel welcome in your homes.

Alan and Halcyon thank you, I will never forget your kindness and great help with my financial certification when I first arrived in New York.

Roosevelt and Shirley thank you both for your advice and inspiration.

Joan and Laurencia you made it much easier for me, a heartfelt thank you.

Kash, Shastri, Robin and Carlene thank you for saving me from myself during my bouts of insanity, I owe my life to you.

TABLE OF CONTENTS

LIST OF TABLES

LIST OF FIGURES

CHAPTER I

INTRODUCTION

Metal clusters are assemblies of atoms and molecules that are weakly bound to each other.[1] There may be from two to several thousand atoms contained in a cluster. It is only in the last twenty years or so that the field of cluster science[2-5] has emerged to stand by itself as a separate and dynamic discipline within the field of chemistry and chemical physics. Cluster science owes its development on a large part to advances in the fields of molecular beams and lasers.[6,7] The study of clusters represent the hope for bridging the understanding of knowledge on the microscopic (atomic) level to the macroscopic understanding of the bulk matter. Scientists have long pondered on the nature of the transition from atomic properties to bulk properties,[8] for instance at what aggregate size does Fe start exhibiting its catalytic effects.[9]

There are two principal categories of clusters, van der Waals or molecular clusters[10] and metal clusters[11] (transition metal, alkali metal and mixed metal clusters). Clusters may be studied either in the gas phase[12] or embedded in inert gas matrices[13]. Metal clusters may be produced using several different cluster sources, sputtering types and jet cooled sources (laser ablation and thermal sources). Laser ablation or vaporization[14] produces ions from refractory metals by the use of a laser to vaporize the metal. The vapor is enveloped

This dissertation contains our contribution to the general body of knowledge concerning metal clusters using two very different experimental approaches, matrix isolated and gas phase metal cluster spectroscopy. The following three spectroscopic techniques were used on matrix isolated neutral metal clusters, absorption, scattering depletion and Raman spectroscopy, while one color photofragmentation spectroscopy was performed on gas phase metal cluster cations. The experiments performed on the matrix isolated clusters enabled us to accurately determine the ω_e, $\omega_e x_e$ and r_e for niobium and vanadium neutral dimers. For the photofragmentation experiment it was necessary to design and build our own apparatus to produce and study gas phase metal cluster ions. A major part of this dissertation deals with the design, building, testing and calibration of the laser vaporization source and mass spectrometer. Photofragmentation spectroscopy carried out on the cationic dimers of niobium illustrated the difficulties encountered when working with the d-d bonding ions. Ion photofragmentation experiments especially in the determination of the spectroscopic properties of transition metal ions is still in its infancy.

in a carrier gas to promote condensation, and finally the vapor/gas mixture is supersonically expanded through a small orifice, producing both neutral and ionic clusters of varying sizes. The thermal (hot oven) technique involves using a heated oven to vaporize the metal, followed by expansion of the metal vapor through a nozzle and subsequent ionization of the expansion.

Much of cluster research has been devoted to studying the size effects of clusters.[15] The structure and properties of clusters have been studied to gain an understanding of how they evolve with increasing size to attain bulk properties (conductivities, etc.). Their reactive properties are studied with a view to better understand catalysis on a molecular level and the development of better catalysts. Much remains to be learned about clusters, especially an understanding of bonding in the late transition series and the effects of d-d bonding orbitals in metal clusters. It may be at least a decade before a truly comprehensive theory of transition metal cluster bonding can be formulated. In the mean time research at the molecular level is being carried out using various techniques and approaches to understand the nature of the cluster and their properties. Another important area of study is the cation <-> neutral <-> anion structure/charge transformation, the study of how the cluster properties and structure are affected by the gain or loss of electrons.

Chapter I References

1. Jousha Jortner, Ber. Bunsenges. Phys. Chem. **88**, 188, (1984).

2. E. Schumacher, M. Kappes, K. Marti, P. Radi, M. Schär and B. Schmidhalter, Ber. Bunsenges. Phys. Chem. **88**, 220, (1984).

3. V. E. Bondybey, Science, **227**, 125 (1985).

4. E. W. Becker. Z. Phys. D- Atoms Molecules and Clusters, **3**, 101 (1986).

5. W. D. Knight, Walt A. deHeer and Winston Saunders, Z. Phys. D- Atoms Molecules and Clusters, **3**, 109 (1986).

6. Joseph Haggin, C&EN March 2nd 1987.

7. W. Begemann, S. Dreihöfer, G. Ganteför, H. R. Siekmann, K. H. Meiwes-Broer and H. O. Lutz, Springer Ser. Mater. Sci., 230 (1988).

8. J. Mater. Res. vol 4, # 3, 704 (1989).

9. Michael A. Duncan and Dennis H. Rouvray, Sci. Amer. 110 (Dec. 1989).

10. Robert Pool, Science, 248, 1186 (1990).

11. R. Stephen Berry, Sci. Amer., Aug. 1990 (pg. 68).

12. Marvin L. Cohen and Walter D. Knight, Phys. Today, Dec. 1990 (pg. 42).

13. Zhendong Hu, Jian-Guo Dong, John R. Lombardi and D. M. Lindsay, J. Chem. Phys. **101**, 1 (1994).

14. Robert F. Curl and R. E. Smalley, Sci. Amer., 54, Oct. 1991.

15. David J. Wales, Science, 271, 925 (1996).
A. P. Alivisatos, Science, 271, 933 (1996).
Gustavo E. Scuseria, Science, 271, 942 (1996).

CHAPTER II

SPECTRA OF MATRIX ISOLATED MASS SELECTED CLUSTERS

II.I INTRODUCTION

Vibrational frequencies of matrix isolated species tend to be quite close to their corresponding gas phase values. Vibrational structures are not common features in matrix isolated absorption spectra, in addition many cluster species seem to have very low fluorescence quantum yields. Spectroscopy on the other hand has been established as a robust technique for the elucidation of vibrational information in small metal clusters.[1] Spectra have been repeated for several diatomic and triatomic cluster species.[2] A common problem with such spectra has been the assignment of the spectral carriers, a perplexing question especially for the larger clusters. This problem of carrier assignment is overcome[3-6] by preparing mono-dispersed (highly enriched) matrix samples using a mass selected cluster ion beam as a deposition source. The work done by Lindsay and Harbich et al. have demonstrated the techniques of excitation and fluorescence spectroscopy.

II.2 EXPERIMENTAL

The cluster source shown in Fig. 2.1 is similar in several aspects to that described by Harbich, Lindsay et. al. in refs. 3 and 4. An intense (typically 10 mA at 2.5 KeV)

argon ion beam from a 'CORDIS' ion source (Rokoin Ionenstrahl-Technologie, Darmstadt, Germany)[7] sputters vanadium cluster ions from a water cooled, vanadium target (Aesar 99.5% purity). The primary beam was collimated by an 8 mm aperture (denoted A1 in Fig. 2.1), which also separates the ion source from the rest of the instrument. A 500 l/s turbo pump (Balzers TPU 510) and mechanical pump backing pump was used to evacuate the ion source. The specially designed sputtering chamber (MDC vacuum products) sits on top of the turbo pump. Typical vacuum pressures when the ion source is being operated are 1×10^{-7} torr sputtering chamber, 1×10^{-8} torr deposition chamber. The pressure decreases to 7×10^{-9} torr in the deposition chamber when the sputtering is off and spectra are being recorded. The angle between the primary and secondary beam lines is about 50°, corresponding closely to the optimum angle of ejection for material sputtered from a metal surface.[8] This angle is adjusted slightly during deposition to optimize ion current.

The target is normally maintained at 700 V. Cluster cations sputtered from the target were extracted with a modified Coultron model -200-B lens system (L2 in Fig. 2.1). The sputtered ions are mass selected using a Wien filter (Coultron 600-B) in conjunction with an approximately 175 mm long drift space and a 6.5 mm diameter aperture (A3). For the vanadium ion (V_2^{+}), the Wien filter was operated at a magnetic field of 2000 G. This corresponds to an electric field of 130 volts for V_2^{+} giving a mass resolution of ($M/\Delta M$)

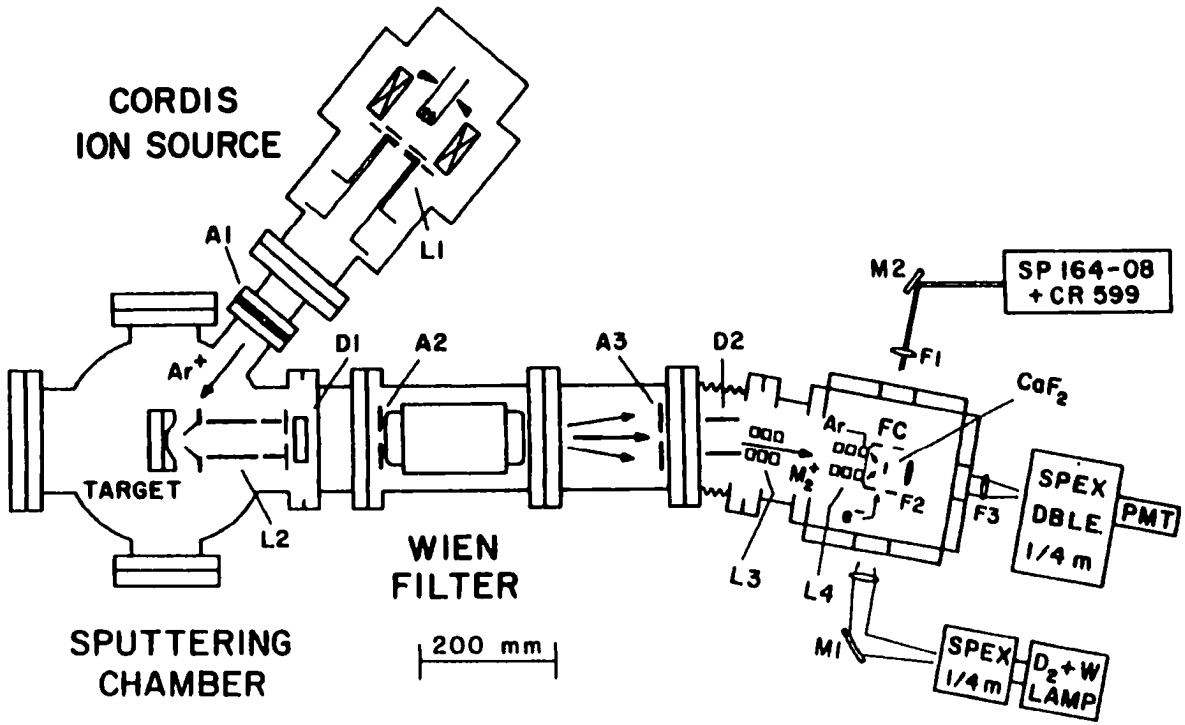

Figure 2.1 Cluster deposition apparatus

of 6-7, sufficient to separate the dimer from the atom and trimer and ensure the absence of oxides. After mass separation the ion beam was bent by 10° (using deflection plates D2 mounted in a short bellows section) and then guided to the deposition region by two Einzel-like lenses L3 and L4. The 10° bend separates dimer ions from sputtered neutral products whose flux may be comparable to or greater than those of the ions. From deposition of silver with and without the 10° bend, we estimated that only 0.1% of the neutral species were deposited in our experiments. We found out in later experiments that floating the secondary beam line (extraction lens, Wien filter, drift space, etc.) to -1KV increases the extractable ion current.

The deposition region is shown in Fig. 2.2. Vanadium dimer ions were co-deposited with argon and electrons on a 45 x 8 x 1 mm polished CaF_2 plate (Maris-Delfour, Paris) mounted (using Wood's metal and an Indium gasket) to a closed cycle cryostat (APD Displex 204-s1/DMX-6). The cryostat temperature was measured using a silicon diode in conjunction with a Scientific Instruments model 5500 temperature controller. Deposition temperatures were typically 20 K. The CaF_2 substrate is surrounded by a "Faraday Cage" (denoted FC in Fig. 2.2). It is composed of two side plates with openings for optical measurements), the lower half of the cryostat radiation shield, the electron source for neutralizing the cluster ions, and the last lens element of L4 which was enclosed by a 90% transmitting Ni mesh. This lens element

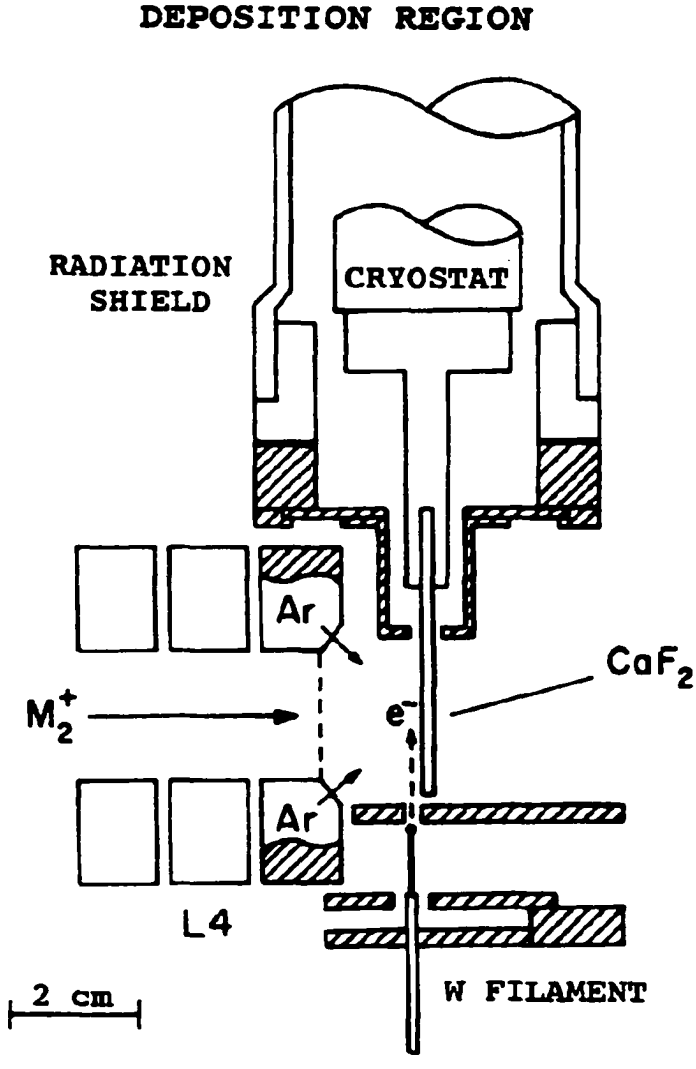

Figure 2.2 Cluster Deposition Region

incorporates a coaxial injector ring (eight 0.5 mm diameter holes) for the entrance of the matrix gas (99.9995% Ar, Alphagaz). The electron source was a Phillips electron microscope filament (0.3 tungsten) on a ceramic base (Ladd Research Industries). The electron source assembly was enclosed by a stainless steel box having an 8 x 1 mm slit positioned so that electrons were introduced about 1-2 mm in front of the CaF_2 substrate. The filament was biased at -3 V with respect to the Faraday plate to ensure that a sufficient number of low energy electrons would reach the matrix target.

Ion currents were monitored using a Faraday plate situated near the deposition window. The rotatability of the cryostat facilitated easy adjustment of the Faraday plate and substrate to measure ion currents as well as prepare matrix samples and record optical spectra. The potential in the deposition region can be defined and controlled, (inspite of the fact that both the matrix and CaF_2 substrate are insulators), by the voltage applied to the Faraday cage. The difference in voltage between the Faraday cage and the target (V_{dep}) determined the dimer deposition energy (eV_{dep}), which for this experiment was maintained at 10 eV. Measurement of the kinetic energy distribution of the arriving ions by applying a retarding potential to the Faraday plate revealed, that it was centered close to $eV_{dep} = 0$ with a halfwidth of about 8 eV, comparable to that reported for sputtered ionic particles.[9] The 700 eV ion beam with an area of 1 cm^2 gave mass selected currents of V^+ (110 nA), V_2^+ (70nA) and V_3^+ (10

nA). The dimer fragmentation was estimated by comparing the intensities of atomic excitation features in a dimer deposition with those obtained from deposition of the atom under similar conditions. Using this method we estimated that 10 - 15 % of the vanadium dimers (neutral bond energy, 2.8 eV)[10] were fragmented at eV_{dep} = 10 eV, a value which is slightly below that found for Ag_2 neutral bond energy, 1.7 eV)[11] deposited in Kr matrices.[6] The ratio of electron current to dimer current (as measured on the Faraday plate) was generally 3:1. It was supposed that since the dimer ionization potential (6.1 eV)[12] was relatively large compared to the bond energy (2.8 eV)[10], the neutralization step takes place on or very near to the matrix surface.

Matrices were grown at around 6 μ/h with an Ar:metal ratio of approximately 10^4:1, which was sufficient to ensure that the dimers remained well isolated both from each other and (more difficult to achieve) from any impurity species. During deposition, the partial pressure of H_2O (the dominant background gas) in the cryostat chamber was generally about 5 x 10^{-9} torr, as measured on a residual gas analyzer (Leybold-Inficon, Quadruvac Q 100). This translated into a better than 95 % probability that a dimer will be surrounded by at least 12 nearest neighbour argon atoms.

II.3 VANADIUM DIMERS

II.3.1 RESULTS

Raman spectra were recorded using both an Ar^{+} laser (Spectra Physics, 164-08) and a dye laser (Coherent, 599-02), focused to an estimated 50 μ spot by a 240 mm focal length lens (F1 in Fig. 2.1). The laser power incident on the sample was typically 50 mW. Plasma lines were removed by predispersing the laser beam with a grating. Scattered light was collected at 90° using f/1 optics (lens F2) and focused onto the slits of a 1/4 m Spex Double-mate monochromator (1800 groove holographic grating) by a 200 mm focal length lens (F3) with a magnification of about 5. The monochromator, modified so as to have an adjustable middle slit) was driven by a Dell 386 computer using a Data Translation (DT 2817) digital I/O board. The mirror (M1 in Fig. 2.1) was mounted on a computer controlled stepping motor (Compumotor A5783), which allowed the focused light to be scanned (in approximately 12 steps) across the 8 mm wide sample. The signal was detected by a cooled (Hamamatsu R943-02) photomultiplier tube (PMT), processed by an amplifier/ discriminator (Uniphoton) and stored by the computer using a specially designed prescalar and the DT2817 digital I/O board.

Figure 2.3 shows a typical spectrum for divanadium in argon matrix. The spectrum was acquired following a 4 hour deposition of 52 nA of V_2^{+} (3 x 10^{11} dimers/sec) at a

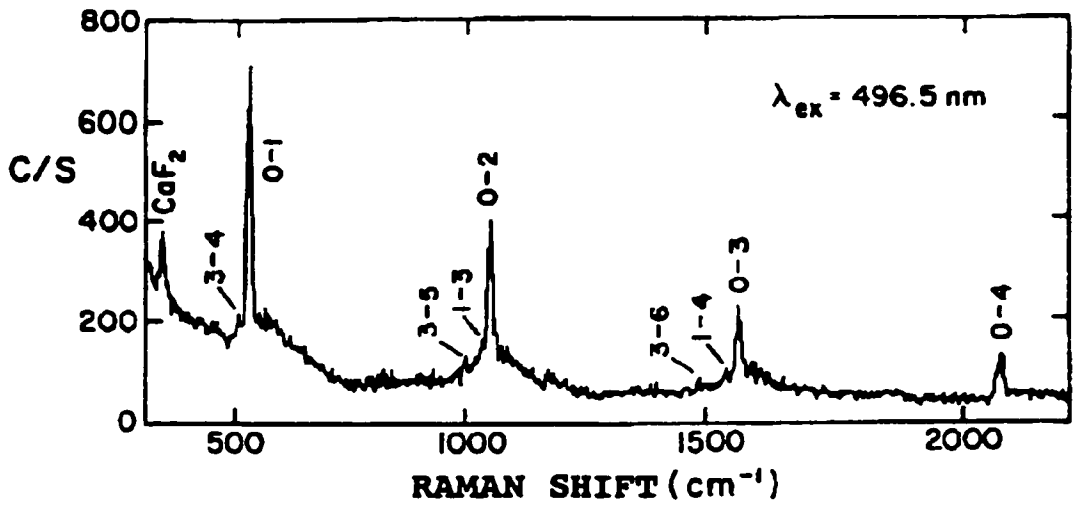

Figure 2.3 Raman spectrum of the Vanadium dimer in an Argon matrix at 20 K.

deposition of 10 eV. Figure 2.3 was recorded using 10 cm^{-1} resolution (200 μ slits) and a "scan rate" of 2000 ms for each 3 cm^{-1} step. Spectra were observed throughout the blue-green region of the ion laser, as well as with dye laser scans using Rhodamine 6G. The principal feature of the divanadium spectra is a progression (n" 0 -> n">0) in the ground $^3\Sigma^+$ state, as previously reported by Cossée et al.[13] Also evident in Fig. 2.3 is the transition from the CaF_2 support (whose 330 cm^{-1} frequency serves as a useful fiducial mark)[14] and several rather weak 'hot band' features which apparently arise because ground state vibrational levels other than n" = 0 may be populated by radiative processes.[13] Weak features, not seen in Fig. 2.3 but observed for some excitation wavelengths, probably correspond to electronic resonance transitions (denoted ERR1 and ERR2 in Ref. 13) to low lying excited electronic states in the dimer. Table 2.1 summarizes the frequency data for four ion laser wavelengths. All spectra were calibrated by scanning through the corresponding ion laser line and further corrected (when possible) by comparison with the CaF_2 frequency.

The Table 2.1 data were analyzed by standard methods to give ω_e" = 536.9 ± 1.1 cm^{-1} and $\omega_e x_e$" = 4.1 ± 0.1 cm^{-1}. Similar parameters were obtained using excitation wavelengths between 560 nm and 575 nm (Rhodamine 6G). These constants were in excellent agreement with those previously obtained (ω_e" = 537.5 cm^{-1} and $\omega_e x_e$" = 4.2 cm^{-1}) from matrices containing a distribution of cluster sizes.[13] Spectra were

TABLE 2.1: Raman Frequency Shifts (cm^{-1}) for the vanadium dimer in an Argon Matrix.

λ_{ex} (nm)	$\upsilon'' = 1$	$\upsilon'' = 2$	$\upsilon'' = 3$	$\upsilon'' = 4$	$\upsilon'' = 5$	$\upsilon'' = 8$
496.5	526.9	1046.2	1557.2	2065.5		
488.0	528.6	1051.4	1560.6	2066.5	2566.4	
472.7			1561.2	2061.3	2557.2	
457.9			1564.6	2065.7	2562.5	3047.8
Mean (σ)	527.8(12)	1048.83	1560.93	2064.82	2562.04	3047.8

also obtained when vanadium dimer cations were deposited in krypton matrices, but these spectra were of poorer quality than those found for argon. The progressions were less extensive, owing to a broadening of the lines with increasing v"; only the fundamental frequencies could be measured with precision. These data give a fundamental frequency, $\Delta G_{1/2}$ = 525.7 ± 2 cm^{-1} for V_2 in krypton. It should also be noted that the fundamental frequencies for both krypton and argon ($\Delta G_{1/2}$ = 528.7 ± 1.2 cm^{-1}) matrices are within 1% of the gas phase value, $\Delta G_{1/2}$ = 529.5(10).[15]

II.3.2 CONCLUSION

We have demonstrated the practicality of measurements on matrix samples formed by depositing mass-selected cluster ions. Such experiments were feasible only in cases where the signal was resonantly enhanced. Thus, our divanadium sample contained about $5x10^{15}$ scatterers/cm^2 and was excited with approximately $1x10^{17}$ photons s^{-1}. Assuming[16] a normal cross section of 10^{-30} cm^2 and a 1% detection efficiency, the expected Raman signal is about 5 Hz. The measured Raman intensity (Fig. 2.3) is about 500 Hz, consistent with a 100-fold enhancement arising from the divanadium absorption band at 494 nm.[17]

II.4 NIOBIUM DIMERS

The deposition of Nb_2 was done as previously described. The Nb_2^+ sample was studied using both Absorption and Raman spectroscopy. For absorption we employed a deuterium or a tungsten lamp, dispersed by a (computer controlled) Spex 1/4 m monochromator (calibrated with a Hg lamp) and focused onto the matrix sample as indicated in Fig. 2.1. Spectra were recorded as described previously. Both the Raman and (as described in more detail below), the absorption measurements were made by collecting the light scattered at 90 degrees to that incident using lens F2 in Fig. 1 (f/1 optics).

II.4.1 SCATTERING DEPLETION SPECTROSCOPY

Figure 2.4 shows a 'scattering depletion spectrum' (SDS) of atomic niobium in an unannealed argon matrix at 13.5 K. The spectrum (recorded with a tungsten/halogen lamp) was acquired following a 2 hour deposition of 32 nA of Nb^+ (64 nA hours) at a deposition energy of 10 eV. Fig. 2.4 was recorded using 1 nm resolution and a "scan rate" of approximately 500 ms/nm. The relatively sharp features between 300 and 450 nm all arise from absorption by atomic niobium and have been reported previously.[18] The broad background extending from 250 - 800 nm was due to a relatively small, but wavelength dependent, difference in scattering and/or collection efficiency in (see later) the reference and signal beams. The weak oscillatory structure most evident at longer wavelengths was caused by interference effects in the thin matrix sample.

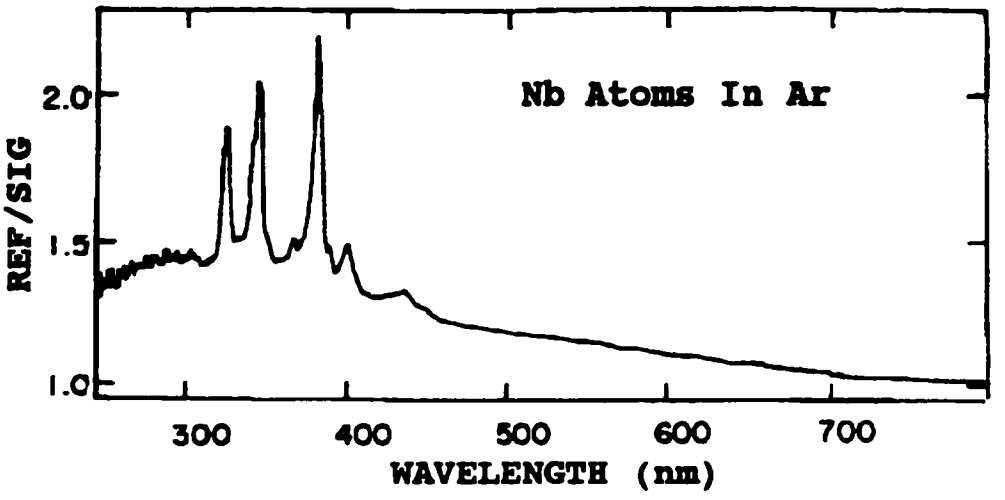

Figure 2.4 Scattering Depletion Spectrum (SDS) of atomic Niobium in an Argon matrix.

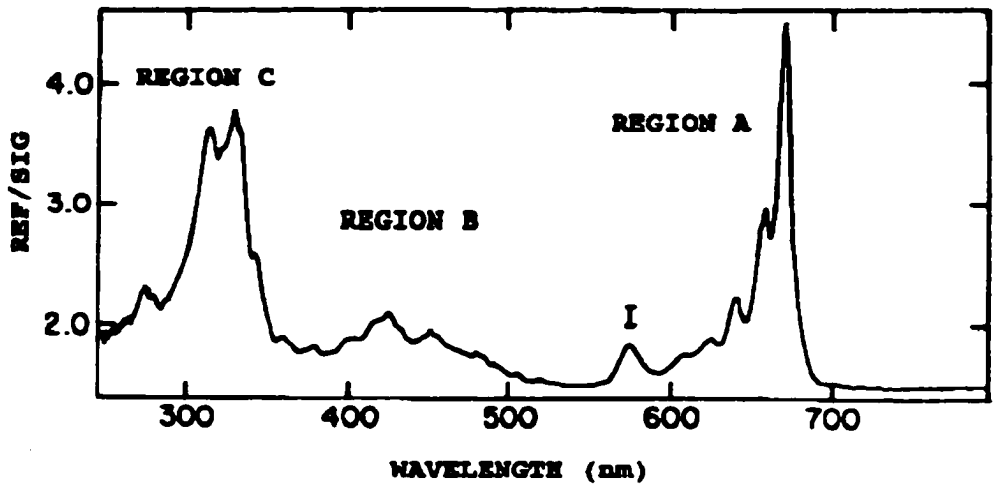

Figure 2.5 Scattering Depletion Spectrum (SDS) of the Niobium dimer in an Argon matrix, showing regions A, B and C.

The ordinate in Fig. 2.4 (the SDS signal) is the ratio of the "reference intensity" to the "signal intensity". The former corresponds to light scattered from a region near the center of the 8 mm wide sample, whereas the latter pertains to that scattered near an edge. Prior to recording Fig. 2.4, the optical density profile of the sample was obtained by recording single beam SDS spectra as a function of lateral position on the sample. It was generally found that the sample was non-uniform, with about twice as much absorption in the center as compared to near an edge. Thus the reference also contains absorption information, but to a lesser degree than the signal. Conventional absorption spectra, using the same signal and reference positions but detecting the light transmitted through the sample, also show the same features evident in Fig. 2.4. However, we find that absorption features in the scattered spectra are approximately 20 -50% more intense than those observed in transmission.

Figure 2.5 is an SDS spectrum of diniobium in an unannealed argon matrix at 14 K. The spectrum was obtained following the deposition of 450 nA hours of Nb_2^+ at an energy of 10 eV. The scan conditions were similar to those used in recording Fig. 2.4. Since the dimer fragmentation was less than 1%, there were essentially no atomic features in this spectrum. Indeed, the presence of atomic niobium could only be detected through excitation spectra which (see, for example, Ref. 4) are very sensitive to atoms. Thus, although absorption spectra have been reported previously for Nb_2

clusters,[19,20] these data were obtained from matrices containing a distribution of cluster sizes. Accordingly, all dimer features between 300 nm and 450 nm were largely obscured by the more intense atomic transitions.

For convenience we separate the absorption spectrum of Nb_2 into three regions. Region A covers the wavelength range 550 - 700 nm and is shown in more detail in Fig. 2.6. This spectrum was made using the same matrix sample as in Fig. 2.5, but was recorded (after annealing to 28 K) with a different grating order to avoid a Wood's anomaly [21] which occurred near 700 nm. The feature marked "I" in both Fig. 2.5 and Fig. 2.6 arose from a contaminant of unknown origin. Interestingly, this impurity band gives a very strong and rich resonance spectrum. As shown by the stick diagram in Fig. 2.6, the A region consists of two overlapping transitions: an intense, sharp feature (which we designate the A' <---- X) at 672.3 nm (14,870 cm^{-1}) [22] and six members of a vibrational progression (denoted A' <---- X) which may be analyzed to give $\omega_0' = 426 \pm 4$ cm^{-1} where this latter frequency corresponds to a (nominal) origin notated v' = 0 in Fig. 2.6. Diniobium transitions near 660 nm have been reported before,[19,20] but the existence of a vibrational progression was apparently not recognized.

Region B (see Fig. 2.5) extends from 550 nm to 340 nm with an intensity maximum at 430 nm. Although this region of the diniobium spectrum is less easy to analyze, it appears to be somewhat structured, consisting of a series of local

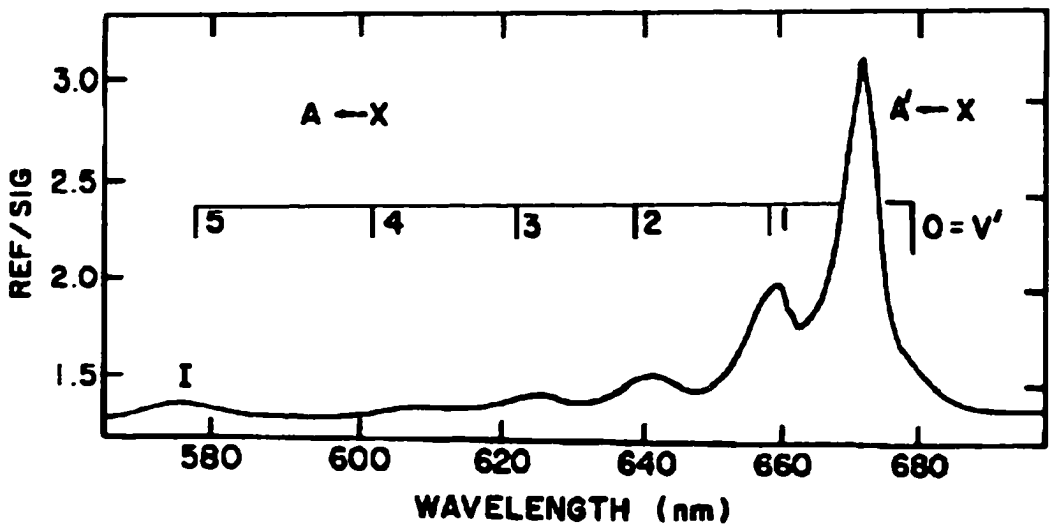

Figure 2.6 Detail of the Niobium dimer "A region" showing two absorption bands.

maxima (often doublets) spaced by around 1300 cm^{-1}. Since an energy separation of this magnitude is too large for a Nb_2 vibrational frequency, we are unable at present to assign this structure. Region C consists of the two intense features at 331 nm and 314 nm plus the previously reported[19] band at 275 nm. The dividing line between Regions B and C is not clear-cut, however. Additional, but weaker, Region C transitions may be seen in absorption spectra (not shown) taken with a deuterium lamp.

II.4.2 RAMAN SPECTROSCOPY

Figure 2.7 shows a typical spectrum for diniobium in argon matrix. The spectrum was acquired following deposition of 200 nA hours of Nb_2^+ at an energy of 10 eV. Fig. 2.7 was recorded using 10 cm^{-1} resolution (200 μ slits) and a "scan rate" of 4000 ms for each 3 cm^{-1} step. The principal feature of the diniobium spectrum was a progression (v" = 0 ----> v" > 0) in the ground state vibrational frequency. Also evident in Fig. 2.7 is the transition from the CaF_2 support, whose 330 cm^{-1} frequency serves as a fiducial mark.[23] Spectra were observed throughout the blue-green region of the ion laser, as well as with dye laser scans using DCM. Figure 2.8 shows the observed variation in the intensity of the signal with the excitation wavelength. The ordinate in this figure gives the relative intensity of the fundamental (at 418 cm^{-1}) scaled by the laser power and the fourth power of the exciting wavelength. The excitation profile bears a strong resemblance

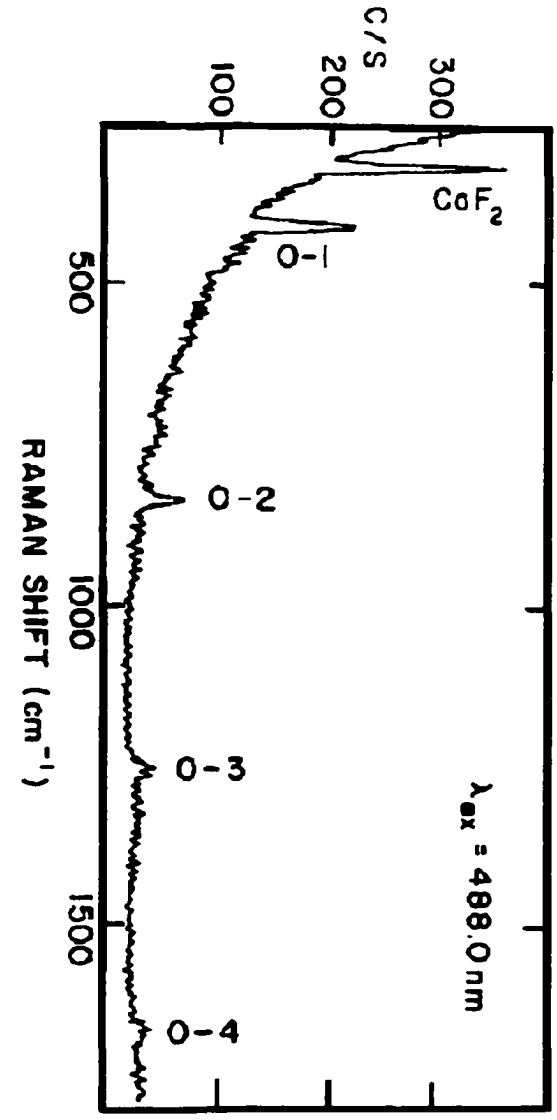

Figure 2.7 Raman spectrum of the Niobium dimer in an Argon matrix at 14K.

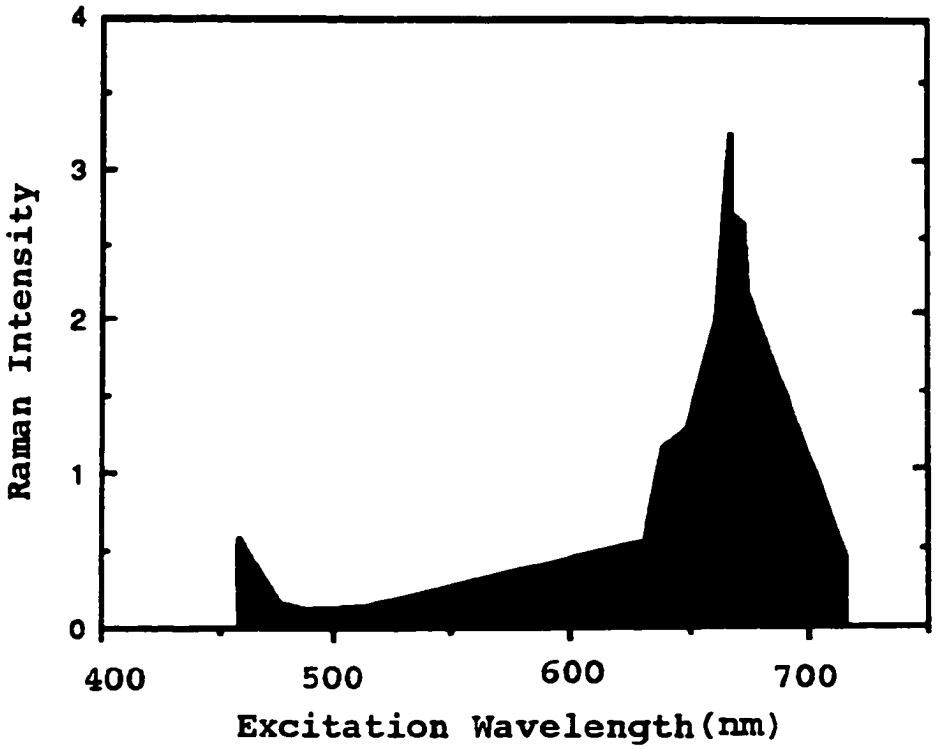

Figure 2.8 Raman Excitation Profile

to the diniobium absorption spectrum (Fig. 2.5). The peak of the excitation profile (near 667 nm) is slightly blue shifted (ca. 120 cm^{-1}) from the strong A'<---- X absorption at 672.3 nm, in approximate accord with the behavior expected for A-term resonance intensities.[24]

In general the diniobium spectra were of poorer quality than those observed for the other Group VIB dimers, V_2 as previously reported. Raman progressions were less extensive and the outermost transitions broadened and sometimes split, presumably due to matrix site effects. Accordingly, the diniobium vibrational constants are not precise as those we reported for V_2. Table 2.2 summarizes the frequency data for eight laser wavelengths. All spectra were calibrated by scanning through the corresponding ion laser line and further corrected by comparison with the CaF_2 frequency. The Table 2.2 data were analyzed by standard methods to give ω_e'' = 420.5 ± 0.5 cm^{-1} and $\omega_e x_e''$ = 0.5 ± 0.3 cm^{-1}. These constants are close to those previously obtained (ω_e'' = 421 cm^{-1} and $\omega_e x_e''$ = 1.4 cm^{-1}) for Nb_2 in a Kr matrix.[20]

II.4.3 DISCUSSION

In previous work, Andrews and Ozin[25] noted that a common feature of many Group VIA and VIB dimers was the occurrence of a structured transition in the low energy region of the dimer absorption spectrum. Based upon the results of Xα calculations, but also making an analogy with the corresponding liganded complexes,[26] these authors assigned the

TABLE 2.2: Raman Frequency Shifts (cm^{-1}) for the niobium dimer in an Argon Matrix

λ_{ex} (nm)	v″ = 1	v″ = 2	v″ = 3	v″ = 4
457.9	416.0	827.0		
465.8	422.0	839.1	1251.4	
472.7	419.2	837.6	1250.7	1674.1
476.5	422.1	842.2	1258.5	1673.8
488.0	421.8	842.2	1252.8	1667.9
496.5	421.1	839.7		
501.7	418.0	839.2		
514.5	422.1	837.2	1256.6	1670.2
Mean (σ)	420.323	838.149	1254.034	1671.530

red absorption features to a $\delta \longrightarrow \delta^*$ transition arising (for Group VB dimers) from a ground state configuration: $d\sigma_g^2 d\pi_u^4 d\delta_g^2$. The observed structure had the appearance of a doublet splitting which was thought to arise from the lifting of the degeneracy of the delta (δ) orbital owing to the matrix environment. Our measurements make this latter conclusion unlikely, at least in the case of Nb_2. Thus, the A region absorption shown in Fig. 2.6 clearly consists of two different types of transitions, implying two electronic symmetries. The sharp (A' <--- X) feature indicate that the upper and lower electronic states have a similar internuclear separation, whereas the overlapping A <--- X progression is characteristic of a Franck-Condon envelope for a molecule in which the excited state potential curve is significantly shifted from that of the ground state. Our results do not, however, permit a definitive identification of the excited states of Nb_2, nor do they allow an assignment of the intriguing structure observed in the B region of the dimer absorption spectrum. Indeed, such a task is rather daunting for combinations of open d-shell elements. Thus, Cotton and Shim[27] find 75 electronic states lying within 1-2 eV of the (predicted) $^1\Sigma_g^+$ ground state of Nb_2. Moreover, the molecular orbital configuration $d\sigma_g^2 d\pi_u^4 d\delta_g^2$ is found to contribute only about 12% to the overall orbital population of the ground state.

II.4.4 CONCLUSION

We have demonstrated the importance of mass selection in the elucidation of spectra of metal clusters. We have shown that "Scattering Depletion Spectroscopy" is a useful technique for absorption measurements, and have observed the first absorption spectrum of the niobium dimer which is free from interference from atoms or higher mass clusters. Spectra obtained throughout the blue-green and red region are in good accord with the optical absorption data.

Chapter II References

1) For example, Jacox reports that "the argon-matrix shift for most diatomic molecules is less than 2%". See, M. E. Jacox, J. Mol. Spectrosc. **113**, 286 (1985).

2) Metal Clusters, edited by M. Moskovits (Wiley, New York, 1986).

3) D. M. Lindsay, F. Meyer, and W. Harbich, Z. Phys. D **12**, 15 (1989).

4) W. Harbich, F. Fedrigo, F. Meyer, D. M. Lindsay, J. Lignieres, J. C. Rivoal and D. Kreisle, J. Chem. Phys. **93**, 8535 (1990).

5) W. Harbich, F. Fedrigo, J. Buttet, and D. M. Lindsay, Optical Spectroscopy on Size Selected Gold Clusters Deposited in Rare Gas Solids, Z. Phys. D **19**, 157 (1991).

6) W. Harbich, F. Fedrigo, J. Buttet, and D. M. Lindsay, Soft Landing of Monodispersed Small Metal Clusters in Rare Gas Solids, Mater. Res. Soc. Symp. Ser. **206**, 369 (1991).

7) R. Keller, in The Physics And Technology of Ion Sources, edited by I. G. Brown (Wiley, New York, 1989), Chap. 7.

8) K. Besocke, S. Berger, W. O. Hofer and U. Littmark, Radiat. Eff. **66**, 35 (1982).

9) See for example, W. Begemann, Ph.D. thesis, Universität Bielefeld (1988).

10) E. M. Spain and M. D. Morse, Int. J. Mass Spectrosc. Ion Phys. **102**, 183 (1990).

11) K. P. Huber and G. Herzberg, Constants of Diatomic Molecules (Van Nostrand, New York, 1979).

12) D. M. Cox, R. L. Whetten, M. R. Zakin, D. J. Trevor, K. C. Reichmann and A. Kaldor, Advances in Laser Science I, edited by W. C. Stwalley and M. Lapp (AIP Conf. Proc. **146**, 1986), pg. 527; A. Kaldor, D. M. Cox, D. J. Trevor and M. R. Zakin, Z. Phys. D **3**, 195 (1986).

13) C. Cossé, M. Fouassier, T. Mejean, M. Tranquille, D. P. DiLella and M. Moskovits, J. Chem. Phys. **73**, 6076 (1980).

14) A. R. Gee, D. C. O'Shea and H. Z. Cummins, Solid State Commun. **4**, 43 (1965).

15) P. R. R. Langridge-Smith, M.D. Morse, G. P. Hansen, R. E. Smalley and A. J. Mercer, J. Chem. Phys. **80**, 593 (1984).

16) W. Demtröder, Laser Spectroscopy (Springer Verlag, Berlin, 1981).

17) T. A. Ford, H. Huber, W. Klotzbücher, E. P. Kündig, M. Moskovits and G. A. Ozin, J. Chem. Phys. **66**, 524 (1977).

18) D. W. Green and D. M. Gruen, J. Chem. Phys. **57**, 4462 (1972).

19) W. Klotzbücher and G. A. Ozin, Inorg. Chem. **16**, 984 (1977).

20) M. Moskovits and W. Limm, Ultramicroscopy **20**, 83 (1986).

21) R. W. Wood, Phil. Mag. **4**,396 (1902)

22) Wavelengths pertain to measurements in air, whereas energies are given in vacuum wavenumbers.

23) A. R. Gee, D. C. O'Shea and H. Z. Cummins, Solid State Commun. **4**, 43 (1965).

24) R. J. H. Clark, Raman, Resonance Raman and Electronic Raman Spectroscopy in Vibronic Processes in Inorganic

Chemistry, ed. by C. D. Flint, NATO ASI Series (Kluwer Academic Publishers, 1989), pg. 301.

25) M. P. Andrews and G. A. Ozin, J. Phys. Chem. **90**, 2852 (1986).

26) M. C. Manning and W. C. Trogler, J. Amer. Chem. Soc. **105**, 5311 (1983).

27) F. A. Cotton and I. Shim, J. Phys. Chem. **89**, 952 (1985).

28) S. P. Walch and C. W. Bauschlicher, in Comparison of ab initio Quantum Chemistry with Experiment, ed by R. J. Bartlett (Reidel, boston, 1985).

CHAPTER III

DOUBLE TOF MASS SPEC. WITH LASER VAPORIZATION SOURCE AND REFLECTRON

III.1 DESIGN CONSIDERATIONS

Our original design considerations were for an instrument to study gas phase cluster photo-fragmentation using a laser vaporization source and time of flight techniques; simplicity and versatility were our guides. Such flexibility would enable us to study different cluster types, van der Waals, metal and semi-metallic clusters. The primary intention was to maximize the production and extraction of ions formed in the expansion, rather than relying on an electron gun or laser to ionize the neutral clusters produced. Ionization tends to add the unwanted benefit of heating up the clusters. The decision to go via the pulsed route was based on a desire to minimize the pumping requirements of the system. Additionally a pulsed system was ideally suited for time of flight (TOF) mass spectrometry techniques. The choice of laser was between a copper vapor laser (CVL) and a second harmonic pulsed YAG (Yttrium Aluminum Garnet) laser. The YAG was chosen because exceedingly high laser powers were not needed to vaporize even the refractory metals.[1-5] The cluster source needed to be as simple as possible to accommodate the dual role of being able to function as both a regular seeded source and a laser vaporization source. The easy availability

of metals either as sheets (easily cut into target disks) or in powdered form (sintered into disks), influenced our decision to forego the use of target rods.[1-6] Though the manipulation of a target rod to obtain a fresh surface was easier, we felt that we could obtain adequate rotation and translation with the use of a hypocycloidal planetary gear assembly.[7] The choice of an on-axis beam and the use of a simple ion repeller mass gate, rather than off-axis beam was again to simplify the construction and reduce the need for extraneous ion deflectors and lens. The option to fragment clusters axially 'head on' as well as trans-axially, was also an important consideration. The instrument as constructed is shown in Figs. 3.1 and 3.2.

III.2 THE LASER VAPORIZATION DUAL TOF MASS SPEC.

III.2.1 INTRODUCTION

The instrument can be viewed as being comprised of three integral parts contained in a vacuum. The vacuum was essential, for gas phase ions would not exist for any significant length of time outside a vacuum. Cluster ions were produced in the laser vaporization source; they were next mass analyzed to view their mass distribution; then mass selected to choose clusters of a particular size and finally laser fragmented to obtain information from which the nature of their structure and bonding could be inferred.

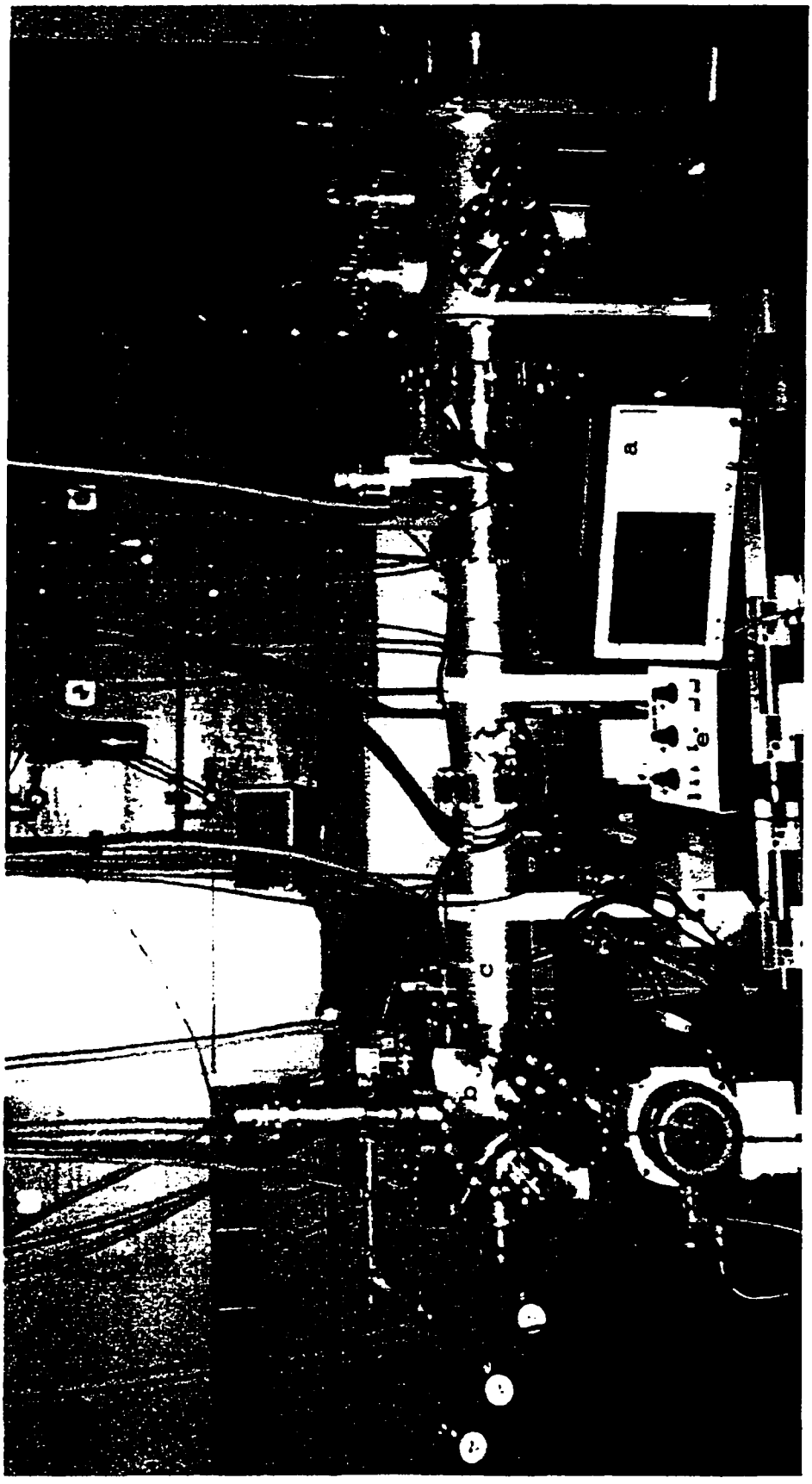

Figure 3.1 Photo of the entire instrument.
a- LeCroy 9450 oscilloscope **b**- Source chamber **c**- Flight tube **d**- turbo pump
e- laser controller **f**- reflectron chamber

Overall View of The Instrument

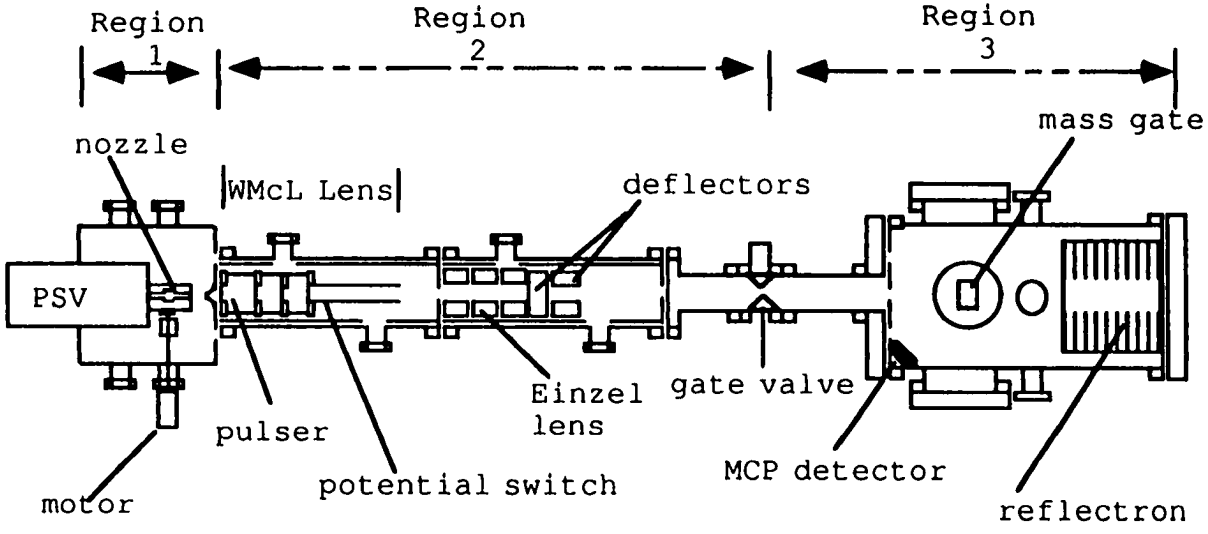

scale: 1 inch = 1 ft

Figure 3.2 :Diagram of Time-of-flight mass spectrometer with laser vaporization source for production of gas phase metal cluster ions. Viewed from the top looking down.

III.2.2 THE VACUUM SYSTEM

The vacuum system consisted of two turbo molecular pumps, a Leybold NT361 (TMP) (pumping speed 355 l/s) and a Balzers TMP500 (pumping speed 500 l/s). Both pumps were water cooled, with the Balzers requiring infrequent oil changes while the Leybold was a low maintenance grease packed pump. Each of the TMP was rough pumped with a Leybold mechanical pump. A Pirani thermal conductivity vacuum gauge and two hot cathode ionization gauges were used to measure vacuum pressures. The vacuum was controlled with the use of a simple interlock which responded to water and power failures and included the option of both automatic and controlled venting.

An important part of our system, designated the 'pump out unit', when viewed as a single entity included the carrier gas lines to the pulsed supersonic valve (PSV) and the PSV inlet reservoir. Experience taught us to pump out the gas lines and inlet reservoir prior to filling with the carrier gas to ensure exclusion of air and the resulting simultaneous production of metal oxide clusters. Despite our extreme measures niobium oxide clusters, which are extremely difficult to eliminate entirely were still produced (shown later). This unit however minimized the amounts of niobium oxide clusters obtained.

The entire system, depicted in Fig. 3.2, consisted of three regions. Region 1 contained the laser vaporization source (LVS), region 2 had the Wiley McLaren TOF mass

spectrometer, ion optics and deflectors and region 3 contained the ion repeller mass gate, reflectron TOF mass spectrometer and a microchannel plate detector (MCP). Regions 1 and 2 were separated by a skimmer, while regions 2 and 3 were separated by a mechanical gate valve (MDC). The gate valve divided the entire vacuum into two separate volumes, which could be closed off and vented separately, for example when doing routine maintenance in the LVS. Compressed nitrogen was used when venting since it was prudent to prevent unnecessary exposure of the MCP detector to air by always keeping the chamber in which it was housed under vacuum. The instrument's total enclosed volume was 50 liters. A total vacuum pressure of 1×10^{-9} torr was easily attained, however during normal operation of the PSV with helium at a stagnation pressure of 150 psig, this increased to 1×10^{-5} torr.

III.2.3 THE LASER VAPORIZATION SOURCE

Clusters were produced in the laser vaporization source, which was the most crucial part of this instrument. Laser vaporization sources which produce metal clusters were pioneered by R. E. Smalley.[1-5] Our source was a modified version of one that was originally designed by Winston A. Saunders.[8] The source shown in Fig. 3.3, consisted of the laser, a pulsed supersonic valve, a Teflon nozzle, a target metal disk and a target rotation assembly with a motor. These were installed in an eight inch cube, which sat above a

Balzers turbo pump. The YAG laser vaporized metal off the target disk, producing a 'superheated plasma'[9] of metal ions.[10] The laser was triggered to fire when the helium pulse was over the target orifice, or in some cases just before it arrived over the target. The helium which was at supersonic flow enveloped the expanding plasma. Plasma collisions within the confines of the dense helium cloud, enabled the metal to condense and initiate cluster growth and formation. Further clustering and cooling of the internal degrees of freedom occurred as the gas expanded supersonically while exiting the nozzle into the surrounding vacuum.[11] The supersonic expansion converts the random thermal motion of the gas and its associated energy into directed center-of-mass motion, reducing the translational temperature of the beam.[10] All the particles in the beam would then travel at about the same velocity as helium, given by the following equation:[4]

$$v \approx \sqrt{\frac{5kT_o}{m_{He}}} \qquad 3.1$$

where m_{He} is the mass of helium, v is supersonic velocity, T_o is the temperature of helium before expansion and k is the Boltzman's constant. This gives a velocity of about 2 x 10^5 cm/s for particles in the beam.

Cluster vaporization was achieved with the use of the 532 nm, (second harmonic) green line of a Spectra Physics GCR-11 YAG pulsed laser. The second harmonic of the YAG had a 7 ns

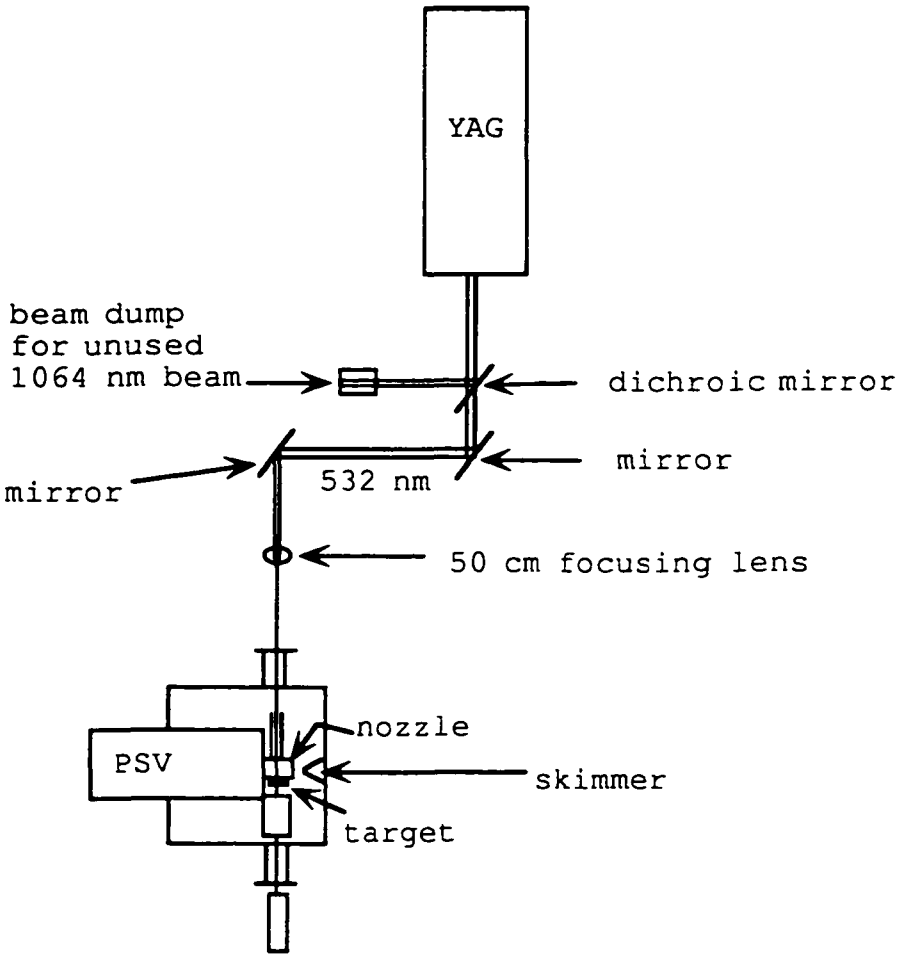

Figure 3.3 Diagram illustrating how the vaporization laser is focused on the target disk.

pulse width, and a pulse energy of 135 mJ at 10 Hz and could be operated at variable repetition rates of 1 - 10 Hz, when externally triggered. Figure 3.3 also indicates how the laser is directed in the source. The fundamental 1064 nm light was separated and directed to a beam dump by a 45° dichroic beam splitter. The 532 nm laser beam was then guided through a window into the source with the use of two mirrors. The laser beam was brought to a sharp focus in the source, from a 6.4 mm beam diameter to a 0.5 mm diameter spot on the target surface. Focusing was achieved by using a 50 cm F focusing lens, to focus the laser down a very narrow (5 mm diam.) Teflon channel. Prior to laser alignment, the gate valve was closed and the vacuum in region 1 was vented. The top and side (8") flanges were next removed to gain access to the target and nozzle. Proper alignment of the laser was accomplished by removing the target together with the target holder and gear assembly, (see Fig. 3.4). Figure 3.5 is a close up photo of the source chamber in the absence of the target holder and gear assembly, showing clearly both the PSV and the Teflon backed nozzle support. The laser was then turned on and allowed to exit the nozzle orfice. A visual inspection of the laser spot on a dark background, was made to determine the shape of the laser spot, and to estimate the degree of laser mis-alignment. The laser beam was then directed into a power meter, which was mounted at the Teflon backed stainless steel block containing the nozzle, (shown in Figs. 3.5, 3.6A and 3.6B). The laser energy was maximized

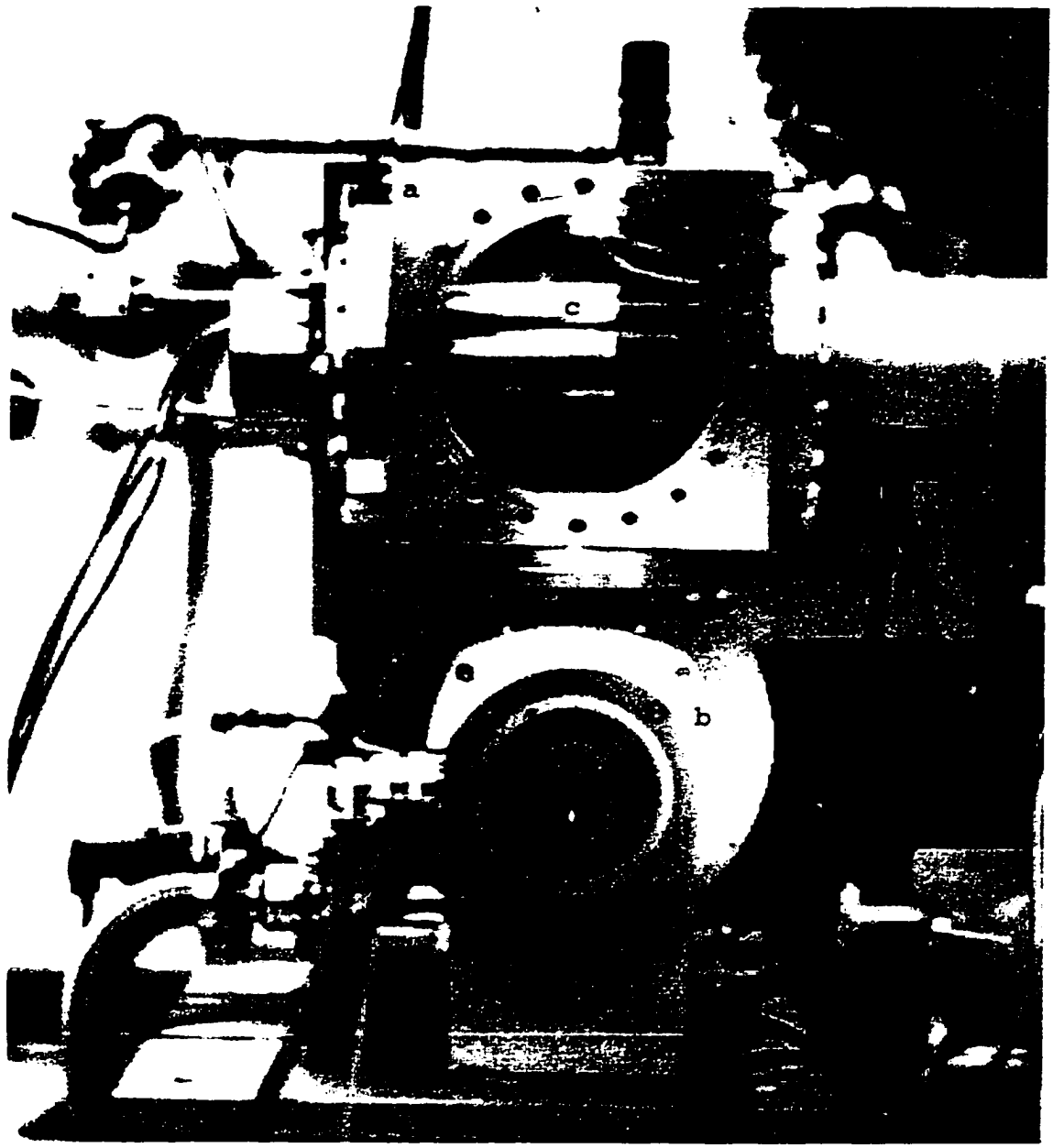

Figure 3.4

Photograph of the source chamber (**a**) which is sitting on the Balzers turbo pump (**b**). The target holder and gear assembly have been removed to allow the PSV (**c**) to be seen.

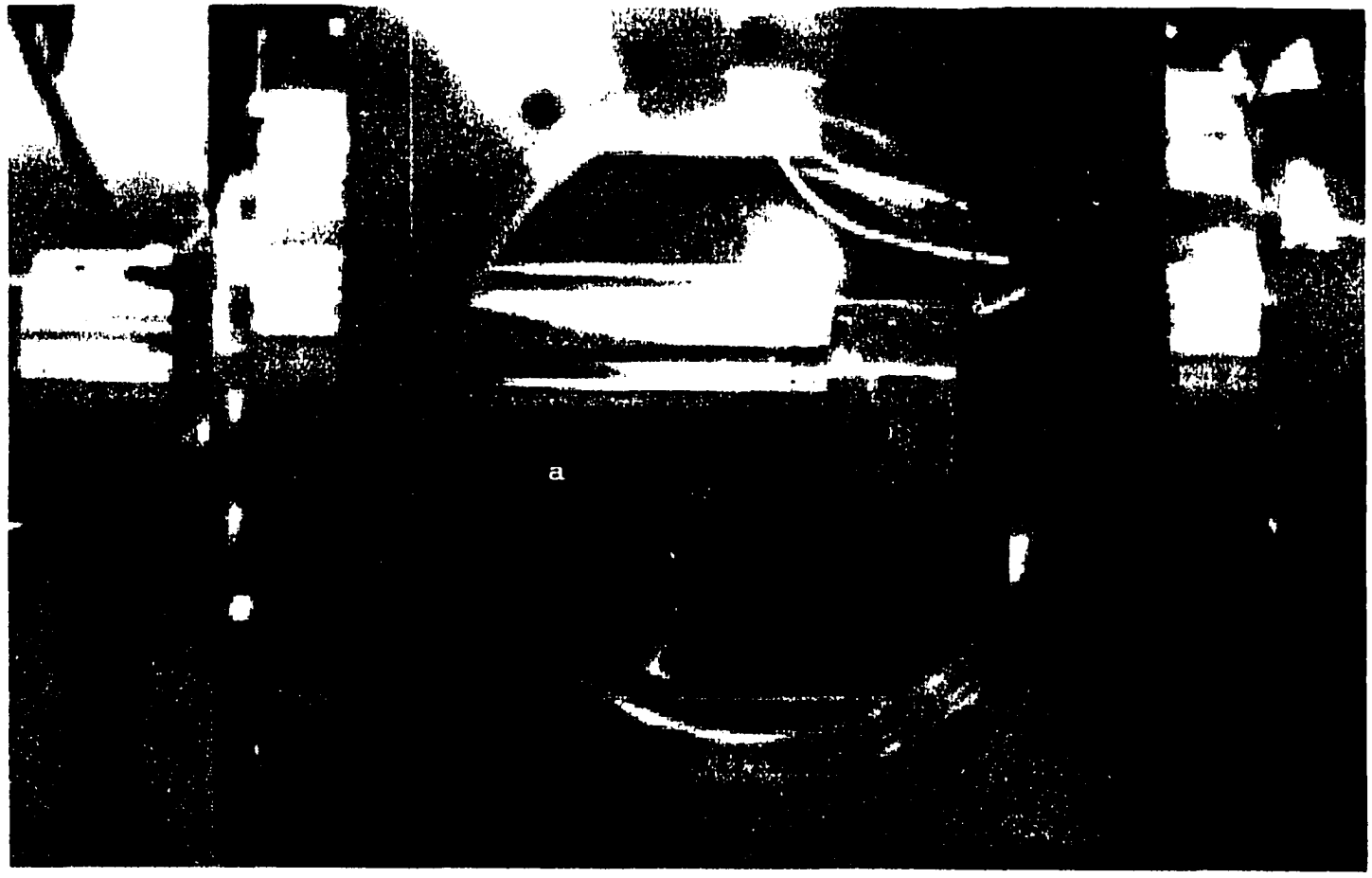

Figure 3.5

Close-up photo of the source chamber showing the PSV (**a**) and the Teflon backed nozzle support (**b**). The dark spot in the center of the nozzle support is the laser orifice.

through the narrow channel by mirror adjustments and the target and gear assembly were reinstalled when the alignment process was completed. A vaporization energy of 20 mJ per pulse was used for the vaporization of niobium.

III.2.4 THE PULSED SUPERSONIC VALVE

The PSV was an R. M. Jordan valve which operated on the magnetic beam repulsion principle pioneered by Dimov.[12] Magnetic beam repulsion allows for the passage of a 5 kA current of 20 ms duration through a pair of parallel conductors in a 'hairpin configuration', with the current traveling in opposite directions. The opposing flows of current set up a magnetic force which lifts the top beam from the O-ring seal over the nozzle and opens the valve. The valve admits carrier gas into the supersonic free expansion nozzle, which then injects gas pulses of varying widths. These gas pulsewidths are determined by the magnitude of the current, the backing pressure of the gas and the elasticity of the 'hairpin' spring. The PSV valve shown in Fig. 3.5 had a 0.5 mm diameter nozzle and could withstand a backing pressure of 150 psig and be operated at a repetition rate up to 10 Hz. The instrument was normally operated at a rate of 4 Hz, since at higher repetition rates there was an increased gas load for the pump to handle, which created a very 'noisy' cluster beam signal. The valve was arranged parallel to the beam axis, with the cluster nozzle assembly attached to the

face of the PSV and directly aligned with the PSV nozzle as shown in Fig. 3.5.

III.2.5 THE CLUSTER SOURCE NOZZLE

The cluster source nozzle (see Figs. 3.6A and 3.6B) was constructed from two cylindrical sections of Teflon. Teflon was the material of choice for nozzles because it was easy to machine and therefore easily facilitated minor modifications. Both nozzle sections were 'almost' identical and were set up in a mirrored configuration. One part of the nozzle section consisted of two regions, a cylindrical channel (1 mm diam. and length 1 cm), opening out into another cylindrical region (5 mm diam. and length 5 mm). The other section, which formed the front part of the nozzle had an additional region which extended out into a 30 degree angle Laval cone, through which cluster beam supersonic expansion occurred. The size and geometry of the nozzle were very important as they determined the cluster size distribution.[10,11] We experimented with various nozzle designs and were still not satisfied with one that could be regarded as ideal.

The body of the Teflon nozzle was threaded into the stainless steel mount (Fig. 3.6B), which was supported on the face of the PSV. The mount which was screwed to the face of the PSV supported and aligned the cluster nozzle as well as the target and it's ancillary apparatus. There was a 1 mm orifice drilled through the mount to allow the laser to impinge on the metal target disk. Both sections of the

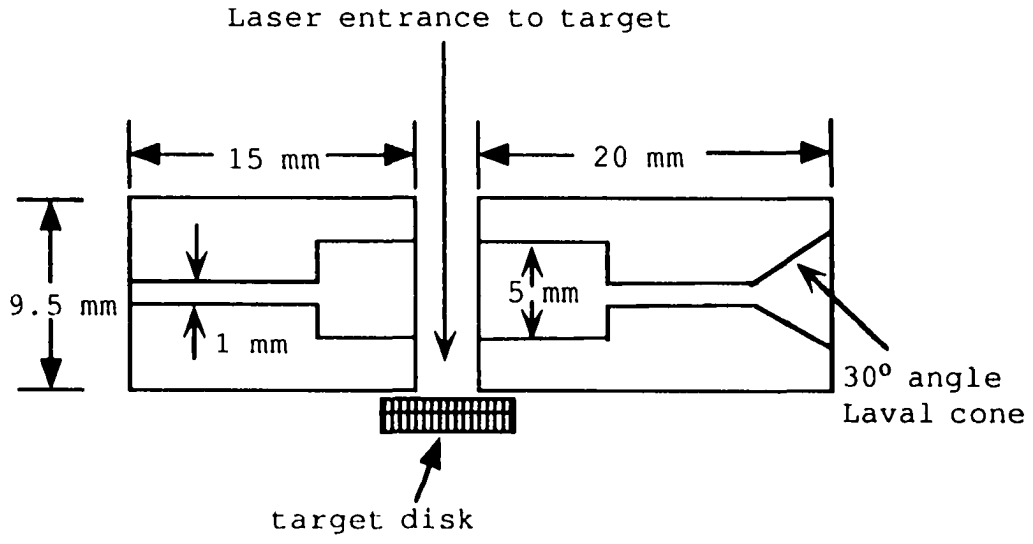

Figure 3.6A Diagram of both halves of the threaded Teflon nozzle insert.

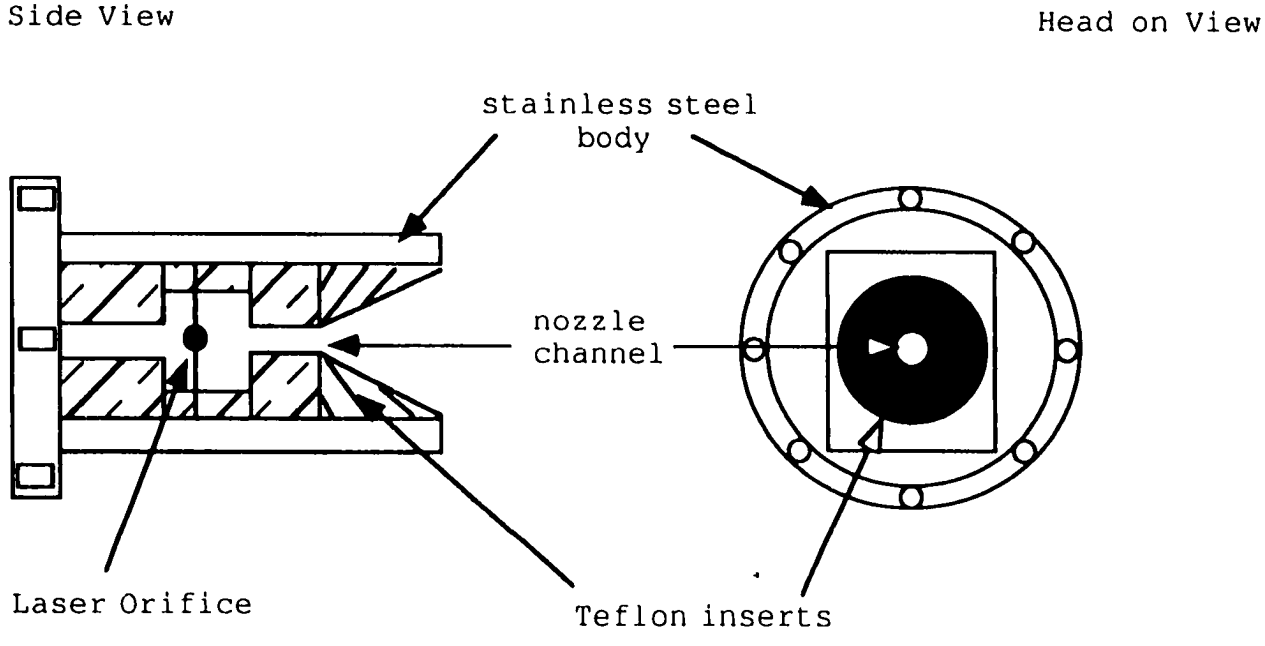

Figure 3.6B Diagram of the nozzle support with the Teflon nozzle inserts. The nozzle support is bolted to the face of the PSV.

cluster nozzle were arranged such that the 5 mm diam. regions faced each other and formed a cavity. The orifice was perpendicular to the nozzle and beam axes and dissected the cavity to allow the entrance of the laser beam, which was tightly focused on the metal target disk. The cavity, affectionately referred to as the 'waiting room' provided the location for the vaporized metal plume to become entrained in the 'puff' of helium arriving from the PSV, and be subjected to collisions and condensation to form clusters.

III.2.6 TARGET ASSEMBLY

The target assembly shown in Figs. 3.7 (A,B,C), consisted of a linear rotation motor, a 35 tooth internal gear, a 22 tooth external gear, a target holder shaft and an offset coupling. The internal gear (N32S2-35), and external gear (P32S26-22) both made of 303 stainless steel, were obtained from Berg Precision Mechanical Components. The gears and shaft were supported on a frame which was attached to the nozzle mount. The internal gear was pressed up against the side of the nozzle mount such that it's center was away from the laser orifice. The benefit of having the external gear 'off-center' was to enable the target to travel an orbital path (circumscribed by a hypocycloid) which would prevent the continuous laser removal of material from one area of the target. The internal gear was fixed in space and supported on a block bolted to the nozzle assembly, (Fig. 3.7A). There was allowance for minor adjustments to the position of the

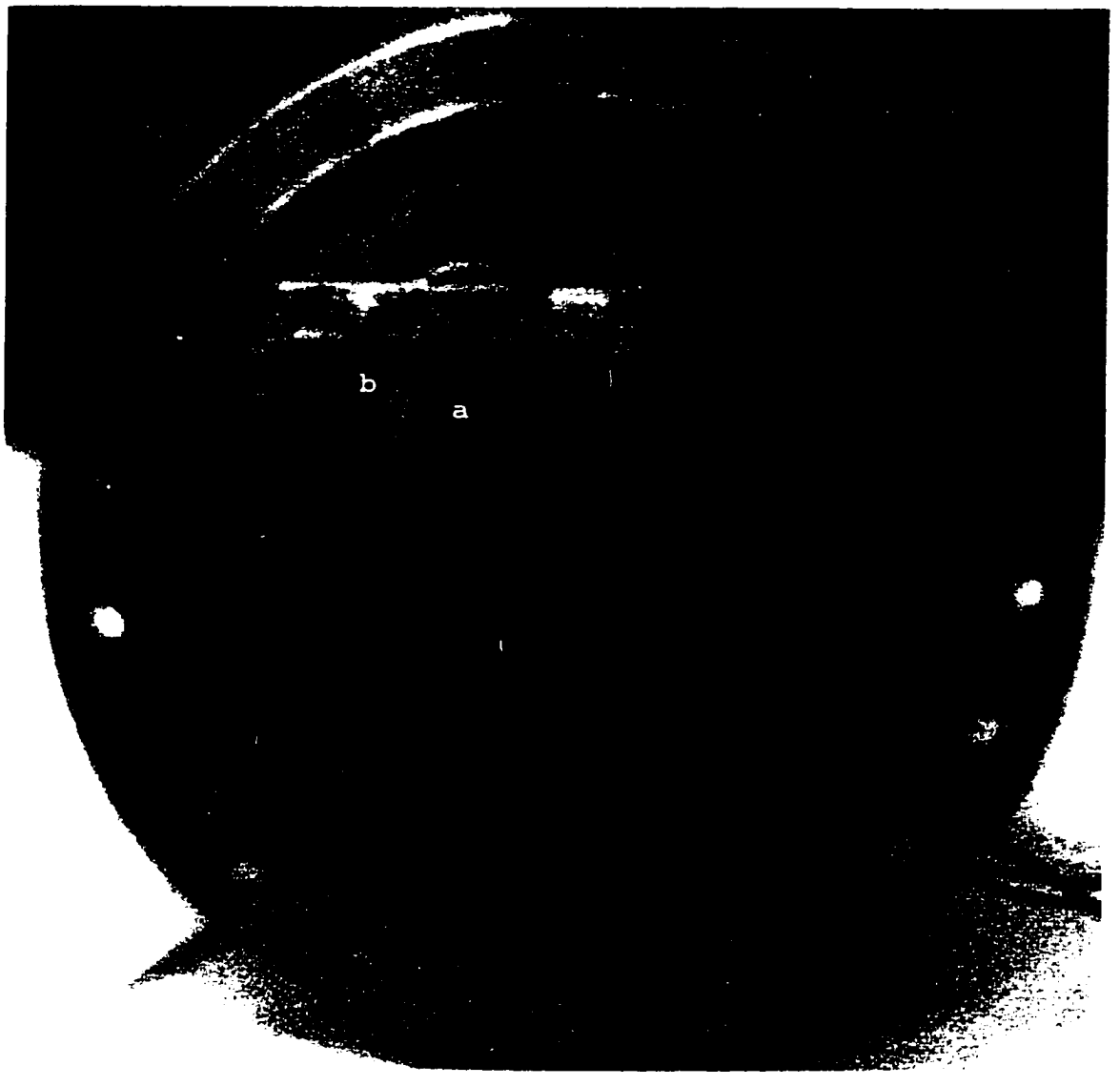

Figure 3.7A

Photograph of the target holder and gear assembly mounted on the 8" flange.
The target (**a**) is facing the viewer. Also visible is the gear assembly which surrounds the target. The front piece denoted (**b**) is the internal gear.

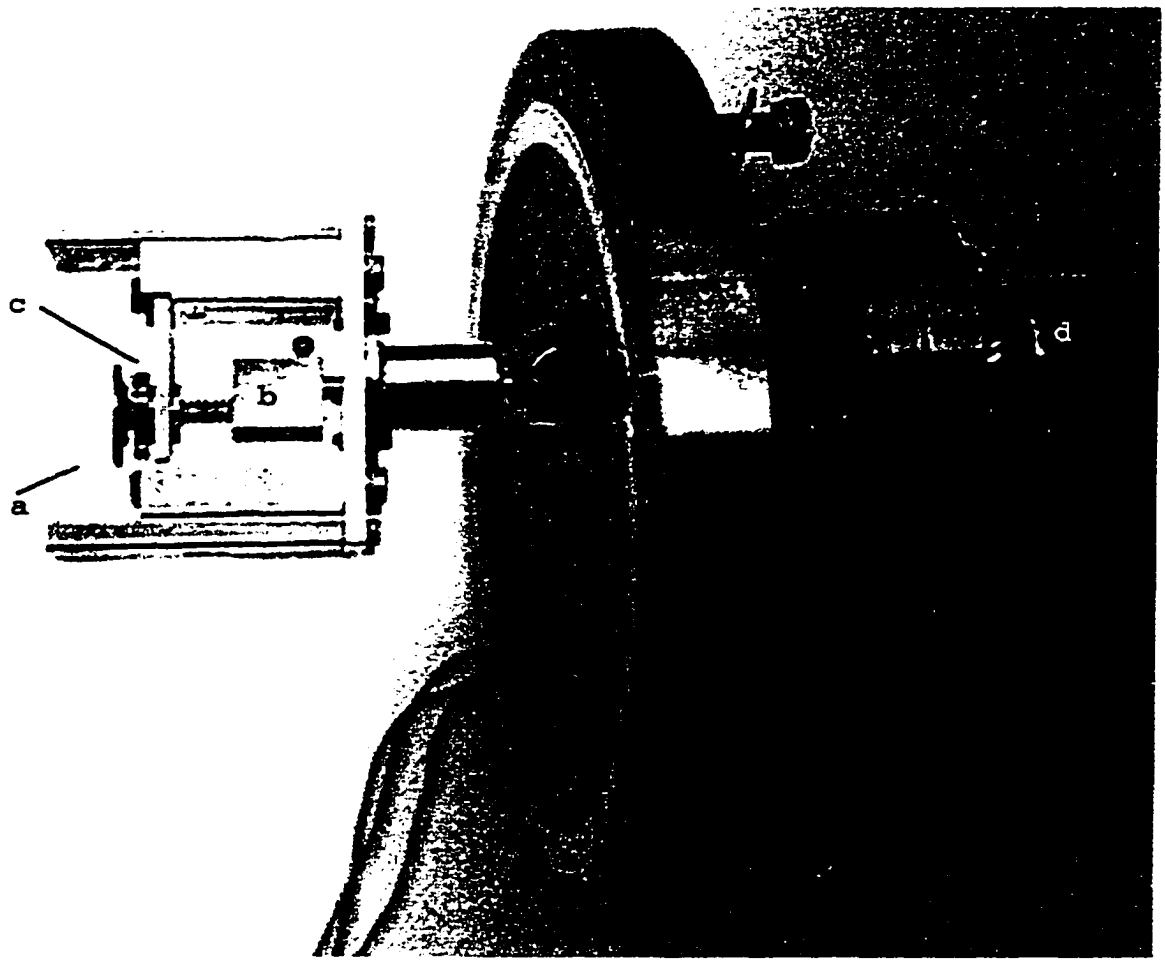

Figure 3.7B

Photo of the side view of the target holder and gear assembly

a- target
b- offset couple
c- external gear
d- the motor which rotates the target

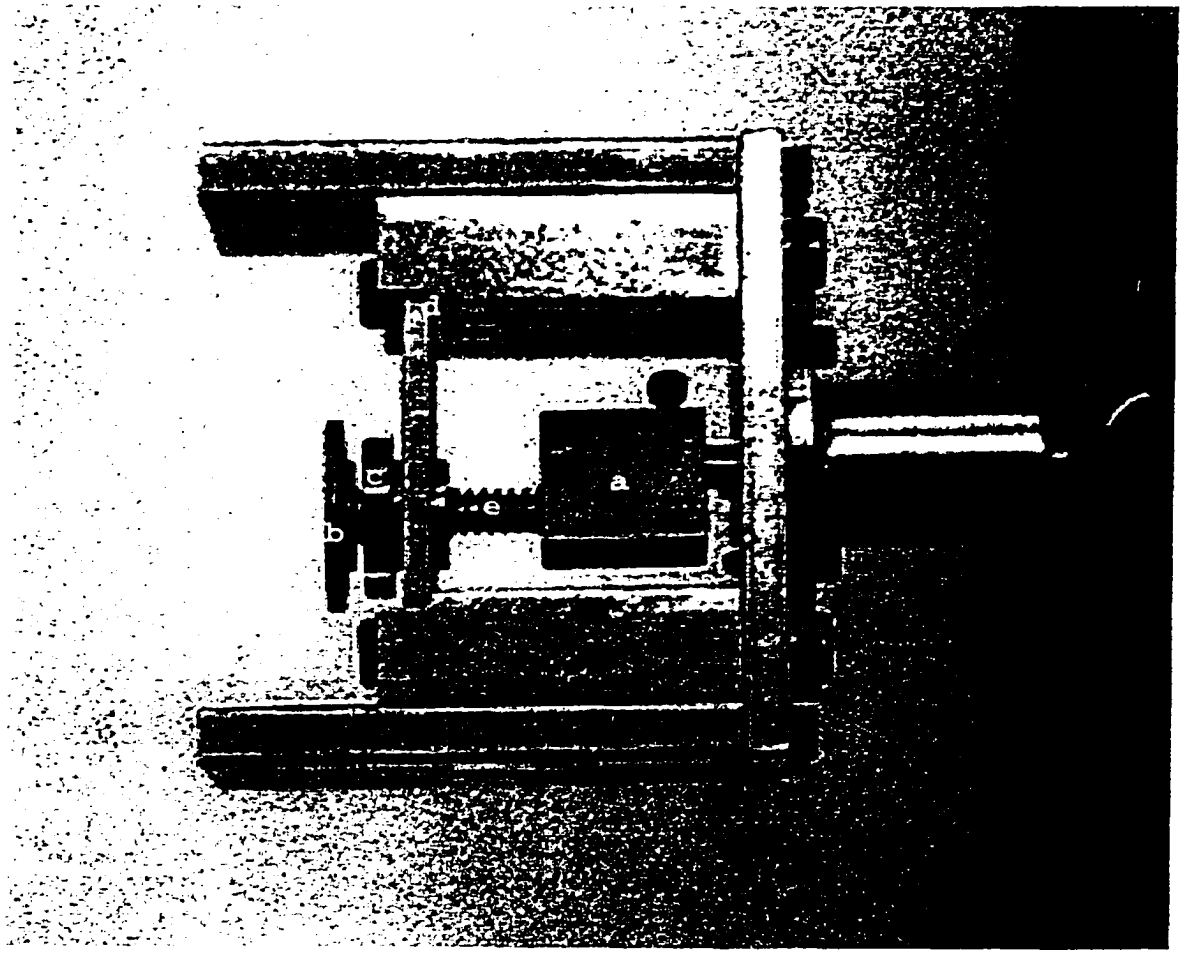

Figure 3.7C

Photo with a close-up view of the target holder and gear assembly

a- target
b- offset auple
c- external gear
d- the block containing the internal gear
e- the target shaft with a spring

internal gear, so that both gears were mechanically aligned. The inner moving gear was centrally affixed to a shaft that supported the target metal disk, shown in Fig. 3.7C. The target was bonded to the shaft with 'Crazy glue', (once the 'Crazy glue' had dried properly it did not outgas 'significantly' under vacuum). The target shaft was coupled to the gear support central shaft by means of an offset couple which was a critical component of the orbital gear arrangement. It allowed a fresh surface to be presented to the laser, thereby preventing the laser from drilling a hole through the target. The target shaft and offset couple were originally crafted from steel and brass respectively, however the brass scored easily and the moving parts eventually jammed. This problem was solved by making both parts out of steel and applying a minuscule amount of molybdenum disulfide vacuum lubricant to their respective contact surfaces. The small amount of molybdenum disulfide used showed no effect on the quality of the vacuum. A small coiled spring was required between the shaft and offset couple to keep the target disk firmly pressed against the orifice on the nozzle housing. Laminated to the nozzle housing was a sheet of Teflon to provide a smooth low friction surface to the metal target pressed up against it. This allowed the target to glide freely with effortless rotation of the gear. The externally mounted linear rotation motor (MDC BRM-275-02) was coupled to the central shaft via a motion feedthrough and supported on a 2.5 inch diam. flange. Our original plans included an

internally mounted stepping motor; however this motor jammed and stopped frequently because the stepping motor over heated when confined in the vacuum chamber. A linear motion motor was cheaper and easier to use since one could slow the rate of rotation by simply decreasing the current to the motor.

The assembly could accommodate targets varying in diameter from 0.8 - 1 inch. These were circular disks of varying thickness up to 0.2 inch, which could be made from either pure metal, sintered powders or composite materials. The targets were prepared by polishing them with emery cloth (medium grade followed by fine grade), and finally with a polishing cloth. A finely polished target was necessary to minimize friction. Targets were thoroughly cleaned with methanol to remove grease and grit and then allowed to dry properly before affixing to the target shaft. It was essential that the target not remain in the same spot for consecutive laser shots, otherwise pits were drilled into it. The orbital rotation of the inner gear enabled the target to present a 'fresh' surface to the laser. Removal of material from the target resulted in the formation of tiny spots. Continuous laser degradation of the spots occurred if the target remained stationary and resulted in a significant decrease or zero cluster ion intensity and the eventual drilling of a hole through the target. Such an event was experienced several times due to malfunctioning of the original stepping motor. Extreme care had to be taken to ensure that the gears were well aligned so that they did not

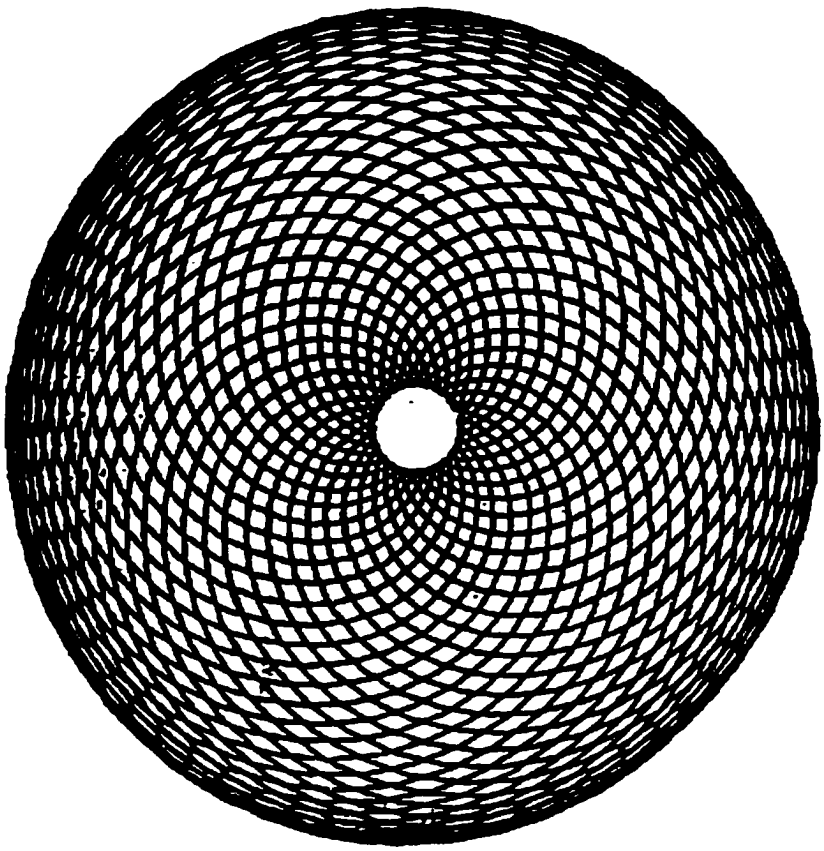

Figure 3.8A

Simulation of the laser burn pattern produced by laser vaporization

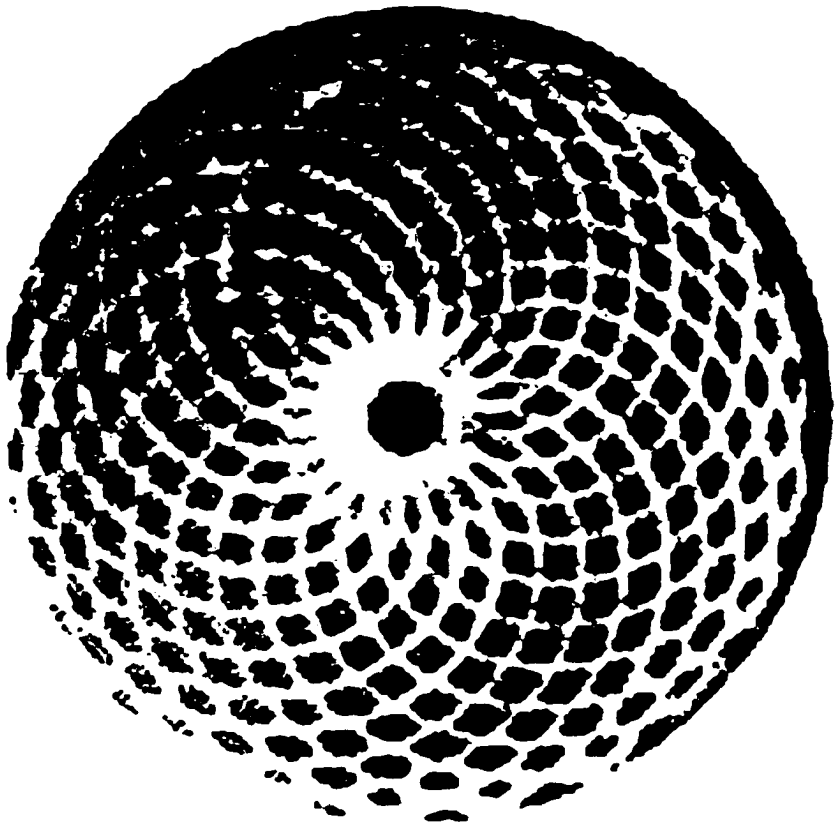

Figure3.8B

Photo of a niobium target after three weeks of use

jam after a few rotations. Abrasions formed on the target by the laser removal of target material results in the emergence of a hypocycloidal pattern (Figure 3.8A) on the surface of the target disk. The simulation is a plot of the equation of the form as follows:

$$x = R \sin (At) \cos (Bt)$$

$$y = R \sin (At) \sin (Bt)$$

When the gears were well aligned and the laser was properly focused on the target disk, the 'rosette' pattern of the hypocycloid shown in Fig. 3.8B, is well defined and symmetrical. Target rotations at the rate of 1 revolution per minute, resulted in a target that was grooved over 95 percent of it's surface area. These grooves were due to the target moving approx. 0.5 mm to the next spot in 0.25 seconds, thereby forming a continuous groove as the target rotated. The target appeared pitted when it rotated too fast, because certain areas made no contact with the laser after traveling the orbital path several times. Once the target rotated slowly and at an even rate, the laser degradation would be fairly even, so that the laser could make several thousand passes over the entire area before the beam quality diminished significantly. A 0.8 inch diameter target would typically last for about two to three weeks before it required surface repolishing.

III.2.7 THE SKIMMER

Supersonic expansions are usually skimmed[13] to produce lower pressure in the detection region and to produce intense beams with a small range of velocities[14]. The skimmer was a nickel plated electroformed cone (1 mm diam. entrance aperture and a 20° angle cone of length 5 cm), manufactured by Beam Dynamics. Cluster ions leaving the nozzle expanded outwards upon ejection. The cluster distribution produced in the cluster source therefore needed skimming to select only those clusters with the components of translation motion mainly in the forward direction. The skimmer collimated the ion packet into a narrow beam of ions. Ions that had their velocity components in other directions were not allowed to enter the mass spectrometer, and were instead deflected off the walls of the skimmer.

III.3 THE PRIMARY MASS SPEC. (LINEAR TOF)

The primary mass spec. utilized the technique of time-of-flight mass spectroscopy to characterize the cluster size distribution. At its simplest, this technique could be viewed as a separation of different masses of ions, by simultaneously pulsing an electric field, which would energize the ions, and then allowing them to drift some fixed distance and become separated due to the differing velocities they have acquired due to their different masses. The technique of time-of-flight mass spectroscopy has undergone a renaissance in the last few years.[15-20] Due to its inherently

pulsed nature, it's marriage to the pulsed laser vaporization cluster source was inevitable. Our system was based on the dual field accelerating system devised by Wiley and McLaren.[15] Upon arrival from the source, ion packets with the same mass may contain both an energy and a spatial spread which create a spread in their arrival times at the detector. In order to compensate for this discrepancy a system consisting of three ion lenses and two different electric fields was devised. This lens arrangement is commonly referred to as the Wiley McLaren time-of-flight system. For positively charged ions, a negative field on the third lens attracts the ions forward, while a positive field on the first lens repels them forward. The second (middle) lens separate both fields which are alternately pulsed on and then off.

The primary mass spectrometer enabled us to obtain a mass spectrum containing the cluster distribution and relative abundance. It consisted of a Wiley McLaren time-of-flight lens assembly, a set of Einzel lens and a pair of ion deflectors. The cluster ion packet, consisting of positive and negative cluster ions and neutral clusters, exit the nozzle and expand out supersonically with a velocity on the order of 2×10^5 cm/s. A 100 μs pulse of helium carrier gas can produce a packet of ionic and neutral clusters of varying masses spread out over a distance of about 10 cm.

III.3.1 WILEY McLAREN LENS

The entire Wiley McLaren (WMcL) assembly begins just after the skimmer. It is an arrangement of three different sets of lenses, shown in Figs. 3.2 and 3.9. The first lens array consists of a series of 4 stainless steel guard rings. The first ring of this lens series had a 90% transmission grid and subsequent rings were separated from each other by sapphire ball insulators. Each guard ring was in electrical contact with its neighbor via a series of 5.6 KΩ resistors which enabled the lens array to provide a uniformly decreasing field when pulsed with a voltage for a short time. This set of lens was maintained at ground potential until pulsed with a positive voltage. Upon arrival within the lens array, the cylindrical volume of ions was subjected to the effects of a rapidly pulsed positive voltage which repelled the cluster cations forward. The 10 cm length of this lens array restricted the ions centered between its ends to an initial length of 10 cm, (later compressed to 1 cm at the WMcL focus). A Kiethley Instrument 245 Power Supply, supplied approximately +1 kV to this lens, commonly referred to as the 'pulser'.

The Wiley McLaren second lens array consisted of an almost identical set of lens as the previous set, including a 90% transmission grid on the first element. Individual guard rings were likewise physically insulated from each other and similarly connected via a series of 470 KΩ resistors, to provide a uniform field. This lens series was kept at ground

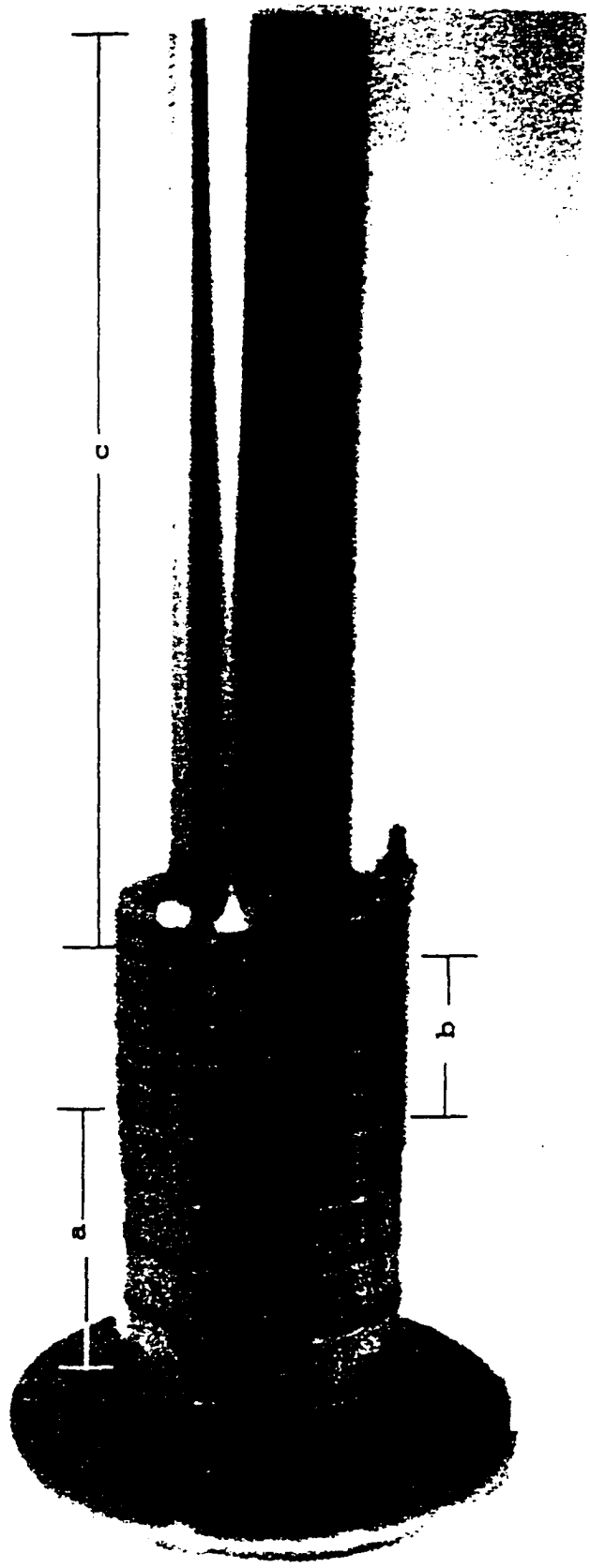

Figure 3.9 Photograph of the Wiley McLaren TOF lens assembly
a- 1st lens array (pulser) **b**- 2nd lens array **c**- 3rd lens array (Pot. Switch)

potential, and served as a transition for the field change from +1 kV at the first lens array to -2 kV at the third lens. The Wiley McLaren third array consisted of a guard ring similar to the others in addition to a 9.5 inches long stainless steel tube. This third set of lens was referred to as the 'potential switch'. It was kept at a potential of -2 kV, which was supplied by a Bertan 205B-03F, high voltage power supply. This lens was rapidly pulsed to ground as the ions entered the potential switch. The field change accelerated the positive ions forward and repelled negative ions off the flight tube axis, neutral clusters were unaffected by either of the charged fields. The ions' ground potential at the end of Wiley McLaren lens system were defined as -2 kV, the potential switch was switched to ground to redefine it to earth ground, causing the ions to be re-referenced to earth ground. The total array about 40 cm long was supported on a triangular arrangement of rods.

Those ions that entered the first lens array early were repelled less strongly than the ones that arrived after, this compensated for the fact that the earlier ones had a higher velocity while the latter ones were slower. By the time they have reached the Wiley McLaren focus 1 meter downstream from the second lens, the slower ions would have caught up to the faster ones and the original ion packet 10 cm long would be compressed to less than 1 cm in length. An ion's arrival time at the focus could be calculated (since we know the various

lens voltage, distances and relative masses of the ions) using equations devised by Wiley and McLaren:

$$T_{total} = T_s + T_d + T_D \qquad 3.2$$

where the time is viewed as the sum of the time for the three different regions of the mass spectrometer as illustrated in Fig 3.10.

$$T_s = 1.02\left(\frac{m}{2U_t}\right)^{\frac{1}{2}}\left[2k_o^{\frac{1}{2}}s_o\right] \qquad 3.3$$

m is the mass of the ion in amu, while U_t, the ion's energy in eV, is given by the following expression:

$$U_t = -v_d + \frac{v_s\, s_o}{s} \qquad 3.4$$

$-V_d$ is the potential switch voltage, V_s is the pulser voltage, s is the distance between the start of the pulser and the second lens and s_o is the distance between the ion and the beginning of the pulser as shown in Fig. 3.10.
k_o is an instrument constant defined as follows:

$$k_o = \frac{(s_o\, v_s + d\, v_d)}{s_o\, v_s} \qquad 3.5$$

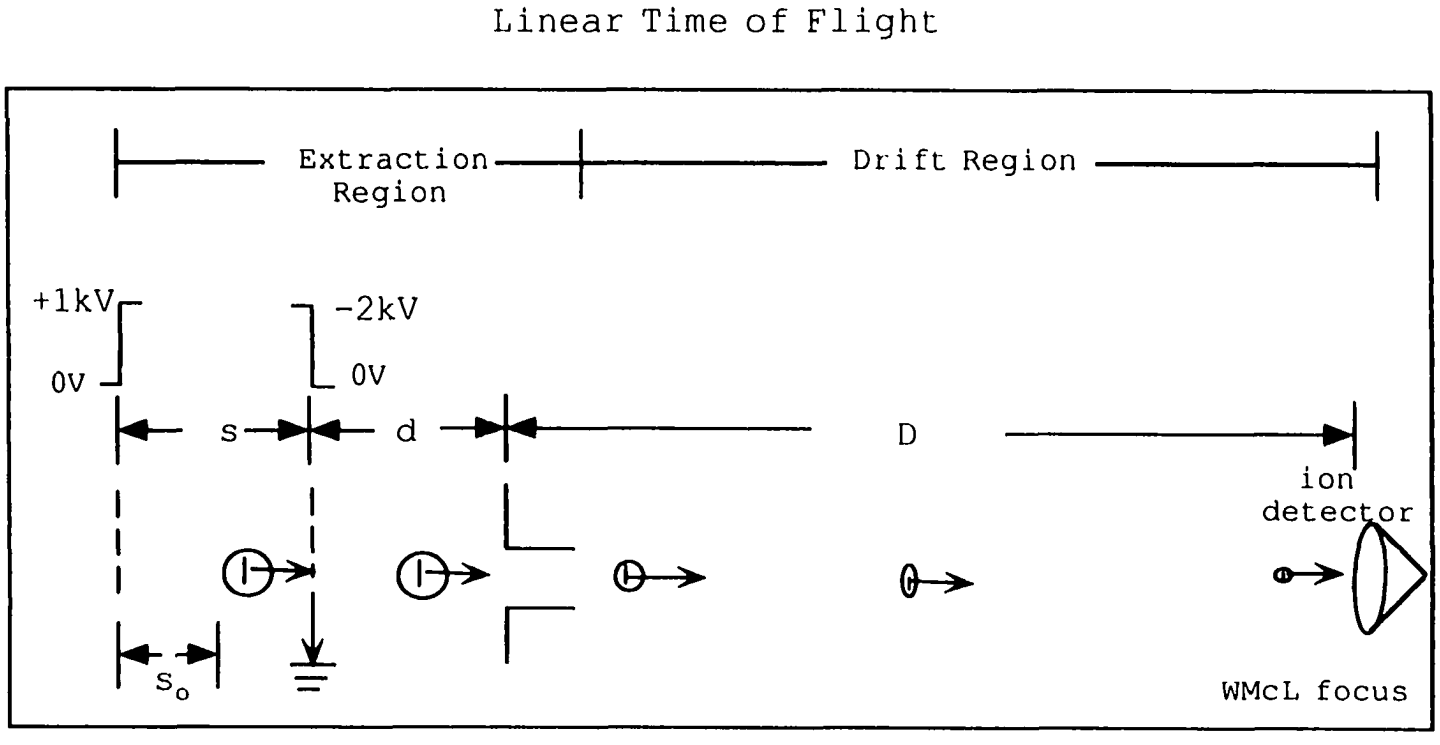

Figure 3.10 Schematic of the Wiley-McLaren TOF lens setup indicating the various regions, voltage pulses and parameters. An ion packet is shown narrowing as it approaches the Wiley-McLaren focus where the detector is located. When mass selection is being performed, the mass gate is situated at the focus.

d is the distance shown and T_d is the time it takes to travel through the distance d given by:

$$T_d = 1.02\left(\frac{m}{2U_t}\right)^{\frac{1}{2}}\left[\frac{2k_o^{\frac{1}{2}}}{k_o^{\frac{1}{2}}+1}\right]d \qquad 3.6$$

T_D is the time it takes to transverse the field free region, where D is the distance (1 m), from start of the potential switch to the Wiley McLaren focus.

$$T_D = 1.02\left(\frac{m}{2U_t}\right)^{\frac{1}{2}}D \qquad 3.7$$

Finally the combined expressions are given in equation 3.8

$$T_{total} = 1.02\left(\frac{m}{2U_t}\right)^{\frac{1}{2}}\left[2k_0^{\frac{1}{2}}s_0 + \frac{2k_0^{\frac{1}{2}}}{k_0^{\frac{1}{2}}+1}d + D\right] \qquad 3.8$$

The Wiley McLaren TOF lens spatially focus the ions with the same charge to mass ratio (q/m) at the mass gate, which was located 1 meter away from the start of the third Wiley McLaren lens. These ions of similar masses which were temporally and spatially compressed (10 cm down to 1 cm), still contained a significant energy spread. Slow ions had been speeded up to meet the fast ions at the transient Wiley McLaren focus. The originally slower ions would eventually

pass the initially faster ions once they have passed the focus and the ion packet would eventually spread out again. It was essential that we did the primary mass selection and laser photo-fragmentation at or near the Wiley McLaren focus, where the ion packet was at it's shortest length; thus the rationale for situating the mass gate.

The width of the ion beam was measured at the mass gate by lowering a metal plate with three apertures, (diam. 0.25 inch, 0.5 inch and 1 inch respectively) across the beam and measuring the ion beam intensity through each aperture. Figure 3.11 shows a plot of ion beam intensity vs the relative lowering of the apertures. The ion beam was shown to have a width of approximately 0.5 inch diameter. The focusing characteristics of the spectrometer are shown in Fig. 3.12, (plot of arrival times of the Nb_2^+ versus it's position away from the grounded front plate). The ions that were further away from the plate achieved a sharper focus at those particular operating voltages. A spreadsheet was used to calculate estimated flight times as well as spread in ion arrival times at various voltage conditions and distances (spreadsheet calculations setup shown in Appendix A.1 and A.2. A mass spectrum of niobium cluster cations is shown in Fig. 3.13A, and Fig. 3.13B shows a plot of ionic mass vs. arrival time (μs), where one observes that the arrival time of the various ions scale as the square root of the mass ($\sqrt{m}$).

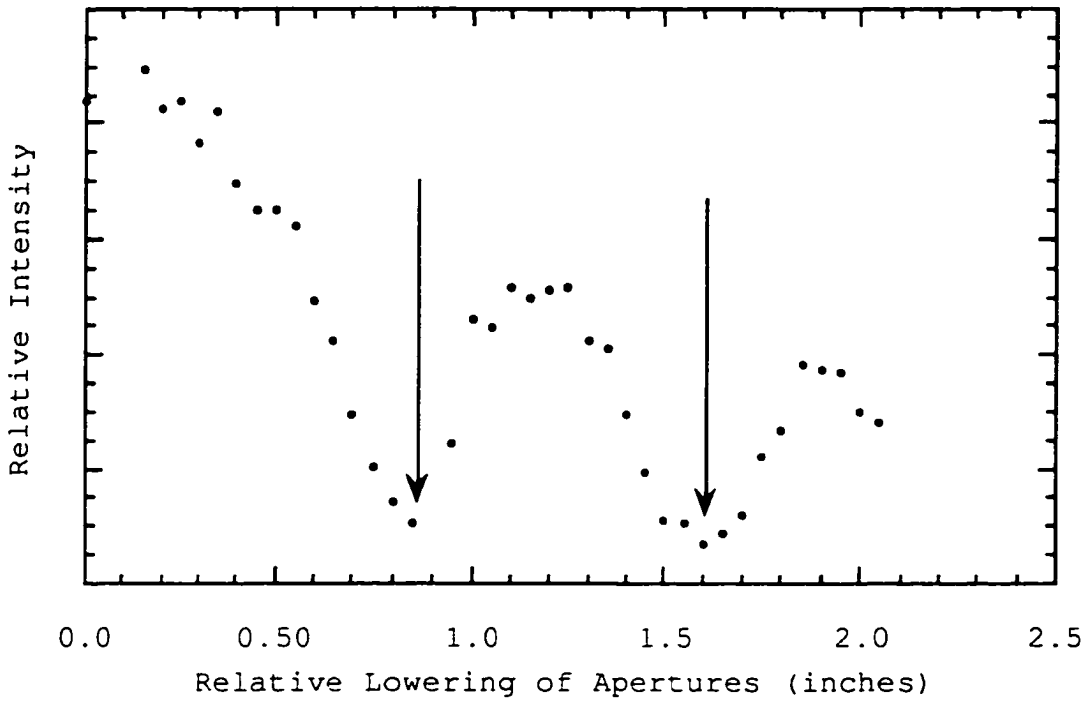

Figure 3.11 Plot of ion intensity vs relative lowering of three different sized apertures (1", 0.5", 0.25"). The beam width was extracted out from the only region on the curve where there is an increase, a maximum and a decrease in ion intensity (shown by the arrows).

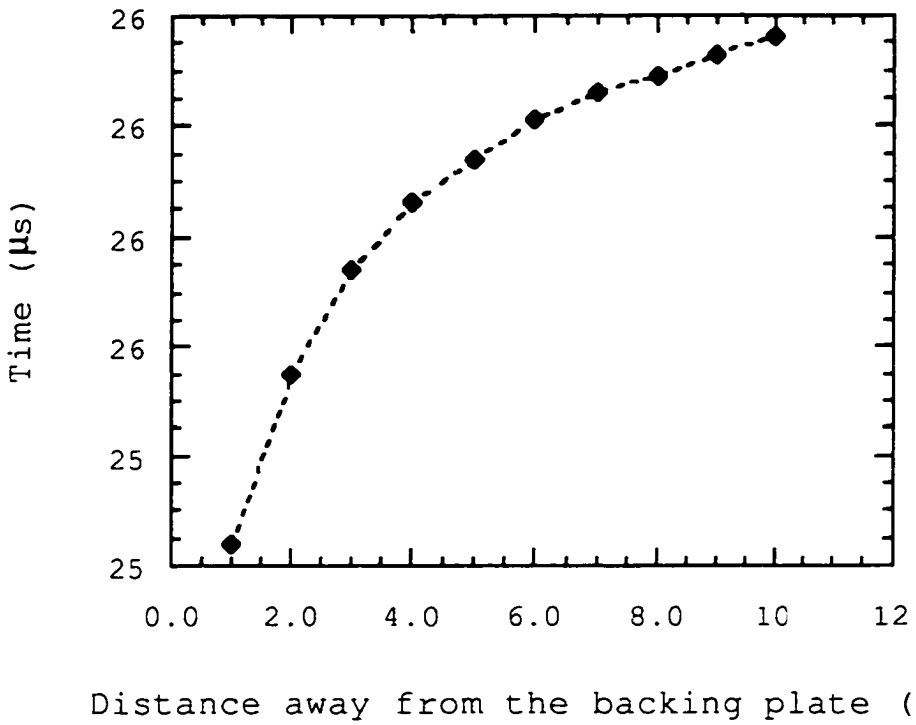

Figure 3.12 Plot of time spread of the arrival time of Nb2+ at the WMcL focus dimer as a function of distance from the backing plate of the first element of the pulser lens.

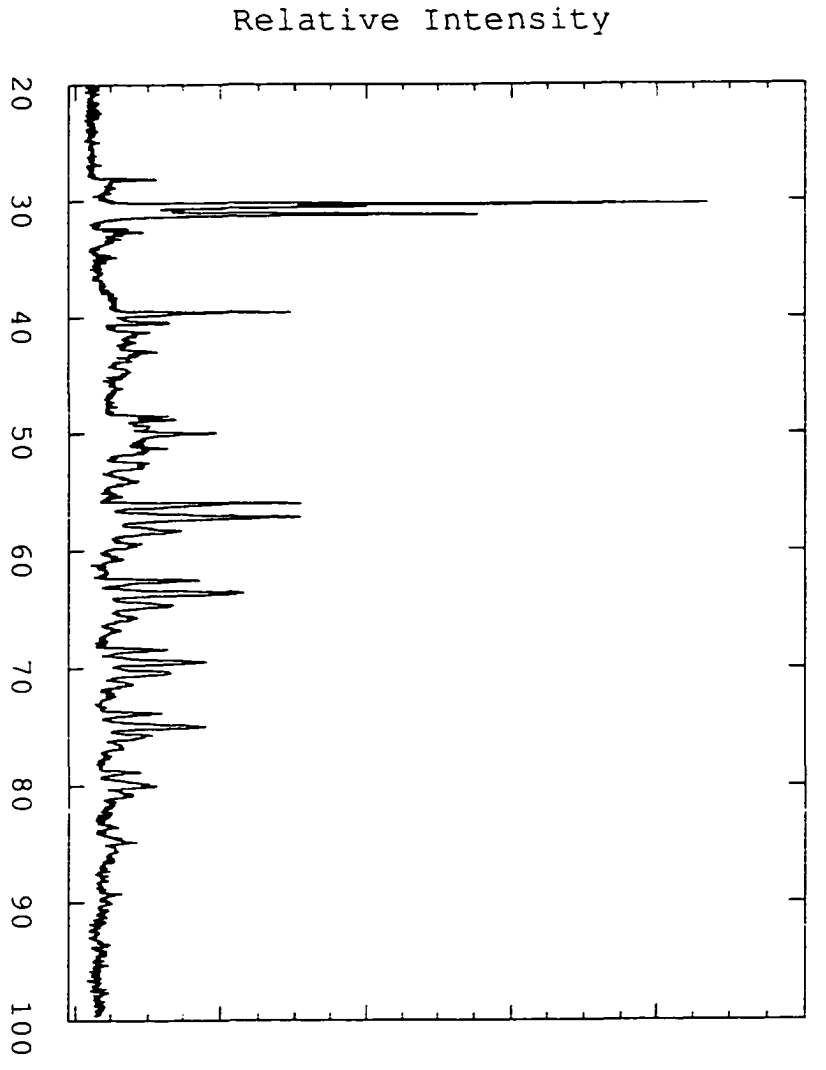

Figure 3.13A Mass spectrum of Nb_n^+ and $Nb_nO_y^+$ cluster cations, where n = (1 -10) and y < 4.

III.3.2 ION LENS & DEFLECTORS

The ion beam required a set of ion lens (Einzel lens) to guide it down the flight tube. These consisted of three stainless steel cylindrical lens located after the TOF lens (see Fig. 3.2). The lens were tuned to focus the ions transversely at the longitudinal focus of the Wiley McLaren TOF mass spec. Using the SIMION (ion simulation software package)[22], we obtained an optimal Einzel lens focusing voltage of 1200 volts. The Einzel lens voltage was supplied by a Bertan high voltage power supply.

The deflectors which were located just after the Einzel lens, are a set of two horizontal and two vertical stainless steel plates. The deflectors deflect ions horizontally and vertically along the beam axis, thereby minimizing the loss of ions along the beam axis. They both required very small voltages to keep the beam aligned. The use of SIMION simulation software in correctly estimating the Einzel lens voltage, minimized the deflector requirement.

III.4 MASS SELECTION, FRAGMENTATION & DETECTION

Our experiment involved selecting a particular sized cluster and subjecting it to irradiation from a YAG pumped dye laser. The effects of the irradiation, (e.g. increase, decrease and absence of fragmentation as well as changes in fragment energies and fragmentation times) could be investigated with the use of a reflectron mass spectrometer

and a dual plate microchannel detector. The reflectron mass spectrometer was also a secondary mass spectrometer which compensated for the energy spread in the ion beam and thus improved the resolution of the instrument.

III.4.1 MASS-GATE

The study of size-selected cluster ions required the isolation of selected ion packets (ions with the same mass). Mass selection was based on the following principle: at the transient focus the ion beam consists of packets of ions grouped according to their masses, lighter ions followed by heavier ones. From spreadsheet calculations, we could easily assign a mass and arrival time to each packet of ions. Knowing the mass and time of a chosen ion packet, we can 'close' the mass-gate thereby blocking entrance to all ions, and 'reopen' it just as 'the selected ions' arrive and then 'close' it again once these ions have passed through the mass-gate.

Mass selection was achieved with the use of a pulsed ion repeller mass-gate, located at the transient focus of the Wiley McLaren lens. The mass-gate was a simple affair consisting of two parallel metal plates, suspended parallel to the path of the cluster beam, one plate was above the ion beam and the other below it. Both plates were biased with a voltage of +300 volts which formed a positive field between the plates and resulted in deflection of positive ions off the flight tube axis. At the precise moment that the ion of

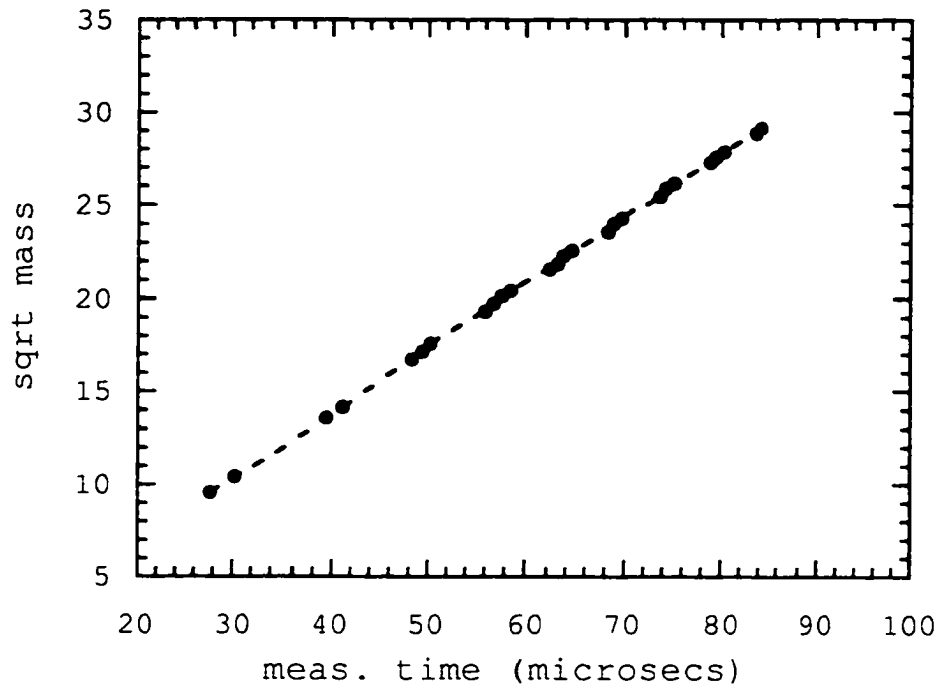

Figure 3.13B Plot of square root of the mass vs the arrival time of ion for niobium and niobium oxides. This plot indicates the linear relationship between $\sqrt{m}$ and the arrival time of the ion.

Nb	NbO		
Nb_2	Nb_2O		
Nb_3	Nb_3O	Nb_3O_2	
Nb_4	Nb_4O	Nb_4O_2	Nb_4O_3
Nb_5	Nb_5O	Nb_5O_2	Nb_5O_3
Nb_6	Nb_6O	Nb_6O_2	
Nb_7	Nb_7O	Nb_7O_2	
Nb_8	Nb_8O	Nb_8O_2	
Nb_9	Nb_9O		

interest approached the mass-gate, the deflection voltage was pulsed to ground thereby enabling the passage of the selected ion species into the reflectron region.

The pulse activating the mass gate needed to be both narrow (on the order of a few hundred ns) and to also have a very fast rise time (on the order of a few ns). Pulse switching was accomplished with a Behlke HTS 31 fast high voltage switch (supplied by Eurotek Inc., NJ, USA) with a turn on rise time of less than 10 ns. It was pulsed to ground for approximately 200 ns (this corresponded to the resolution of the counter timer plug-in board which was limited to 200 ns) giving the ability to select ion packets approximately 400 ns apart. Once the mass selected ions were through the mass gate the voltage was pulsed on again, preventing the passage of other ionic masses. When the mass gate was off, all ions were admitted to the reflectron mass spectrometer. Figure 3.14A shows a mass spectrum of Niobium cluster ions (transmission of all ions) with the mass gate off and Fig. 3.14B shows a mass spectrum of one ion,(transmission of a selected cluster ion) when the mass gate was turned on.

III.4.2 SECONDARY MASS SEPARATION

Secondary mass separation was achieved with the use of an R. M. Jordan single stage reflectron mass spectrometer. The reflectron assembly which was 20 cm deep and 15 cm in diameter, consisted of a combination of plates with grids and mesh which when powered, combined to create a uniform

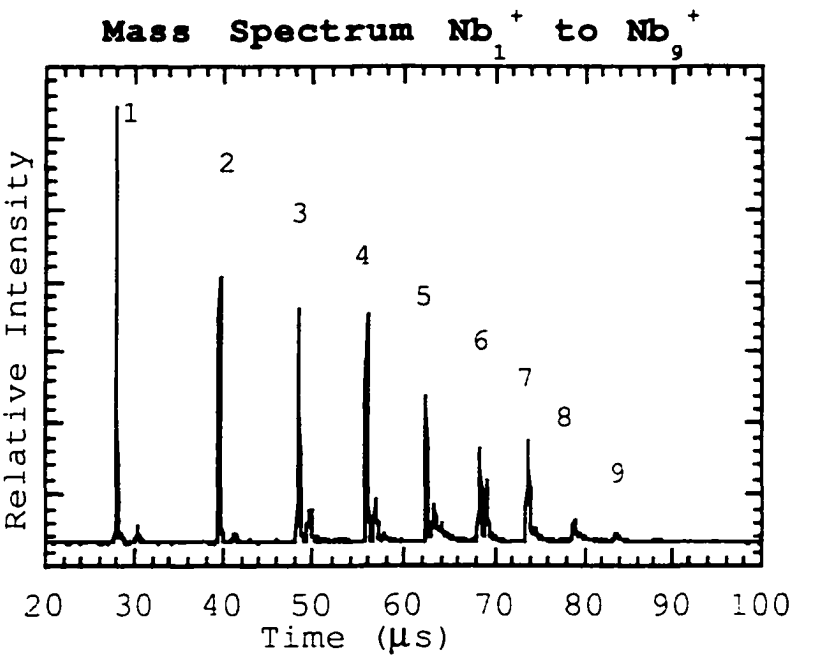

Figure 3.14A Mass spectrum of niobium cluster cations Nb_1^+ to Nb_9^+ in the absence of the mass gate.

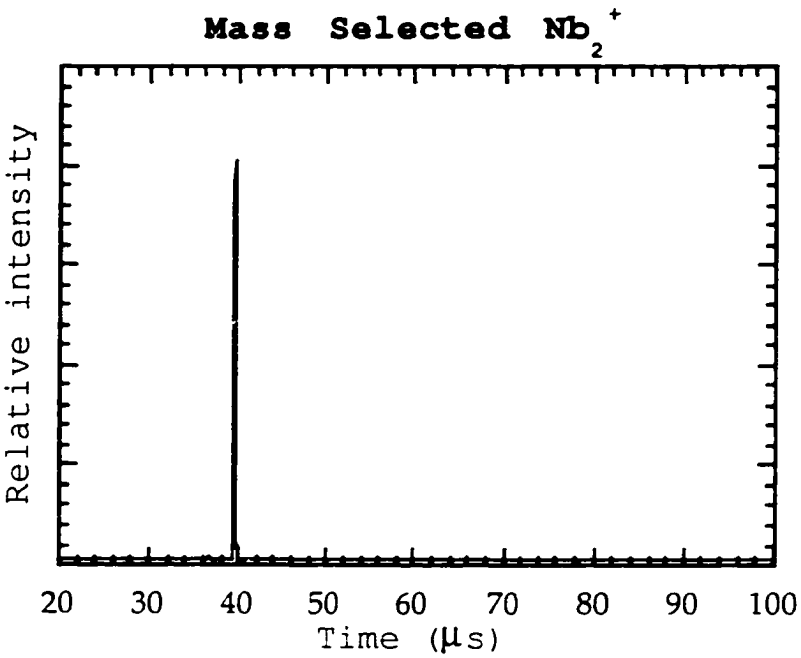

Figure 3.14B Mass spectrum of mass selected Nb_2^+ when the mass gate is on.

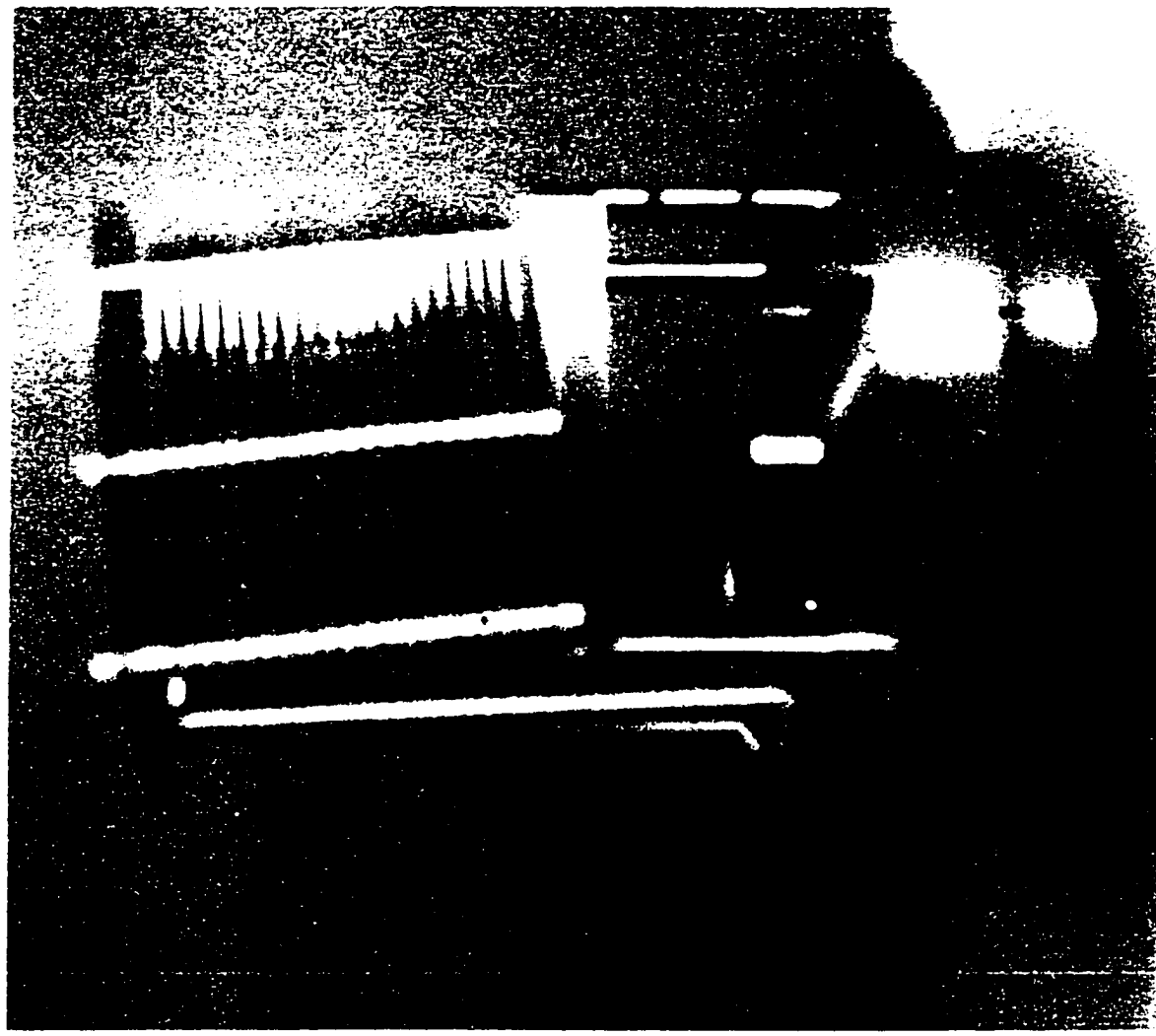

Figure 3.15

Photo of the reflectron TOF assembly mounted on the 12" flange. Clearly visible in the photo, are the plates with grids.

electric field within the reflectron. It was inclined at an angle of 6°, and situated just after the mass gate (see Figs. 3.1 and 3.2). Figure 3.15 is a photograph of the reflectron mounted on a 12" flange. The reflectron was housed in a large 'T-shaped' chamber (12" diam.). A large chamber was required so that the ion beam, when reflected by the reflectron's 'ion mirror', curved around and was focused on the detector located at the lower front of the chamber. The entrance to the reflectron was held at the beam potential of 3 kV and the rear was biased so that ions of interest were reflected at 50% - 90% of the total depth.

The reflectron was an ion reflector based on the system pioneered by Mamyrin et al.[21] It compensated for the energy spread present in the ion packet which was due to the distribution of initial ion positions along the length of the extraction cylinder. Ion packets of the same mass were spatially and temporally compressed at the WMcL linear TOF focus, however once past the focus they were decompressed because of their original spread in energy. The reflectron resolved problems due to the energy spread in the ions. High energy ions of the same mass penetrated deeper through the reflecting fields than low energy ions of 'the same' mass. Ions that penetrated deeper, spent more time in the reflectron and so allowed low energy ions to catch up at a focal plane in the field free region as they exited the reflectron. Narrower mass peaks well spaced in time (better resolution) was the result. Ions of different masses entering

the reflectron coincidentally focus in a manner such that the heavier ions penetrated deeper into the reflectron and thus arrived at the focus where the detector is located, after the lighter ions had arrived. In this manner when ions were photofragmented the daughter fragments could be resolved from the parent ions even though they would have had the same energy, when they entered the reflectron.

The equations used to calculate the time spent in the reflectron (t_{ref}) were developed as follows: The axes (x, y) were set up with origin at the entrance point of the reflectron. The positive x-axis was parallel to the incoming beam, and positive y-axis was defined so that the z-axis was perpendicular to the paper (a right hand coordinate system) with ions moving from left to right, (Fig. 3.16).

$$F_x = \frac{mdv_x}{dt} = -eE_x = -eE\cos(\phi) \qquad 3.9a$$

$$F_y = \frac{mdv_y}{dt} = -eE_y = -eE\sin(\phi) \qquad 3.9b$$

where the subscripts x and y refer to the x and y components, and F, v, m and e are force, velocity, mass of the parent ion and charge of the ion respectively, E is the electric field strength and ϕ is the tilt angle of the reflectron (ions are deflected by 2ϕ).

$$v_x(t) = \frac{-eE\cos(\phi)t}{m} + v_x(0) \qquad 3.10a$$

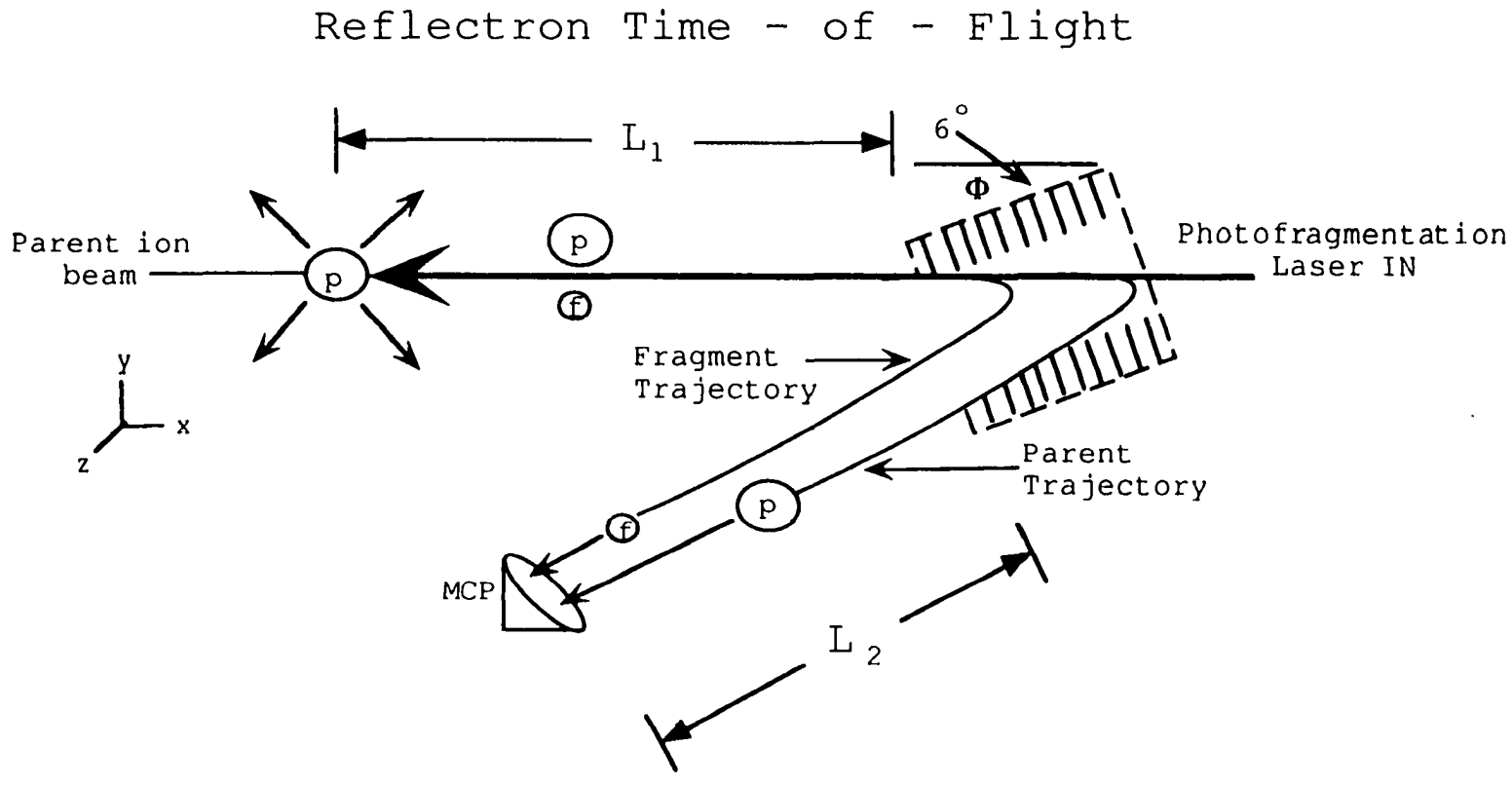

Figure 3.16 Schematic of reflectron TOF showing an ion (p) breaking up to produce a fragment ion (f). The trajectories of both ions are shown entering and exiting the reflectron. Also shown are the free flight regions L_1 and L_2 and the coordinate axes.

$$v_y(t) = \frac{-eE\sin(\phi)t}{m} + v_y(0) \qquad 3.10b$$

$v_x(0) = \sqrt{\frac{2U}{m}}$ and $v_y(0) = 0$ where U is the ion kinetic energy

The energy of the ions are the same before entering and after exiting reflectron.

$$\frac{2U}{m} = \left(v_x(t)\right)^2 + \left(v_y(t)\right)^2 = \left[\frac{-eE\cos(\phi)t}{m} + \sqrt{\frac{2U}{m}}\right]^2 + \left[\frac{-eE\sin(\phi)t}{m}\right]^2 \qquad 3.11$$

solving for t by squaring, canceling and using $\sin^2\phi + \cos^2\phi = 1$ gives

$$t = \frac{2m\cos(\phi)}{(eE)\sqrt{\frac{m}{2U}}} \qquad 3.12$$

The factor of 2 comes about because the ions make two passes through the reflectron (going in and coming out).

$$t_{ref} = \frac{2D}{V_{ref}}\cos(\phi)m^*\left(\frac{2U}{m}\right)^{\frac{1}{2}} \qquad 3.13$$

where t_{ref}, m^* can be either the mass of the parent or daughter ion (when calculating parent arrival or daughter

arrival respectively), D is the depth of the reflectron and V_{ref} is the reflectron voltage.

The time spent in the field free region t_L is given as follows:

$$t_L = L\cos(\phi)\left(\frac{m}{2U}\right)^{\frac{1}{2}} \qquad 3.14$$

where $L = L_1 + L_2$ (L_1 is the length of the region from WMcL focus to the beginning of the reflectron and L_2 the length of the region from the beginning of the reflectron to the detector). Time spent in both the field free region and the reflectron, t_{total} is given by:

$$t_{total} = L\cos(\phi)\left(\frac{m}{2U}\right)^{\frac{1}{2}} + \frac{2D}{V_{ref}}\cos(\phi)m^*\left(\frac{2U}{m}\right)^{\frac{1}{2}} \qquad 3.15$$

Arrival times of ions through the reflectron and total flight times (from pulser through reflectron and to the detector) were also calculated using a spreadsheet calculation.

III.4.3 FRAGMENTATION LASER

The fragmentation laser was a Spectra Physics YAG pumped PDL-3 Dye laser system. There were two configurations for cluster fragmentation, (1) coaxial fragmentation, (collinear and counter propagating to the ion beam) and (2) trans-axial,

(perpendicular to the ion beam). In the perpendicular configuration, the laser entered through a side port and intersects the clusters as they emerged from the mass gate. This configuration involved a measure of difficulty especially in the space/time overlap between the cluster beam and the pulsed laser. The following advantages of this arrangement are as follows: (1) absence of a noisy background due to photo-ions from the laser hitting the mesh or other metal hardware, (2) no significant laser reflections off the metal walls within the chamber would reach the detector, (3) it was easier to monitor the laser power by measuring it as it exited the chamber after interaction with the cluster ions. The axial configuration was chosen because it was simpler to do and gave an earlier success. The laser entered the chamber through the rear of the reflectron TOF, and was positioned to interact with the clusters at the linear TOF focus (mass gate). This point was ideal for fragmenting the clusters because the ion packets had been spatially and temporally compressed to their smallest dimensions thereby providing the best overlap between the laser and cluster beam. Co-axial fragmentation however had some significant drawbacks, which were: (1) By going through the reflectron, the laser encountered some of the wire meshes which provided field uniformity, laser/mesh interactions gave rise to ejected photo-ions which reach the microchannel plate detector and created a noisy signal at times, (2) The laser could hit everything coming down the flight tube, including

larger ions, before they arrived at the mass gate. Laser beam/ion beam overlap alignment presented problems which were aggravated by the non-uniform laser beam power density profile and variations in laser pointing when dyes were changed. One also assumed that the cluster density was uniform across the collimated beam however this was not necessarily so, therefore on-axis alignment could still result in detected ions not being exposed to the laser pulse and thereby creates a nondepletable background. The laser was slightly diverged to produce a quasi uniform beam. Power measurements were made by passing the laser through a glass slide set at a 45° angle and measuring the power of the 90° reflected light with a very sensitive power meter. The glass slide was calibrated at different powers and and wavelengths to correlate the laser's reflected and transmitted powers. Laser fluence was determined by assuming that the pulse energy was uniformly distributed over a circle of radius 0.5 cm, to give an area of 0.785 cm^2.

III.4.4 ION DETECTION

Mass spectra were obtained by adjusting the extraction voltages and associated delays, together with the ion optics until the spatial focus of the mass spec. was at the ion detector. At first we used a large Faraday plate with the output to an oscilloscope to obtain crude mass spectra, however we finally opted for two dual microchannel plate

detectors (Galileo MCP-18B), a 40 mm & a 25 mm diameter, supplied by R M Jordan & Co. Each detector was coupled to a 50 Ω anode assembly. One MCP can be situated at the end of the flight tube in the absence of the reflectron the other which was enclosed in conical structure, was positioned at the lower front of the reflectron chamber directly in the path of ions exiting the reflectron (see Fig. 3.2). Microchannel plate detectors are costly, fragile and tend to degrade with use, however they were ideally suited for handling fast ion pulses and provided high gain with a sub-nanosecond rise time. The signal from the MCP was acquired using a LeCroy 9450A digital oscilloscope to display a fresh cluster mass spectrum at the 4 Hz repetition rate of the experiment.

III.5 CONCLUSION

The laser vaporization coupled dual TOF mass spec. cluster apparatus was assembled over the period of afew years. It operation was a bit complicated at first but with time and practice ptotocols were set up for standard operating procedures. The instrument was able to produce clusters from all the metals which were tested. The mass spectra were very accurate as will be explained in the next chapter.

Chapter III References

1) Y. Liu, Q. L. Zhang, F. K. Tittel, R. F. Curl and R. E. Smalley, J. Chem. Phys., **85**, 7434 (1986).

2) D. E. Powers, S. G. Hansen, M. E. Geusic, D. L. Michalopoulos and R. E. Smalley, J. Chem. Phys., **78**, 2286 (1983).

3) P. J. Brucat, L. S. Zheng, C. L. Pettiette, S. Yang and R. E. Smalley, J. Chem. Phys., **84**, 3078 (1986).

4) D. E. Powers, S. G. Hansen, M. E. Geusic, A. C. Puiu, J. B. Hopkins, T. G. Dietz, M. A. Duncan, P. R. R. Langridge-Smith and R. E. Smalley, J. Chem. Phys., **86**, 2556 (1982).

5) Shigeo Maruyama, Lila R. Anderson and Richard E. Smalley, Rev. Sci. Instrum., **61**, 3686 (1990).

6) Paolo Milani and Walt A. deHeer, Rev. Sci. Instrum., **61**, 1835 (1990).

7) Pritha Gangopadhyay and James M. Lisy Rev. Sci. Instrum., **62**, 502 (1991).

8) Winston A. Saunders, Department of Physics, Swiss Federal Institute of Technology - Lausanne, Switzerland.

9) P. K. Carroll and E.T. Kennedy, Contemp. Phys., **22**, 61, (1981).

10) Paul C. Engelking, Chem. Rev., **91**, 399 (1991).

11) Otto F. Hagena, Rev. Sci. Instrum., **63**, 2374 (1992).

12) G.I. Dimov Pribory I Tekhnika Eksperimenta, Nuclear Physics Institute, Academy of Sciences of the USSR, No. 5, pp. 168- 171, (1968).

13) John M. Hayes, Chem. Rev., **87**, 745 (1987).

14) J. M. Pendlebury and K. F. Smith, Contemp. Phys., **28**, 3, (1987).

15) W. C. Wiley and I. H. McLaren, Rev. Sci. Inst., **26**, 1150, (1955).

16) J. A. Syage and J. Steadman, Rev. Sci. Instrum., **61**, 1204 (1990).

17) a) Hellmut Haberland, Hans Kornmeier, Christoph Ludewigt, Andreas Risch and Martin Schmidt, Rev. Sci. Instrum., **62**, 2368 (1991).

b) Hellmut Haberland, Hans Kornmeier, Christoph Ludewigt, Andreas Risch and Martin Schmidt, Rev. Sci. Instrum., **62**, 2621 (1991)

18) D. S. Cornett, M. Peschke, K. LaiHing, P. Y. Cheng, K. F. Willey and M. A. Duncan, Rev. Sci. Instrum., **63**, 2177 (1992).

19) R. T. Laaksonen, D. A. Goetsch, D. W. Owens, D. M. Poirier, F. Stepniak and J. H. Weaver, Rev. Sci. Instrum., **65**, 2267 (1994).

20) W. Begemann, S. Dreihöfer, G. Ganteför, H. R. Siekmann, K. H. Meiwes-Broer and H. O. Lutz, Springer Ser. Mater. Sci., 230 (1988).

21) B. A. Mamyrin, V. I. Karataev, D. V. Shmikk and V. A. Zagulin, Sov. Phys.-JETP.,**37**, 45 (1973).

22 SIMION PC Version 4.0, courtesy D. A. Dahl, Idaho Natl. Lab. Idaho Falls, ID 83415, USA.

CHAPTER IV

INSTRUMENT CONTROL AND DATA ACQUISITION

IV.1 INTRODUCTION

Combined software and hardware control enabled the instrument to function and thus acquire and store data effectively. Figure 4.1 gives an outline of the experiment. The operator was required to set the parameters that determined cluster distribution and intensity, while the computer coordinated the functions of the different components which made up the laser vaporization dual TOF mass spec. Inherent delays between the various devices required microsecond adjustments to synchronize the individual event each controlled. The entire experiment was a combination of several synchronized events. Timing parameters were set by the operator and controlled by the computer. The pulsed supersonic valve initiated the cycle with a burst of helium, followed by the vaporization laser which fired at the peak of the helium pulse. This burst of laser power effectively vaporized material from the rotating metal target disk. Smalley[1-5] et al. have determined that the vaporization laser should be fired at the peak of the helium pulse when it's density over the target is at the highest so that the vaporized metal can be effectively blanketed and thermalized. The potential switch which was maintained at a negative

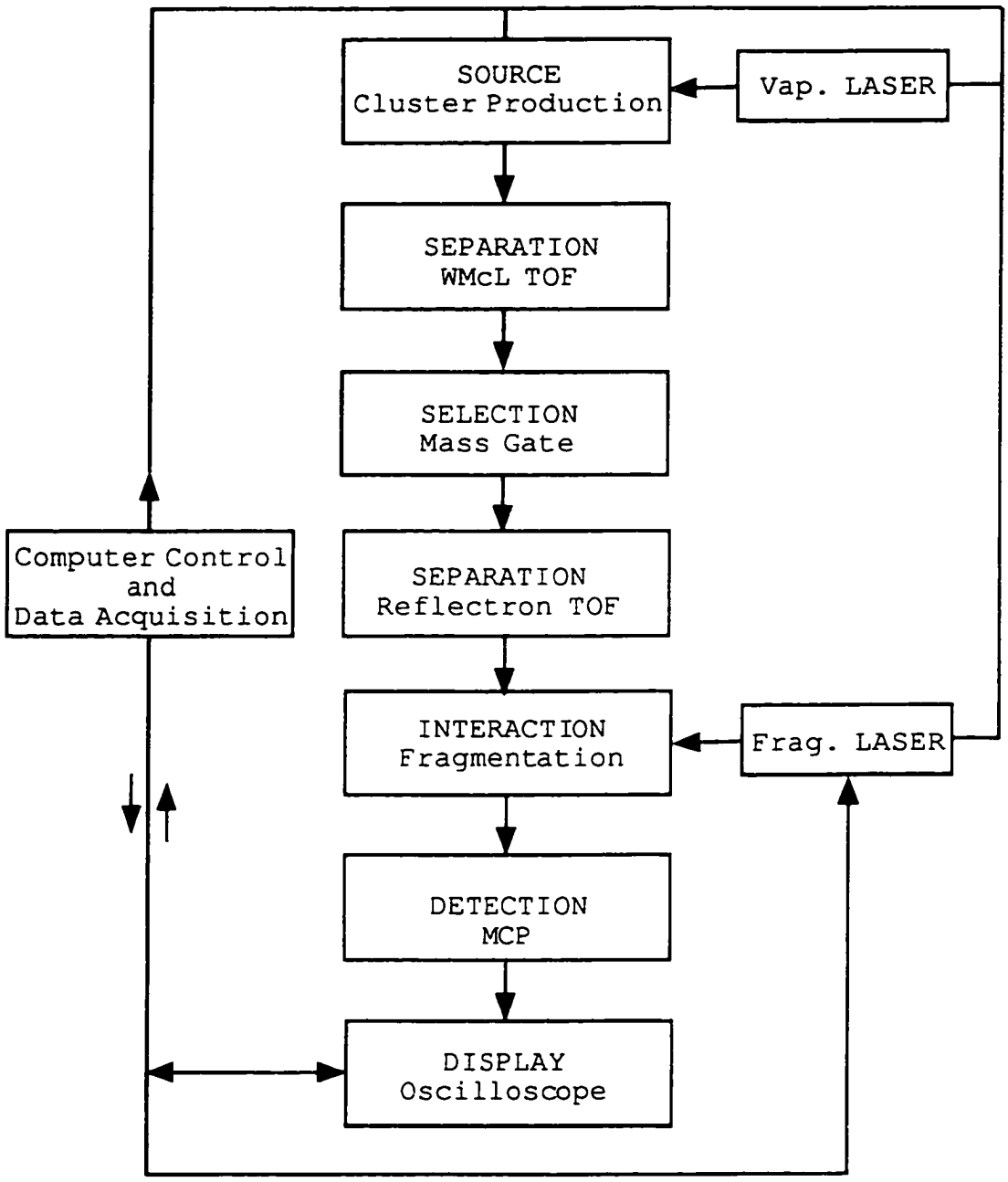

Figure 4.1 Block diagram illustrating the data acquisition and control outline.

potential of -2 kV (it was necessary to supply it with -2.4 kV to obtain an effective output voltage of -2 kV) for the purpose of studying positively charged cluster ions was pulsed to ground potential next. A negatively charged field induced by the potential switch provides an attraction to the positively charged clusters increasing their velocity in the forward direction.[6] Within a few microseconds of the pulsing of the potential switch, the first WMcL lens (pulser), is switched from ground potential to a positive potential of +850 V. This field provides a forward 'kick' to the positive ions. During the 'tuning' of the source the mass gate was kept at ground potential to allow the passage of all ions to the detector. *Tuning* refers to the act of adjusting the control parameters e.g. voltages, timing delays, laser power and helium backing pressure. An optimized cluster ion distribution exhibited peak repetitiveness, maximized stable intensities and smooth peaks with narrow widths.

Mass selection occurred by the turning on/off of an electrical field which deflected ions off the flight tube axis effectively blocking their passage. This electrical field which is kept at +300 V was pulsed off (to ground potential) to coincide with the arrival of a chosen cluster mass. By pulsing the field off for extremely short time periods (200 ns) it is possible to isolate clusters of a particular size and thereby enable the study of individual cluster species.

Following cluster mass selection, the isolated cluster species were observed closely on the oscilloscope using an expanded timescale to determine whether metastable fragmentation was occuring. Metastable fragmentation of vibrationally hot clusters is a normal occurrence in molecular beams whereby a small proportion of ions break apart enroute to the detector, producing daughter ion fragments.[4] It cannot be totally eliminated, however it could be minimized by adjusting the source conditions to prevent over heating of the cluster ions produced. Minimization of metastables was a necessary step because to observe effective frgmentation, there must be a maximum cluster intensity with a minimum metastable ion production. It would be difficult to distinguish between daughter ions from laser induced fragmentation and daughter ions from metastable decomposition if the production of metastable ions was left unchecked. Figure 4.2A shows the Nb_4^+ cation together with Nb_3^+, Nb_2^+ and Nb^+ ion produced from metastable Nb_4^+ ions in the absence of the fragmentation laser, while Fig. 4.2B show the daughter ions produced by laser induced fragmentation. Following the elimination or minimization of metastable decomposition, proper overlap between the fragmentation dye laser and the cluster beam was necessary to achieve maximum cluster fragmentation.

The cycle of events, began with the pulsing of the supersonic valve and ended with the measurement of the dye laser power. Although it could be performed at a rate of 10

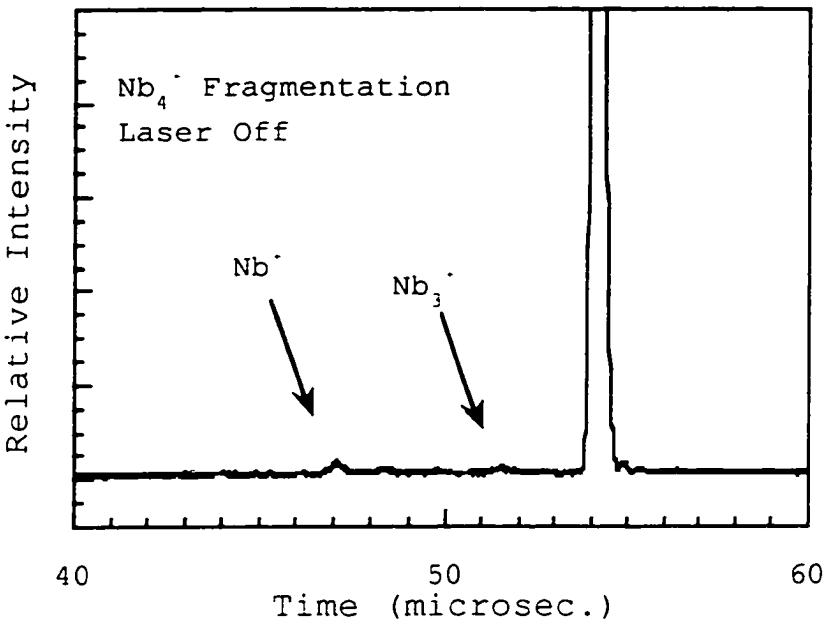

Figure 4.2A Mass spectrum of Nb_4^+ showing some metastable daughter ions (Nb^+ and Nb_3^+). The Nb_4^+ peak is off scale because this plot has been expanded to show the metastable fragment ions.

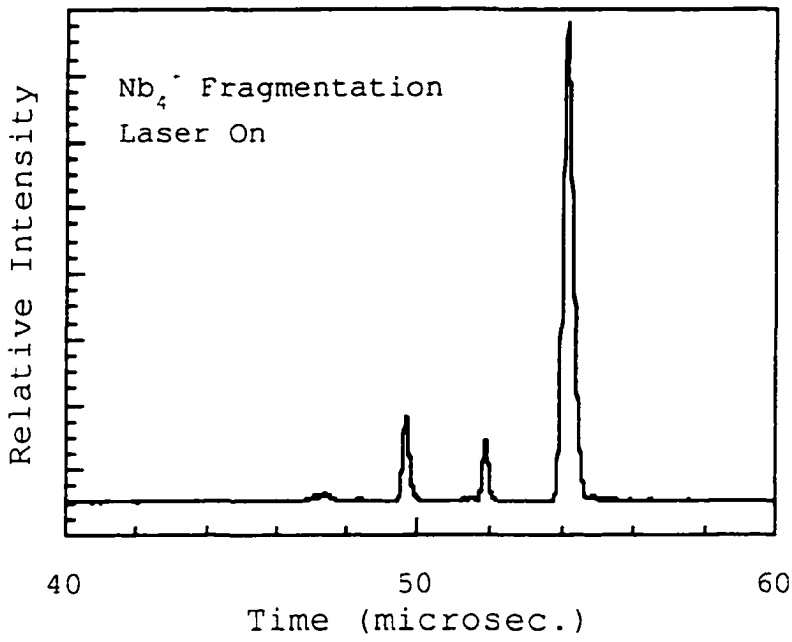

Figure 4.2B Mass spectrum of Nb4+ after fragmentation to produce daughter ions (Nb^+, Nb_2^+, Nb_3^+)

Hz, the existing conditions favored operating at 4 Hz. The signal acquired by the oscilloscope was averaged for 400 shots of the laser or approximately 100 seconds, after which the intensities of the parent and daughter peaks and the average background intensity were extracted and stored by the computer. The dye laser wavelength was incrementally scanned while a waveform plot of cluster intensity versus wavelength was updated on the computer monitor.

IV.2 CONTROL & DATA ACQUISITION HARDWARE

A Dell Dimension XPS 60 personal computer with an Intel pentium microprocessor, two serial ports (RS 232), a 540 megabytes hard drive and 24 megabytes of random access memory, running Microsoft Windows 3.2 operating system coordinated the operation of the various devices. The data acquisition and control system included three National Instruments interface boards (PC TIO-10 Data Acquisition board, Lab PC+ Data Acquisition board, and a IEEE 488.2 AT-GPIB). The PCTIO-10 and the LabPC+ Data Acquisition boards were connected via individual 50 pin ribbon cable to two 50 pin I/O connector blocks installed in a rack mounted panel. Each instrument was attached to the panel via BNC cabling. The GPIB board was connected directly to the LeCroy 9450A oscilloscope and the dye laser PDL-3 scanning motor/indexer was connected via a 3-pin cable (transmit, receive and ground) to the serial port of the Dell XPS-60.

The PCTIO-10 is a timing and digital I/O board which had ten channels of 16 bit counter/timers with defined, adjustable pulse widths and delays. The counter/timer channels were generally used for event counting, pulse generation, square wave generation and frequency measurement. These could be controlled by using several gating methods, software, level and edge gating. Counter/timers were used primarily for pulse generation to control the various devices. Two of the counter/timers output pulses with programmable delays and pulse widths at a resolution of 200 ns while the other eight counter/timers output pulses at a resolution of up to 1 μs.

Counter/timer TTL output pulses were used to control both lasers, the PSV, potential switch, pulser and mass gate. One of the high resolution (200 ns) counter/timer output was used by the fragmentation laser, while the other was used to control the mass gate. The mass gate 'open' time window needed to be as narrow as possible to allow the passage of only one cluster specie and the exclusion of other cluster species. A small time window also ensured that the timing of fragmentation laser could be adjusted to fire at the precise moment. Both lasers were flash lamp triggered rather than 'Q-switch' triggered because of the presence of a significant delay between the Q-switch firing and the flash lamp energy output which varied from laser shot to laser shot. Laser power was manually controlled while the PSV was both TTL triggered and manually adjusted to fine tune the firing delay

and vary the current which determined the extent to which the valve nozzle opened.

The LabPC+ DAQ board was a multifunction analog, digital and timing I/O board with eight analog inputs, two 12-bit DACs, twenty-four lines of TTL-compatible digital input and output and three 16-bit counter/timers. Analog input/output functions of this board were utilized to acquire readings from both the power meter (Scientech AC2301 /2216) and the Spex monochromator which was used for wavelength calibration. The analog output of the power meter facilitated the conversion and recording of the voltages produced during the measurement of laser power. Power measurement from 0.1 mW to 30 W were possible.

The AT-GPIB was a standard IEEE talker, listener and controller used for communicating with the oscilloscope. It read the number of averages the oscilloscope acquired, polled it to determine when acquisition had ended and relayed the information back to the computer. The computer next communicated with the dye laser via the serial port to indicate a wavelength increment. It then returned to the oscilloscope, retrieved the peak intensities and cleared the oscilloscope for the next series of averages.

Two oscilloscopes were used in the operation of the instrument. A Hameg 20 MHz dual channel digital oscilloscope (HM 205-3), was used to determine the time adjustments between the PSV, vaporization laser and the pulser. The LeCroy 9450A digital oscilloscope (dual channel with a

bandwidth of 300 MHz, programmable via RS-232-C or GPIB and with its own LabView software drivers) was used to acquire and store the signal from the microchannel plate detector, measure delays and the timing and adjusting of the fragmentation laser.. It featured 8 bit ADCs, 50 kilobytes of non-volatile acquisition memory per channel, 200 kilobytes of waveform storage memory and a very sophisticated triggering system. Additional features included the capacity to perform mathematical analysis on two separate waveforms while they were being acquired and the ability to have four waveform simultaneously displayed on screen.

The operation of the Wiley McLaren TOF mass spectrometer and mass gate relied heavily on the fast switching of high voltages (+300 V, +850 V, -2.4 kV) of different polarities. High voltage switches were triggered to power the potential switch, pulser and mass gate. These switches had very fast rise times, on the order of 10 ns. The identical switches were wired using different circuit configurations based on the characteristics of the required output pulse, (Fig 4.3A, B and C):

- switch circuit 1 (pulser) was wired such that it switched from 0 V to +850 V
- switch circuit 2 (potential switch) was wired so that it switched from -2.4 kV to 0 V
- switch circuit 3 (mass gate) was wired so that it switched from +300 V to 0 V

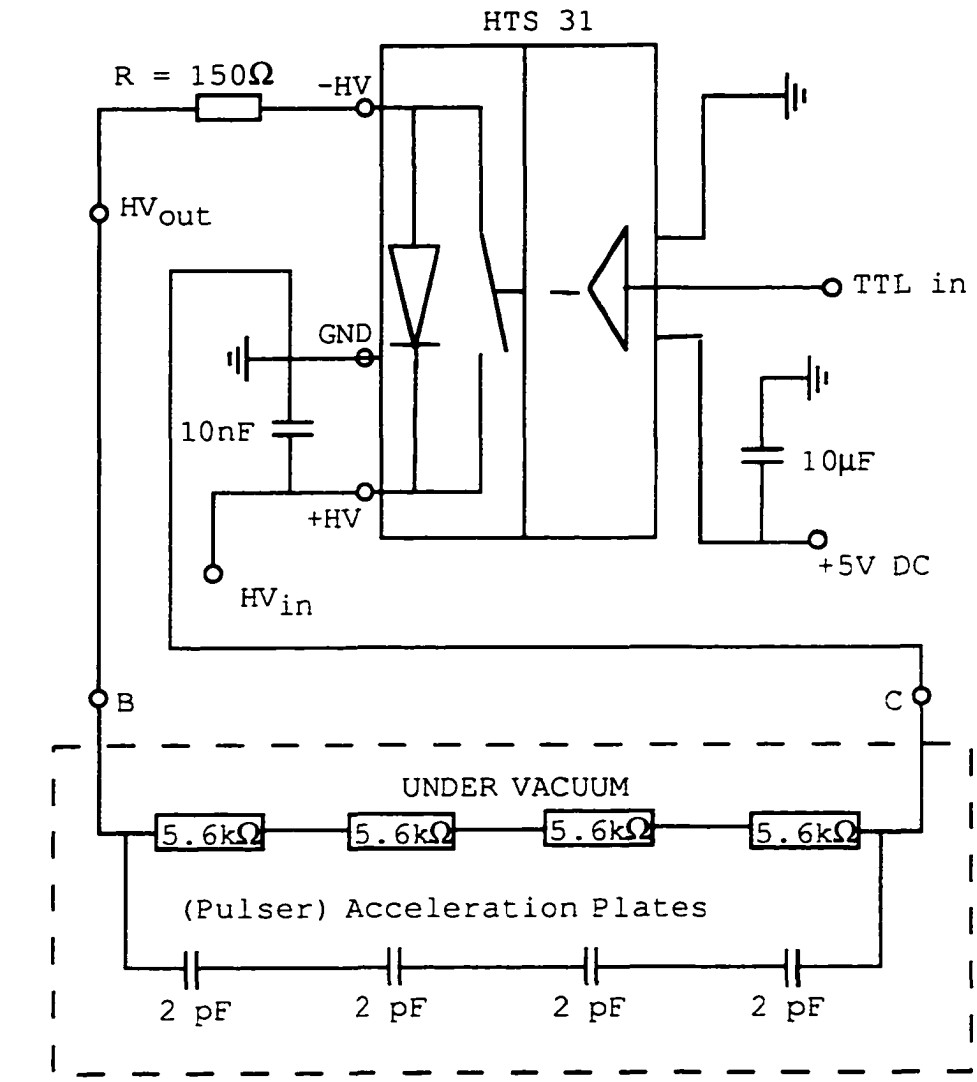

R_{BC} = 27.98 kΩ (in vacuum)
HV_{in} = 850V DC
voltage magnitude HV_{in} = HV_{out}

Characteristics of output pulse are shown at right

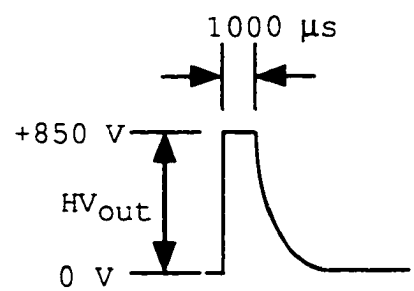

Figure 4.3A Pulser circuit diagram

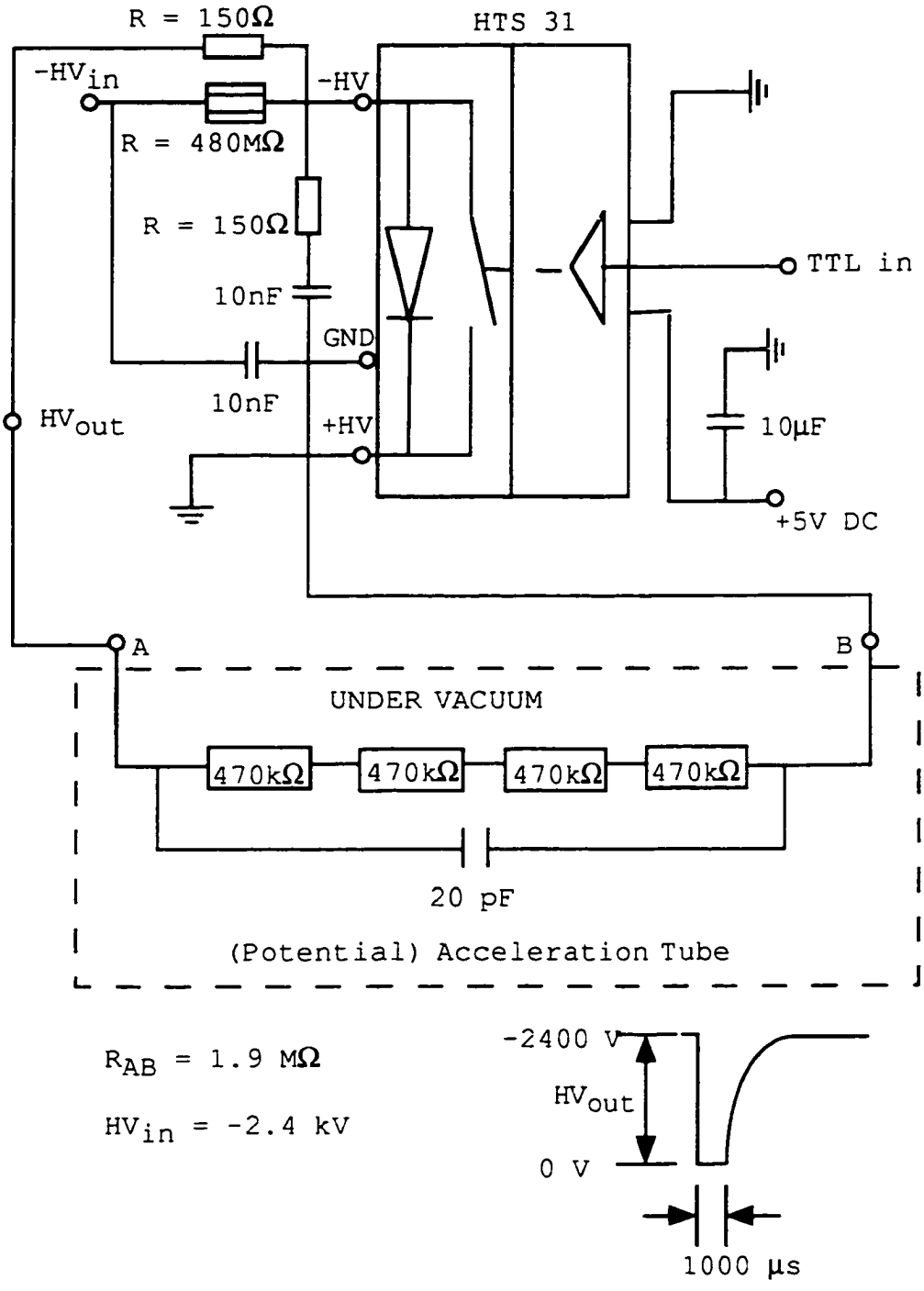

Figure 4.3B Potential switch circuit diagram

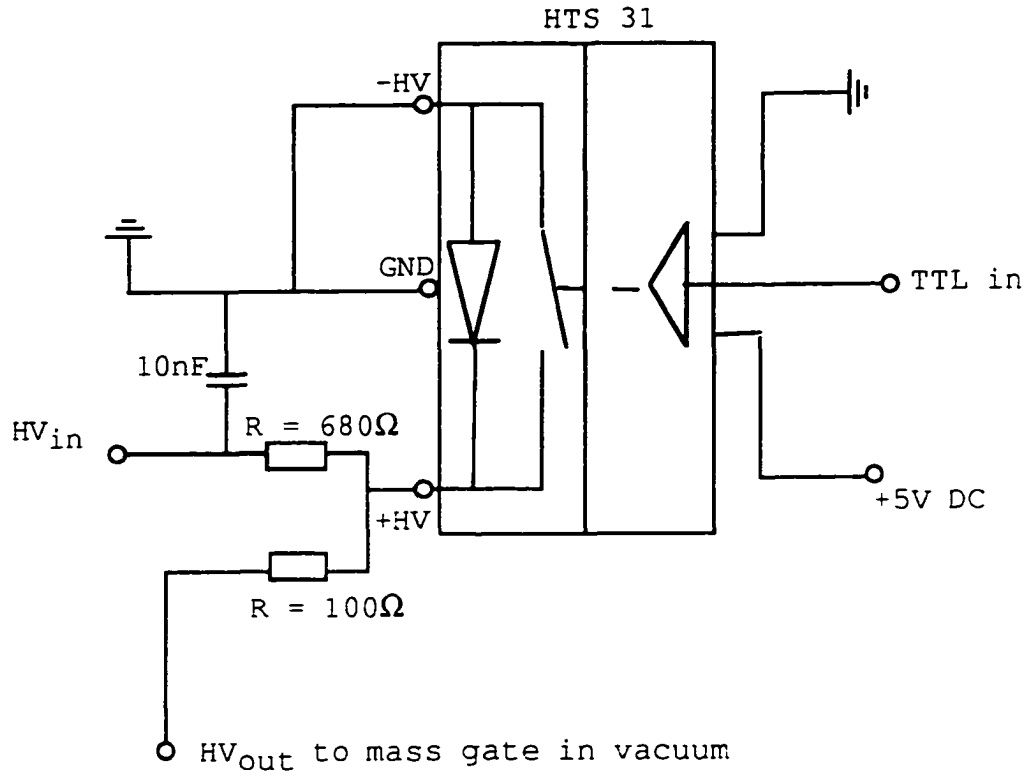

HV$_{in}$ = +300 V

HV$_{in}$ = HV$_{out}$

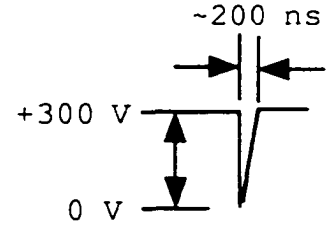

Figure 4.3C Mass Gate circuit diagram

These circuits helped to prevent short circuit, reduced ringing, and were instrumental in rise time adjustment and capacitative power dissipation.

IV.3 DATA ACQUISITION SOFTWARE

The control and acquisition software was written using software developed by National Instruments, LabVIEW 3.1.1 for Windows. LabVIEW was first introduced in 1986 and has been at the forefront of a new instrumentation approach called virtual instrumentation. LabVIEW, an acronym for Laboratory Virtual Instrument Engineering Workbench is a graphical programming system for data acquisition and control with an innovative programming method, whereby you graphically assemble software objects called virtual instruments to create a program.[7,8] This programming system gave the flexibility of a powerful programming language without the accompanying difficulty and complexity associated with other programming languages. In the early development of the instrument we used Microsoft QuickBasic 4.5 (DOS 6 ver.) to control the data acquisition. This worked quite well for each of the instruments separately; however when trying to integrate the separate components into a single entity with a user friendly interface and graphics, the programming tasks assumed huge proportions and difficulties.

National Instruments has also developed control and acquisition software for each of it's computer plug in board. This software simplified the task of data acquisition and

instrument control and enabled the integration of different computer plug-in boards. The software developers anticipated most of the tasks that these boards were required to perform, and have written general software codes which could be adjusted, rewritten and integrated for the performance of these tasks. The general functions were collected in various function libraries, graphical user interface (gui) libraries, analysis libraries, input/output libraries for GPIB, data acquisition (DAQ) and serial interfaces. The DAQ VI library contained functions to acquire and output data with all National Instrument plug-in boards. Lab VIEW programming has the following advantages:

- The creation of a front panel which was the interface for the instrument operator. This interface consisted of control objects, numerical inputs and displays, Boolean switches and graphs through which the operator can effect commands and recieve feedback.
- Construction of a graphical block diagram by selecting icons which represented various functions from the function menu. These icons were connected to each other with on screen 'wires'to enable the passage of data from one function block to another. Function blocks ranged from simple arithmetic functions, to acquisition and analysis routines and advanced file input/output operations.
- LabVIEW for windows has a data flow language architecture which distinguishes it from the control flow architecture of languages like FORTRAN AND PASCAL. Dataflow programming

makes it possible to specify a desired order of execution because the execution order is determined by the flow of data between function blocks, and not by sequential lines of text. This is the single most important feature of LabVIEW, since it enables the performance of different tasks simultaneously.

- LabView contained virtual instrument modules. Computer programs in LabVIEW were constructed in what can be regarded as Virtual Electronic Instruments (VI). These virtual instrument programs could be operated as 'stand alones' enabling the performance of several tasks simultaneously or may be combined into integrated units for synchronized operation.
- The speed of LabView programs was comparable to that of compiled C programs, which enabled productive graphical programming without sacrificing program execution speed.

The LabVIEW instrument control program was a combination of two programs. One of the program was a 'stand alone' which controlled the function of the PC TIO-10, which output TTL pulses to facilitate the operation of each device. This program configured and gated the counter/timers for pulse output. The other program was dependent on the first and was concerned mainly with acquiring the data generated. The second program performed the following: (1) configured the analog input of the LAB PC+ to be gated by the PCTIO-10 for acquisition of the power measurements from the analog output

of the power meter, (2) controlled the scanning of the dye laser via the serial port, (3) communicated comands to send and retrieve data from the oscilloscope via the GPIB and (4) converted the acquired data to a plot of relative intensity versus wavelength which was then saved. Appendix B1 contains a sample of the control software written in LabVIEW.

IV.4 INSTRUMENT OPERATION & CONTROL

Successful operation of the instrument depended on the careful synchronization between the various devices. Design of the operating procedure proceeded with the PC TIO-10 as the first level controller since it was responsible for controlling six different devices. The PC TIO-10 was programmed to produce a frequency adjustable square wave on counter/timer #1. This square wave, adjustable from 1 to 10 Hz, was hard wired to the gate of every counter on the PCTIO-10 board. All the other counters were configured to be gated on the rising edge of the square wave, which enabled them to begin counting simultaneously. Once triggered the counter waited for a user specified delay then output TTL pulses for a duration specified by the user input pulsewidth. The square wave determined the repetition rate of the experiment by triggering all the devices once, during the rising edge cycle of this square wave. A graphical user interface (GUI), was set up so that the counters which output the TTL pulses could have their pulse widths and delays varied by the operator inputting new values of these parameters onscreen. This

adjustment of pulse widths and delays was responsible for synchronizing the operation of the different devices.

There is usually a time delay between the arrival of TTL (trigger) pulses at a device, and the actual performance of the required response, dependent on the mechanical action required to enable the response. Measurement of these time (physical response) delays were critical to synchronizing the operation of the instrument as a single entity. The PSV had two adjustable delays, (a coarse delay of 300 μs - 4.5 ms and fine tuning delay of ± 100 μs), between the arrival of the TTL pulses at the pulsed supersonic valve and the actual opening of the valve to deliver a pulse of gas. The Spectra Physics GCR-11 Laser was designed such that it could be fired by triggering either the Q-switch or the flash lamp. It was found that a more reproducible delay of ~ 120 μs was obtained by triggering the flash lamp instead of the Q-switch.

Pulse sequence is outlined in Figs. 4.4A and 4.4B the rising edge of the square wave marks time 'zero'. At time 'zero' a TTL pulse of delay 120 μs and pulsewidth 10 μs was sent to the PSV. A combination of the backing pressure behind the valve and the valve current determined the length of time the valve remained open, therefore the width of the gas pulse could be varied between 60 μs and 150 μs. The leading edge of this pulse took less than 20 μs to travel the (2 cm) distance to arrive over the target. The opening of the valve could be observed by monitoring the valve sync. output on the oscilloscope. Laser radiation was timed to arrive at the

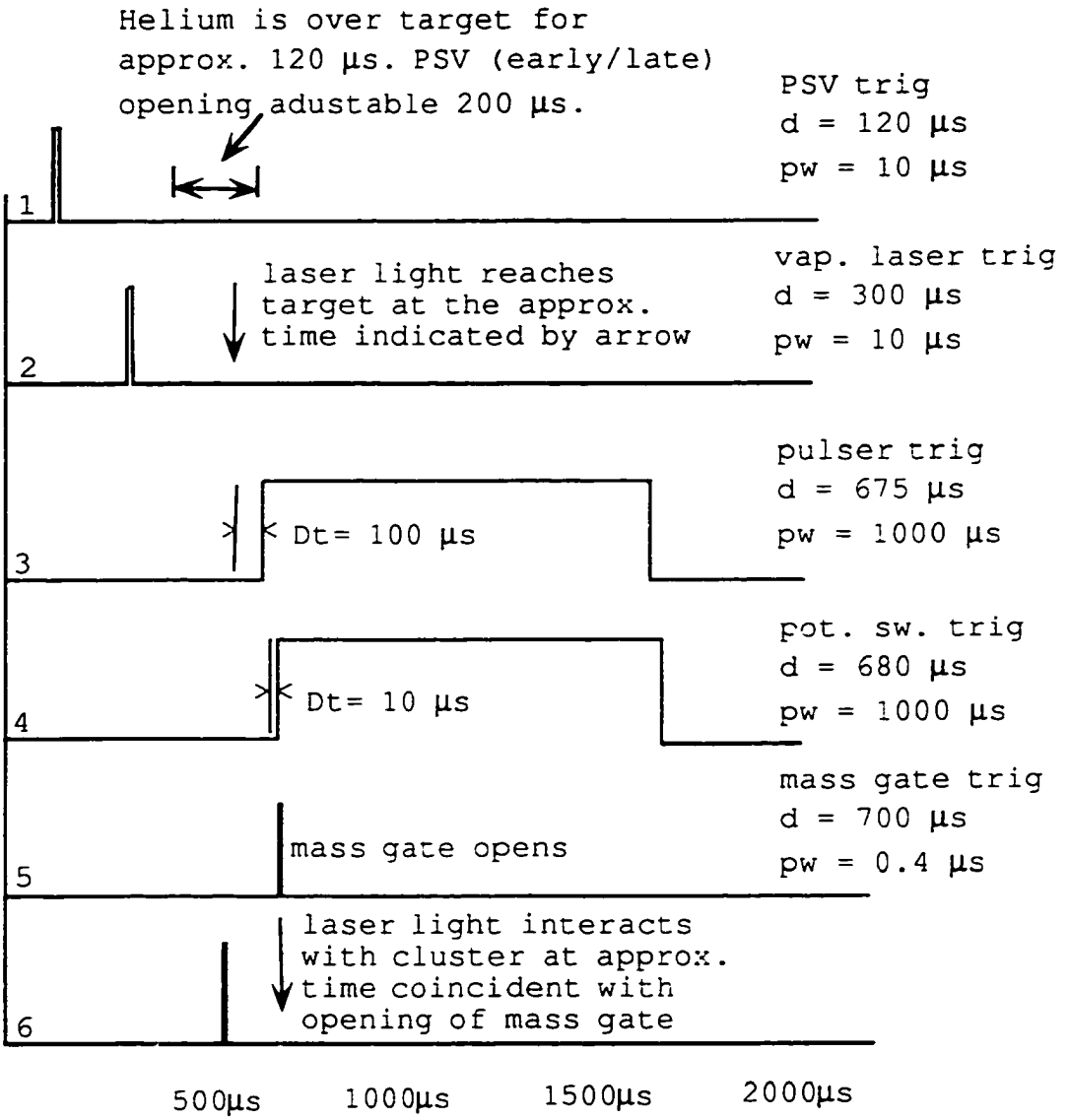

FIG. 4.4A. Diagram outlining the timing sequence of the TTL pulses propagated by the computer plug-in board PC-TIO-10.The times shown are for the Nb_2^+ ion. Letters "d" and "pw"refers to delay and pulsewidth respectively.

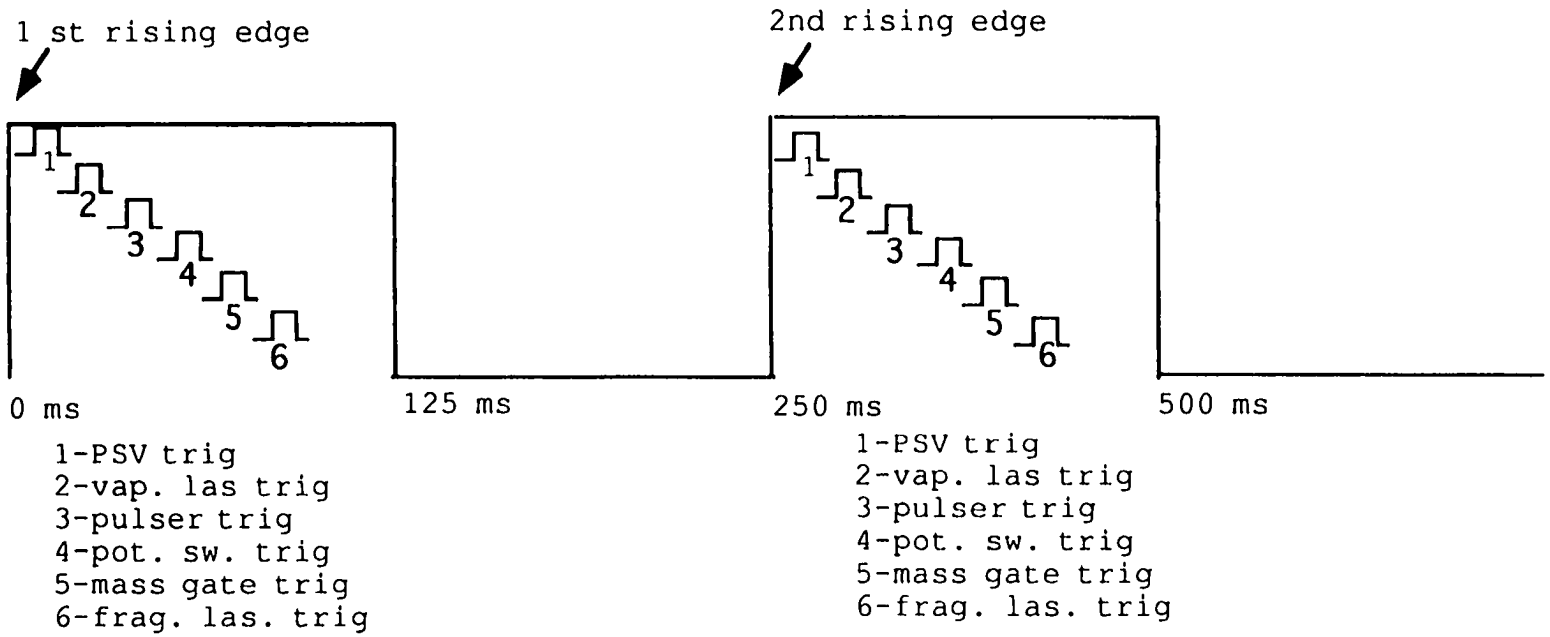

Figure 4.4B Diagram showing two cycles of the 4 Hz square wave. After the first rising edge at 0 ms the 6 devices are triggered and again at the second rising edge at 250 ms and so on at each rising edge of the square wave, four times per second.

target between 340 μs and 440 μs after the initial TTL pulsing of the valve. Since the laser had a 120 μs delay between TTL arrival and light generation, it required TTL pulses between 220 μs to 320 μs after the initial TTL pulse to the supersonic valve. Instead of varying the laser delay, it was easier to set the laser to be triggered 300 μs after the triggering of the PSV. In this way the PSV could then be manually adjusted (fine delay ± 100 μs) so that the arrival of the peak of the helium pulse would coincide with the arrival of the laser at the target.

Arrival of the cluster packet at the first Wiley-McLaren lens occurred about 100 μs (time to travel the 20 cm distance from the nozzle exit to the first Wiley Mclaren lens) after the laser was fired. The first lens was pulsed from ground potential to +850 V when the ion packet was between the first and second lens, about 675 μs after time 'zero'. Switching of potential switch from -2 kV to ground potential occurred between 2 μs to 20 μs after the pulser, depending on which section of the cluster distribution one wished to view. The difference in time between the pulser and potential switch gave a time window over which the cluster distribution could be seen. A time window of (Pulser - Pot. Switch) $\Delta t \sim 5$ μs allowed the viewing of Nb^+, NbO^+ and helium cations, $\Delta t \sim 10$ μs (Nb_2^+ to $Nb_7^+$and $Nb_xO_y^+$), $\Delta t > 15$ μs (Nb_8^+ to Nb_{13}^+). Since it was not possible to view the entire mass distribution simultaneously because of the Pulser - Pot. Switch time window, the LeCroy 9450 made it possible to store

segments of the mass distribution and then sum all the segments of the mass dstribution to get a comprehensive mass spectrum. Typical tuning parameters for niobium cluster ions were as follows:

PSV to Laser delay ~ 120 μs

Laser to Pulser delay ~100 μs

Pulser to Potential Switch delay (dependent on cluster mass) ~ 5 - 15 μs

Helium backing pressure to the valve ~ 140 psig

PSV delay (variable)

PSV current. ~ 3.2 kA

Laser power ~ 20 mJ/pulse

Einzel lens and deflector voltages were set at the beginning of the instrument's operation, and did not require adjustment since these voltages were experimentally determined as well as simulated using SIMION[9]. The mass gate was pulsed from +300 V to ground potential when the ion packet of interest approached, this occurs circa. 700 μs after time 'zero' The gate was usually kept open for a minimum of 200 ns. Light from the fragmentation laser was timed to interact with the ion packet about 2 μs after the opening of the mass gate, therefore this was pulsed about 560 μs after time zero, to compensate for the approx. 140 ms physical delay of the fragmentation dye laser. The pulsing of the mass gate and the fragmentation laser required the high resolution 200 ns counter-timer output to allow small incremental adjustments

for tuning the cluster beam. The various pulse delays given previously were adjusted to suit the cluster beam conditions at the time of tuning.

The microchannel plate detector was biased at 2.4 kV, while the reflectron voltage was set at 3 kV. Infrequently there was need to increase the microchannel plate detector voltage to amplify signals, which were very weak. Scanning of the reflectron voltage was a technique used to determine whether a peak observed was a 'real' daughter peak or a noise transient. When the reflectron voltage is scanned to lower voltages real daughter peaks are expected to arrive at the detector with the same arrival time as the parent peak, when the voltage has been decreased proportional to the ratio of the mass of the daughter ion relative to the mass of the parent ion corresponding to a voltage given by:

$$\frac{\text{mass of daughter}}{\text{mass of parent}} \times 3000 \text{ volts} \qquad (4.1)$$

Typically Nb_4^+ has an arrival time at the detector of 55 μs when the reflectron voltage (V_{ref}) is 3000 V

Nb_4^+ arrival time 55 μs @ V_{ref} = 3000 V

Nb_3^+ arrival time 55 μs @ V_{ref} = 2250 V

Nb_2^+ arrival time 55 μs @ V_{ref} = 1500 V

Nb^+ arrival time 55 μs @ V_{ref} = 750 V

IV.5 DATA ACQUISITION

The Lab PC+ DAQ board, serial port and the GPIB DAQ board are combined to form the data acquisition system. Mass spectra corresponding to both the parent and daughter ions were acquired and averaged using the LeCroy 9450A oscilloscope. The oscilloscope that was connected to the computer via the GPIB, was polled during the waveform acquisition to determine when the entire waveform had been acquired and averaged. After acquisition the waveforn was retrieved by the computer and peak intensities, minimas and maximas were determined. The Lab PC+ DAQ board provided an analog input, which made it possible to read the voltage output of a digital power meter. The fragmentation laser lamp sync. output was used to trigger the acquisition of the analog output from the power meter (Scientech AC2301/2216). Analog output voltage readings from the power meter were acquired by the computer using LabVIEW and reconverted to power (mW). Peak intensities backgrounds and laser power were used to calculate the relative intensity of the daughter ion which was then plotted onscreen as a function of the wavelength. After waveform retrieval from the oscilloscope, the computer signals the dye laser via serial port to move to a new wavelength. The final step in the data acquisition cycle is the clearing of both the waveform buffer and the oscilloscope screen via the GPIB before starting acquisition again. The numbered frames of the data acquisition software given in the appendix shows the actual order of the preceding

events as they occur. The entire cycle of 400 waveform averages at a rep. rate of 4 Hz takes less than 2 minutes.

IV.6 CALIBRATION

The instrument was calibrated using xenon gas and then tested using several different metals and composites. The following metals and composites were tried in the source, Fe, Al, Co, Cr, Ni, Ti, V, Cu, Nb, Ta, Si, C, TiC, VC and Mo. They all demonstrated excellent potential for future cluster ion spectroscopy. The first major calibration step was the introduction into the pulsed supersonic valve of a mixture of the helium together with xenon and its seven naturally occurring isotopes. The resulting mass spectrum displayed several peaks corresponding to separation of the xenon isotopes. It was rewarding to observe the peaks being resolved as we varied the tuning parameters of the instrument, carrier gas backing pressure, psv current, adjustment of the delays between the psv/pulser and the psv/potential switch.

Figures 4.5 show some xenon mass spectra at different delays of the PSV. Spectrum (a) indicates what happens when the pulser has been turned on too late, peaks 6 and 7 are resolved but peaks 1 and 2 and peaks 3,4 and 5 are unresolved. Spectrum (b) the pulser has been turned on too early, peak 1 is resolved, peaks 6 and 7 are partially resolved however they both have two humps indicating that the peaks have both an early and a late component. Spectrum (c)

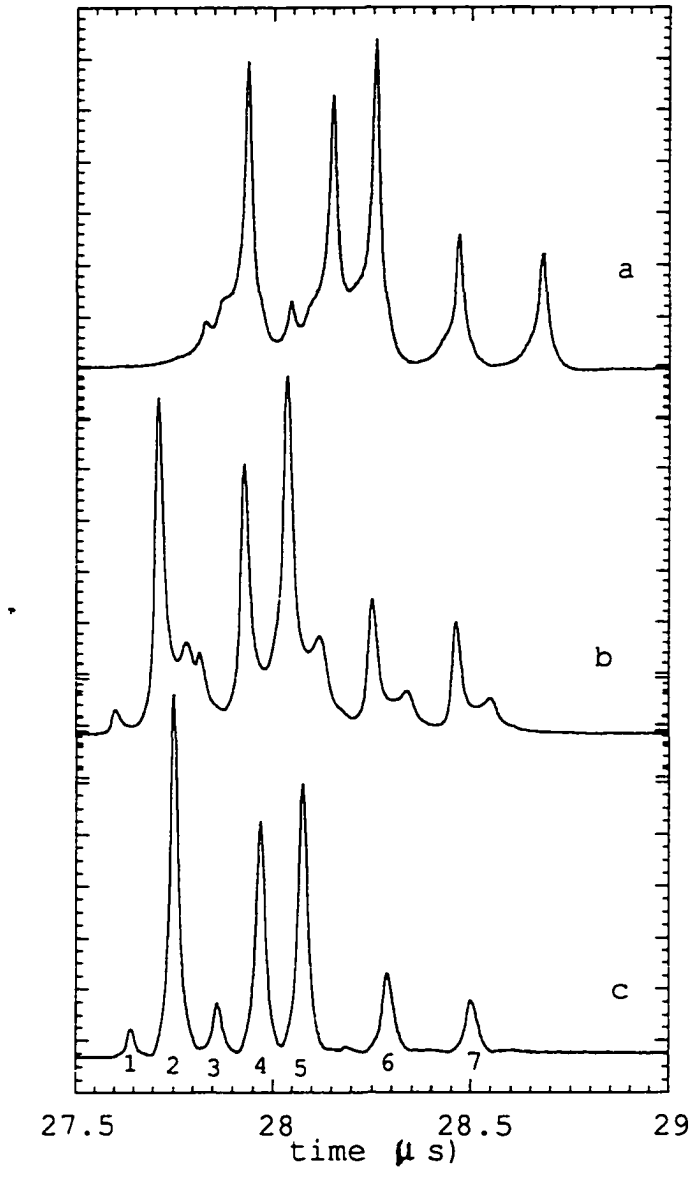

Figure 4.5 Mass spectra showing the separation of xenon isotopes.

1:	Xe^{128}	4:	Xe^{131}	7:	Xe^{136}
2:	Xe^{129}	5:	Xe^{132}		
3:	Xe^{130}	6:	Xe^{134}		

indicates a well resolved spectrum of the xenon isotopes [isotopic mass and intensities, Xe^{128} (4%), Xe^{129} (26.4%), Xe^{130} (6%), Xe^{131} (21.2%), Xe^{132} (26.9%), Xe^{134} (10.4%) and Xe^{136} (8.9%)][10]. There is one slight discrepancy on the resolved spectrum, peak Xe^{129} is shown slightly more intense than Xe^{132}, this is a tuning artifact. It occurs when the tuning conditions are not balanced this leads to an ion distribution that is skewed in favor of the lower masses. It does not however, significantly affect the accuracy of our mass spectrum as shown in Fig. 4.6. Figure 4.7A show copper monomer isotopes (Cu^{65}, Cu^{63}) together with the xenon isotopes respectively. In the case of the Cu^{+} isotopes one can observe that the intensities are proportional to the ratio of the isotopic masses Cu^{65} (30.91%) and Cu^{63} (69.9%).

IV.7 AN INTERLUDE WITH CARBON CLUSTER CATIONS

Carbon cluster ions have been studied and characterized, by several research groups over the years. The most well known of this family of clusters has been carbon-60, discovered by Smalley[2-6] et al. Carbon cluster ions were therefore an excellent specie to characterize and test the performance of the laser vaporization source since there existed in the literature many mass spectra and dissociation studies of carbon clusters.[11-15] Carbon also provided excellent oppurtunities on which to test cluster mass selection and photofragmentation.

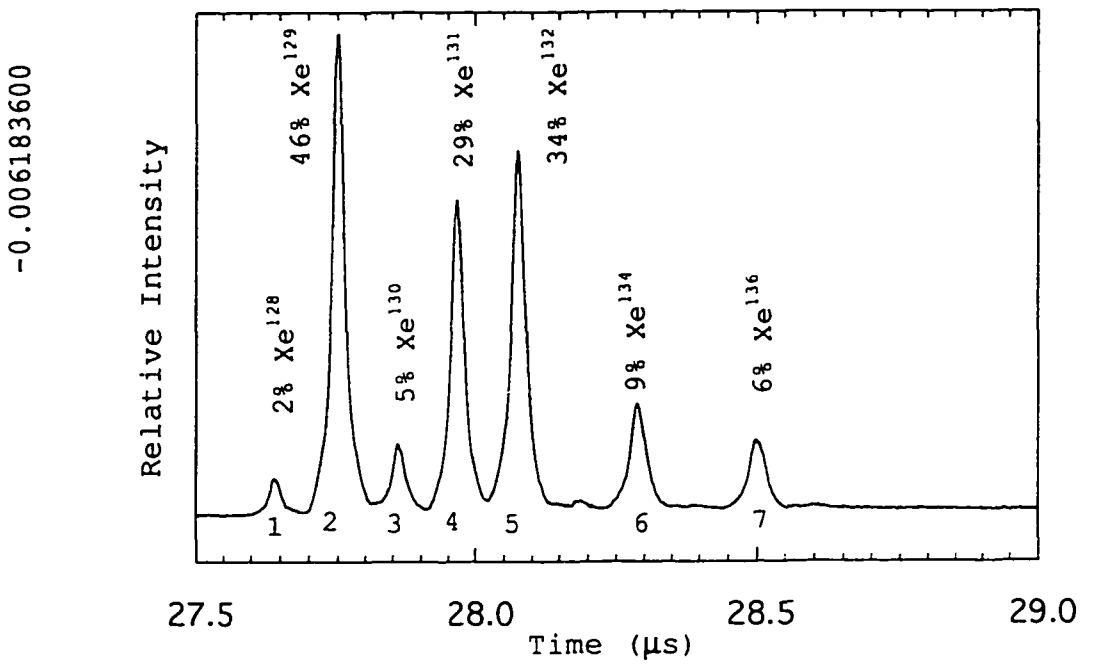

Figure 4.6 Mass spectrum of Xenon isotopes

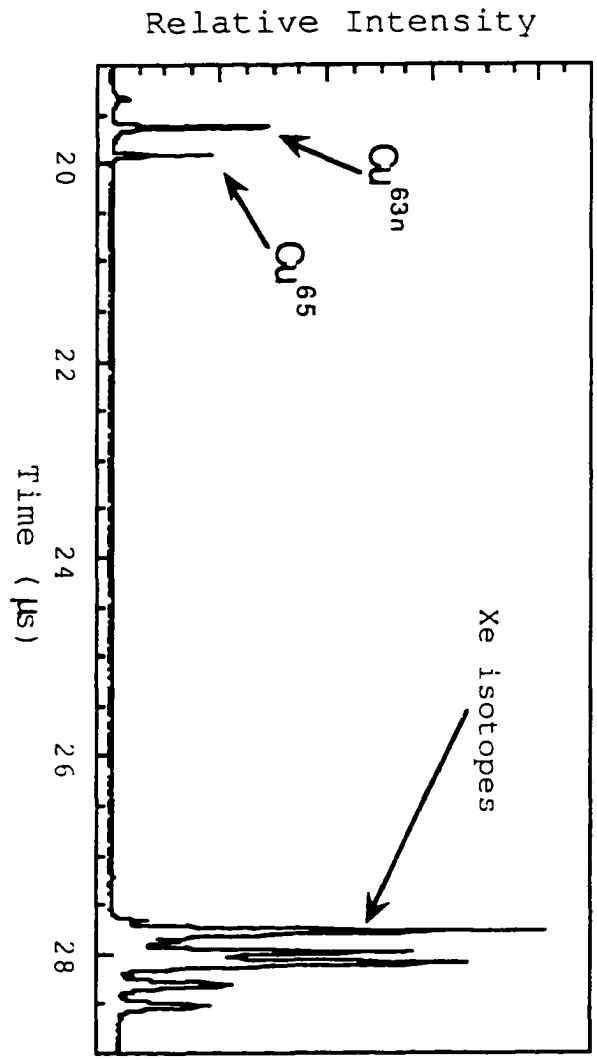

Figure 4.7A Mass spectrum showing the separation of copper isotopes and xenon isotopes.

Carbon clusters were easily produced and therefore presented excellent prospects to gain experience in tuning the source and varying the cluster production. It was soon possible to extend the cluster distribution out to C_{60} and beyond (see Fig. 4.8). The C_{60} (buckminsterfullerene) peak stood out by having a stronger intensity than it's closest neighbours, indicating an especially stable structure. This stability is due to this cluster having an exceptional symmetry whereby strain is alleviated in the cluster by having pentagonal and hexagonal rings of carbon atoms arranged in a giant cage like a 'soccer ball'.[11-15] Also evident was the alternating intensities (even numbered clusters have increased intensity compared to the odd numbered ones) seen for the larger carbon clusters, from C_{50} onwards.

Carbon cluster cations (C_{25}^+ to C_{34}^+) were mass selected and subjected to laser irradiation (YAG 2nd harmonic, 532 nm). It was observed for ions C_n^+, for $n < 32$ that these ions fragment by breaking off C_3 units, (Fig. 4.9). This behaviour is in accord with that observed by O'Brien[11], Geusic[12-14] and Bouyer[15].

The testing and calibration with xenon and carbon was very successful and indicated that our instrument was working well beyond our expectations.

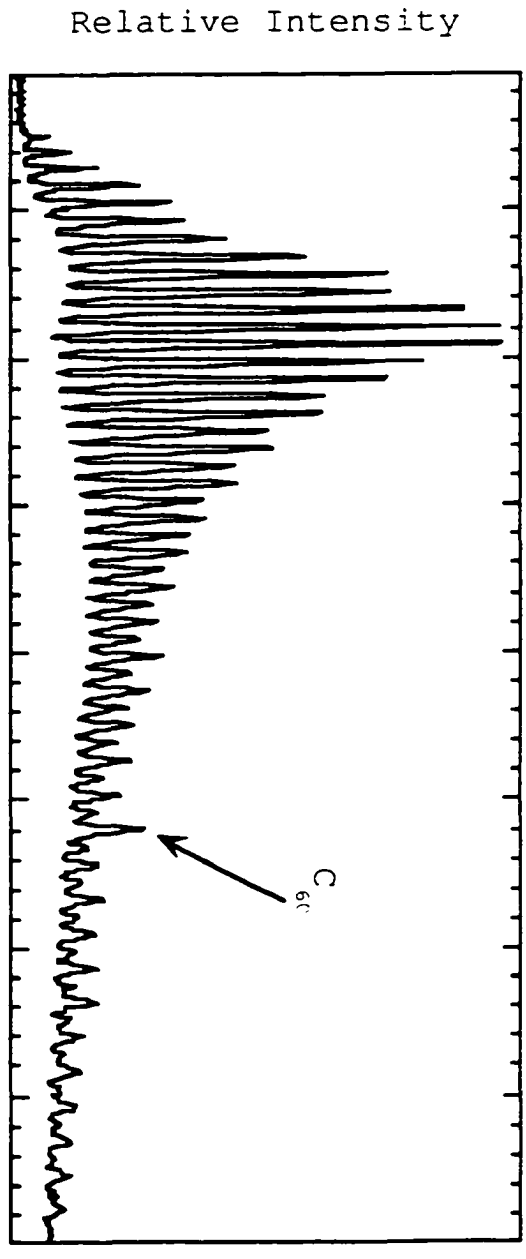

Figure 4.8 Mass spectrum of carbon cluster cations from C_{20}^{+} to C_{80}^{+}.

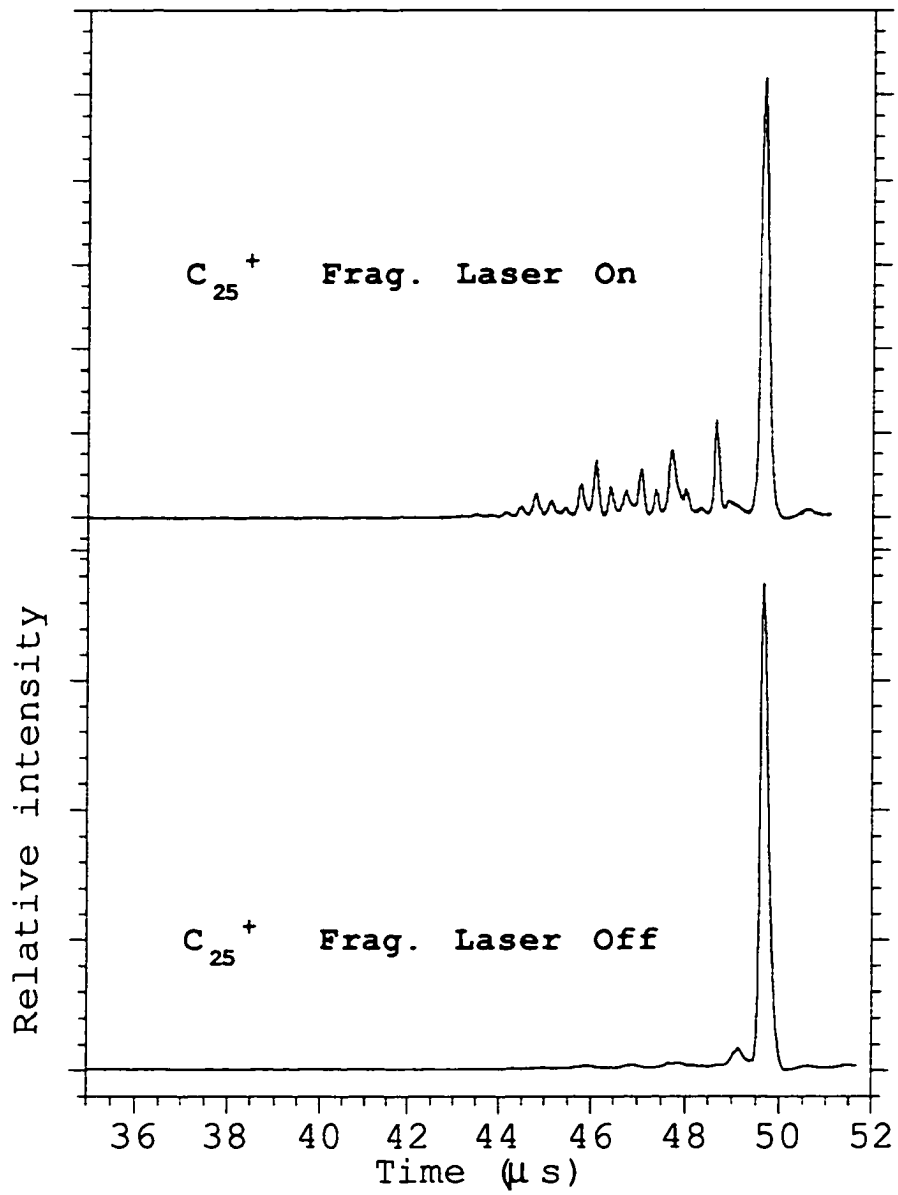

Figure 4.9 Mass spectrum showing the photofragmentation of C25+. The laser is OFF in the lower spectrum and ON in the upper spectrum.

Chapter IV References:

1. R.E.Smalley, Laser Chem., Vol. 2, 167 (1983).

2. Y. Liu, Q. L. Zhang, F. K. Tittel, R. F. Curl and R. E. Smalley, J. Chem. Phys., **85**, 7434 (1986).

3. D. E. Powers, S. G. Hansen, M. E. Geusic, D. L. Michalopoulos and R. E. Smalley, J. Chem. Phys., **78**, 2286 (1983).

4. P. J. Brucat, L. S. Zheng, C. L. Pettiette, S. Yang and R. E. Smalley, J. Chem. Phys., **84**, 3078 (1986).

5. D. E. Powers, S. G. Hansen, M. E. Geusic, A. C. Puiu, J. B. Hopkins, T. G. Dietz, M. A. Duncan, P. R. R. Langridge-Smith and R. E. Smalley, J. Chem. Phys., **86**, 2556 (1982).

6. W. C. Wiley and I. H. McLaren, Rev. Sci. Inst., **26**, 1150, (1955).

7. Wieslaw J. Stryjewski, Rev. Sci. Inst., **62**, 1921, (1991).

8. Gary W. Johnson, LabVIEW Graphical Programming :Practical Applications in instrumentation and Control (McGraw-Hill New York, 1994).

9. SIMION PC Version 4.0, courtesy D. A. Dahl, Idaho Natl. Lab. Idaho Falls, ID 83415, USA.

10. HandBook of Chemistry and Physics 78th edition, (CRC Press Inc. Boca Raton,1997).

11. S. C. O'Brien, J. R. Heath, R. F.Curl and R. E. Smalley, J. Chem. Phys., **88**, 220 (1988).

12. M. E. Geusic, M.F. Jarrold, T. J. McIlrath, R. R. Freeman and W. L. Brown, J. Chem. Phys., **86**, 3864 (1987).

13. M. E. Geusic, T. J. McIlrath, M.F. Jarrold, L. A. Bloomfield, R. R. Freeman and W. L. Brown, J. Chem. Phys., **84**, 2421 (1986).

14. M. E. Geusic, M.F. Jarrold, T. J. McIlrath, L. A. Bloomfield, R. R. Freeman and W. L. Brown, Z. Phys. D-Atoms Molecules and Clusters 3, 309-317 (1986).

15. R. Bouyer, P. Roussel, P. Monchicourt, M. Perdrix and P. Pradel, J. Chem. Phys., **100**, 8912 (1994).

CHAPTER V

PHOTOFRAGMENTATION SPECTROSCOPY OF THE NIOBIUM DIMER CATION

V.I ION PHOTOFRAGMENTATION SPECTROSCOPY

Ion photofragmentation spectroscopy otherwise known as ion photodissociation spectroscopy refers to any study using ion dissociation, in which a photofragment is observed directly as the carrier of the information sought.[1] It can also be viewed as optical spectroscopy performed on gas phase ions. The difference however is instead of measuring the change of photon flux through the sample, the 'effect' of the photons on the sample is observed.[2] Ion dissociation can occur when an ion absorbs one or more photons of total energy greater than the bond energy of a particular state. This may occur because of several reasons[3-9]: (1) excitation directly into a repulsive state from which dissociation occurs directly, (2) absorption to a bound excited state, followed by internal conversion to a lower electronic state whose energy may be greater than the bond dissociation energy, resulting in dissociation, (3) dissociation via the absorption of more than one photon. The simplest example of case 3 is infrared multiphoton dissociation which does not involve excitation to a different electronic state, only rapid sequential absorption of photons to reach the dissociation limit at the top of the Morse potential well.

Case 1 is termed direct dissociation and may be characterized by a 'structure-less' absorption spectrum for the parent ion and would tend to occur very fast, on a timescale of about 100 femtoseconds. Case 2 on the other hand presents several interesting possibilities because of the predissociation phenomenon that makes it occur on a longer timescale (t > 1 picosecond). This phenomenon may be characterized by a structured absorption spectrum, which indicates the presence of a potential well for the excited state, followed by dissociation (brought about by tunneling through a potential barrier or by change of electronic state near a curve crossing).[3] A 'structured' absorption spectrum (narrow peaks that have a semblance of order) may contain details (vibronic and rovibronic states) of the predissociation mechanism for the ion. Figure 5.1 gives a conceptual illustration of dissociation and predissociation.

The detection of ionized fragments produced in ion dissociation, provide information such as the dissociation channels, measurement of the photodissociation cross section and dissociation energies. Photodissociation cross sections are essentially equivalent to absorption spectra when predissociation occurs rapidly.[9] Detailed studies of the photofragments may also be carried out to determine the kinetic energy, angular distribution and internal energy of an ion. Laser induced fluorescence (LIF) and resonant two photon ionization (R2PI), two of the best spectral techniques used in the spectroscopy of ions, encounter difficulties when

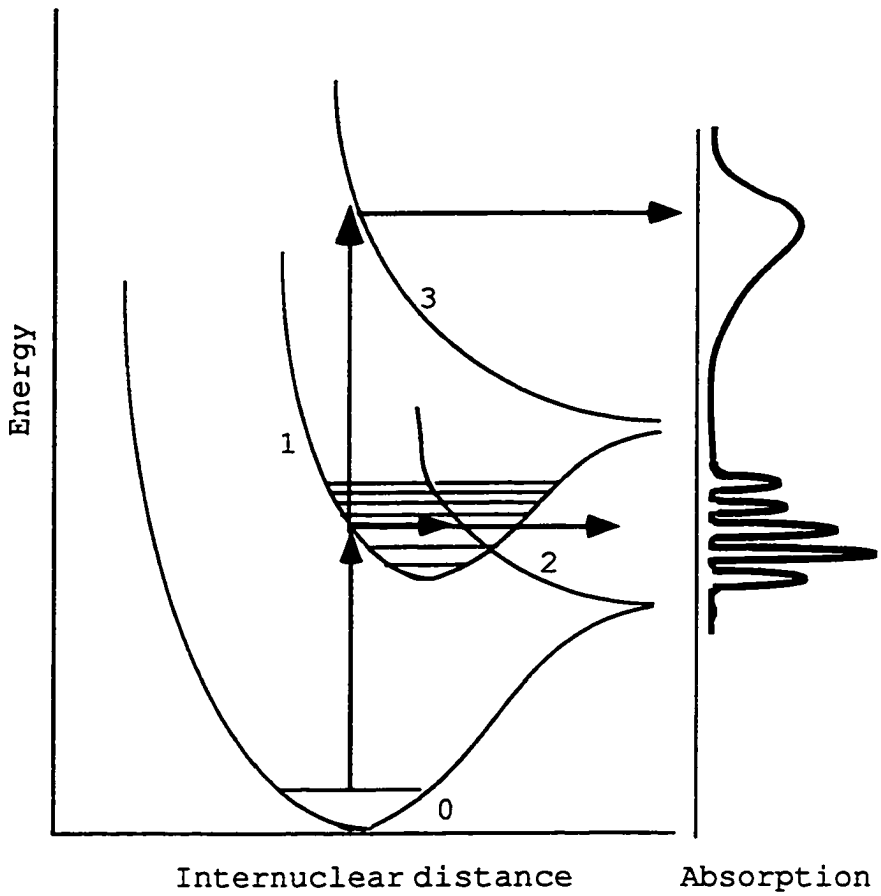

Figure 5.1 A conceptual diagram illustrating dissociation and photodissociation for cases 1, 2 and 3.

applied to metal cluster studies. They both require that the laser induced transition to an excited electronic state have a long enough lifetime for its fluorescence (LIF) or lowered ionization potential (R2PI) to be detected. In transition metal clusters, there exist many close low lying electronic states with the possibility of a dense manifold of vibronic states. Radiationless transition between these states will be very rapid preventing the detection of LIF and R2PI and rendering both techniques ineffective;[4,5] photodissociation spectroscopy overcomes this problem.

In the case of photodissociation spectroscopy, the only requirement to obtain a dissociation spectrum is that the cluster dissociates upon photon absorption. This could be carried out either as a single color dissociation or as a two color dissociation using two different color lasers. One of the laser may be set at a frequency to excite the ion to a virtual state, while the other would be scanned to dissociate the ion as a function of the laser wavelength or vice versa. A primary difficulty of photofragmentation experiments had been the production of ions in sufficient densities, a problem which is only now being overcome. Typically ions would be produced by using an ArF laser to ionize neutrals clusters produced in an expansion.[6] This however has the unfortunate tendency of producing ions in various states of excitation, which when photofragmented result in congested spectra. The preferred method is to use a cluster ion source

with a supersonic expansion to produces 'cooler' ions. The cooling collisions experienced by these ions lead to drastic reduction of the temperatures for the translational (T_t), vibrational (T_v) and rotational (T_r) degrees of freedom, compared to the temperature of the environment. Possible temperatures obtained by this method are T_t < 20K, T_v < 100 K and T_r < 50K. The level of cooling achieved in the ion is heavily dependent on the prevailing source conditions at the time.[10,11] Cooling the ions does not necessarily imply that one would obtain uncongested spectra. If the ion contains a high density of states as is expected for some transition metal ions, the possibility exists that unquenched low lying states might be observed under conditions, that would normally be expected to cool them to their electronic ground state, resulting in a congested spectrum.[12,13]

V.2 PHOTOFRAGMENTATION OF $(Nb_2)^+$

V.2.1 INTRODUCTION

Niobium a Group VA transition metal, belongs to the 4d transition series with a valence electronic configuration $4d^45s^1$, giving it oxidation states of +2, +3, +4 and +5. Niobium which has no known isotopes and a propensity for clustering has been the subject of many studies, including reactivities, binding energies, spectroscopic studies, dissociation energies and theoretical studies. There is

however, very little information concerning the nature of the bond in the niobium dimer cation.[5,14-21] This 4d transition dimer cation has resisted several attempts to probe the nature of its bonding. Niobium's lack of isotopes enables it to have a simple mass spectrum, except for the oxides which it readily forms, as seen previously in Fig. 3.13. Since we had examined the neutral dimer in argon matrices using absorption spectroscopy[17], the first experiment attempted with the photofragmentation mass spec., was a probe of the niobium dimer cation, Nb_2^+.

V.2.2 EXPERIMENTAL

Niobium clusters were generated in the vaporization source by vaporizing niobium metal (Goodfellow, 99.99%), then mass analyzed in the Wiley McLaren TOF mass spectrometer. Dimer cations were mass selected and fragmented with light of varying wavelength from a YAG-pumped PDL-3 dye laser. Typical scan conditions were as follows:

Laser energy	=	18 mJ/pulse
PSV/Laser delay	=	150 μs
PSV current	=	3.2 kA
Laser/Pulser delay	=	90 μs
Pulser voltage	=	850 V
Pulser/Pot Switch delay	=	10 μs
Pot. Switch voltage	=	2000 kV
He backing pressure	=	140psig

Mass gate voltage	=	300 V
Reflectron voltage	=	3000 V
Einzel lens voltage	=	1200 V
Deflector voltage	=	60 V
MCP voltage	=	2400 V
Frag. Las/mass gate delay	=	1 μs
Frag. Laser power	=	10 mW-20 mW

The intensities of both the daughter ion (Nb^+) and the parent ion Nb_2^+ were collected as a function of the dye laser wavelength. Four hundred shots were averaged at each wavelength increment and the result stored by the computer. Intensities of the parent and daughter ions and the background level were measured in volts, with the laser power and wavelength in mW and nm respectively. Parent ion intensity was on average about 2.5 V ± 1 V. Relative intensities were calculated by normalizing the daughter ion intensity to the parent intensity by using the following equation:

$$\frac{\text{Daughter intensity}}{(\text{Parent intensity} + \text{daughter intensity})(\text{Fluence})} \qquad 5.1$$

A total of seven overlapping dye scans were used to cover the range from 500 nm to 625 nm (21000 cm^{-1} - 15000 cm^{-1}). Scans were performed using the following dyes: Rhodamine 590, Coumarin 500, Coumarin 540A, DCM, Sulfarhodamine 640, Kiton Red 610 and Fluorescein 548.Wavelength shifting of those dyes were also carried out to cover areas in between the dye

range. Fluences for the yellow dyes were typically 20 mW/cm^2, while that of theblue dyes tended to be much lower, 10 mW/cm^2. Additional experimental details can be found in chapters III and IV.

V.2.3 RESULTS

Fragmentation of Nb_2^+ produces Nb and Nb^+; with only Nb^+ being detectable. Figures 5.2A and 5.2B show laser on and laser off mass spectra for Nb_2^+. The intense peak in the laser off spectrum is Nb_2^+, while the laser on shows both Nb_2^+ and Nb^+. Fluence dependent studies were performed in an attempt to determine whether the absorption process was a one photon, two photon or even a three photon process. Figure 5.3 show the results of these fluence dependent studies at different wavelengths. The nonlinearity in the curves at the different wavelengths negates the possibility that the absorption was a one photon process[5,22], however the determination of whether the absorption was a two photon or three photon process was still unclear. Ideally a homogenous light field of known absolute flux should be used to determine the per ion absorption rate as a function of intensity. The YAG with which the dye laser is pumped has a Gaussian profile. This resulting intensity profile is not flat and therefore some areas of the laser beam are more intense than others. Additionally the YAG misfired at times and the power varied ± 10% from pulse to pulse. Effects

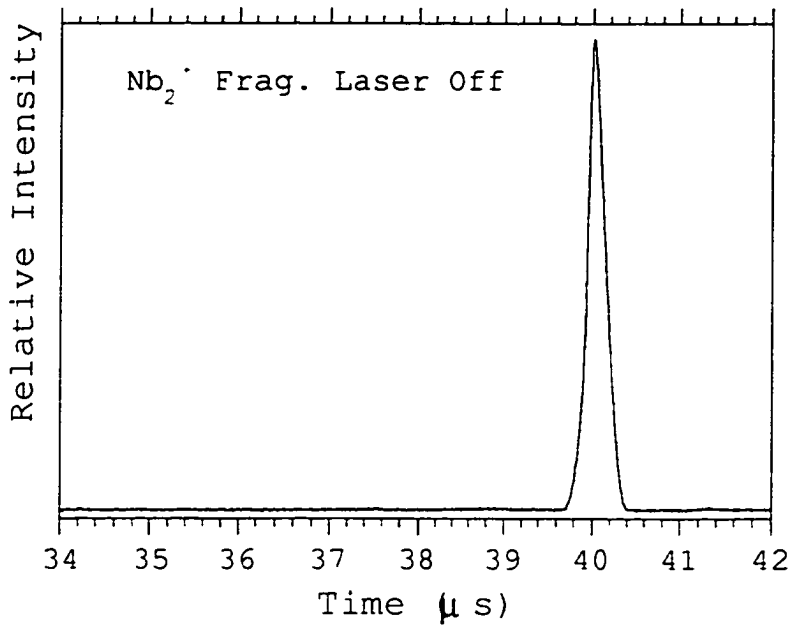

Figure 5.2A Mass spectrum of Nb_2^+ with the fragmentation laser OFF.

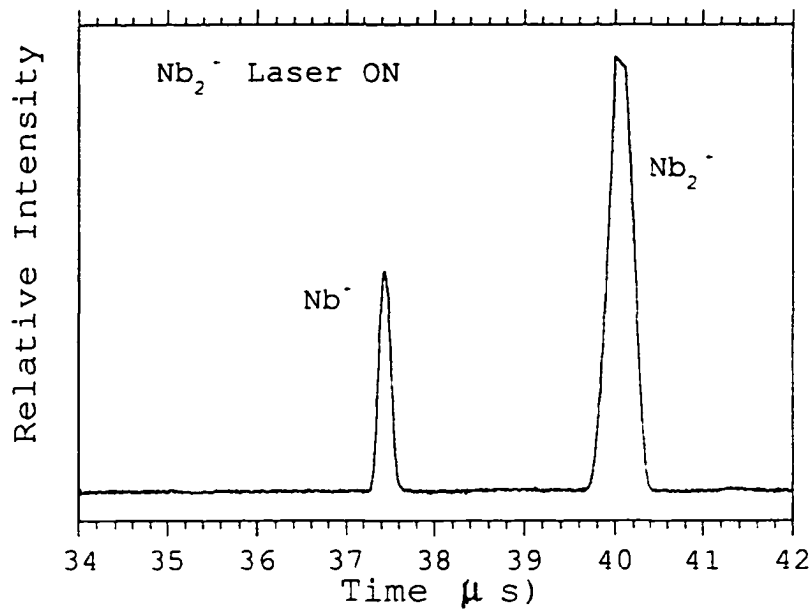

Figure 5.2B Mass spectrum of Nb_2^+ and Nb^+ produced with the fragmentation laser ON.

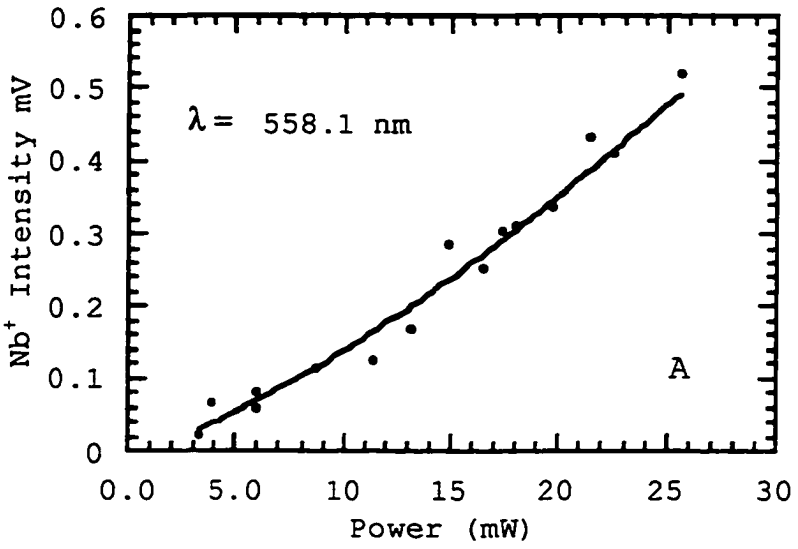

Figure 5.3A Plot of Nb^+ intensity vs laser power for fluence dependence studies of Nb_2^+ at λ= 558.1 nm.

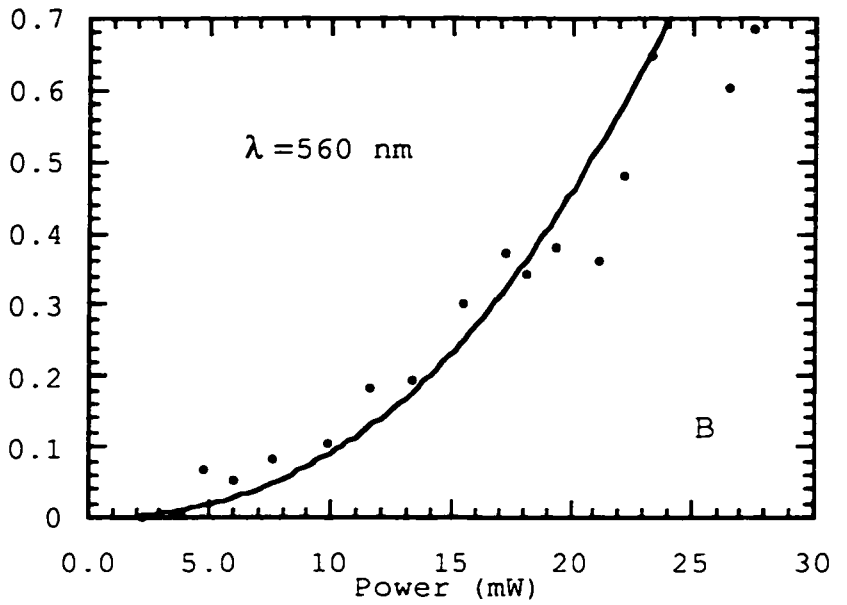

Figure 5.3B Plot of Nb^+ intensity vs laser power for fluence dependence studies of Nb_2^+ at λ= 560 nm.

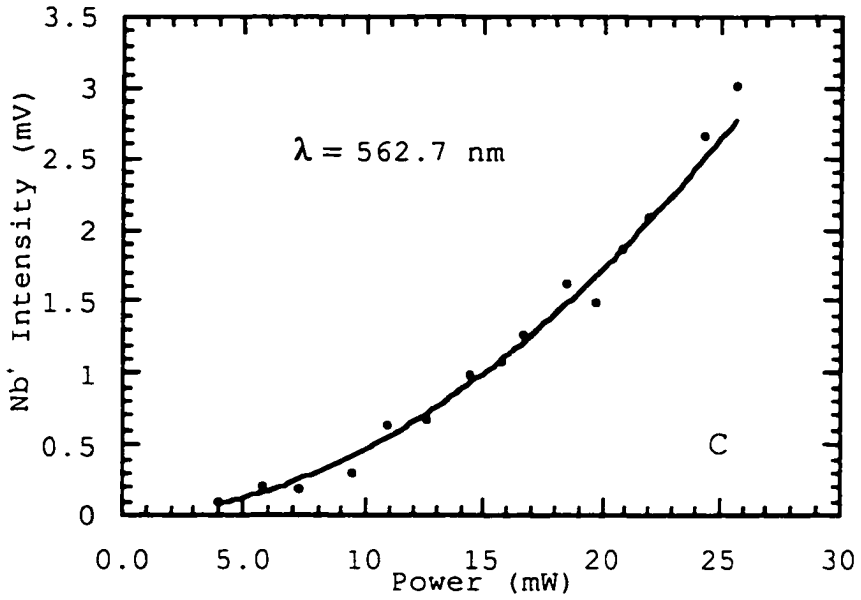

Figure 5.3C Plot of Nb^+ intensity vs laser power for fluence dependence studies of Nb_2^+ at λ= 562.7 nm.

caused by the mismatch in the laser/ion beam overlap and saturation at high laser power only serve to aggravate the problem. These effects when summed could bring about the appearance of a reduction in the order of the process, when the daughter intensity is plotted against the laser power. The curve for a two photon process may appear linear and be incorrectly inferred as a one photon process, or a three photon process may appear to be a two photon process.[5] The curves in Fig. 5.3 (A,B,C) have a high degree of curvature therefore one can easily dismiss the possibility of one photon process; these are all second order plots. Additional information supporting this view comes from knowing that the bond dissociation energy[18] of Nb_2^+ is 5.87 eV, this coupled to the fact that our power studies were over the range 558 nm to 562 nm ~ 2.3 eV, a three photon process was the minimum possibility. Figure 5.4 shows a possible dissociation scheme for a three photon process.

Figure 5.5 presents the vibronic spectrum of Nb_2^+ taken at a resolution of 0.02 nm, 50 points per nm. There are several sharp features visible between 16000 cm^{-1} and 18450 cm^{-1}; all were reproducible. The frequencies and intensities are listed in Table 5.1. The overall majority of these vibronic features were red degraded, indicative of an increase in bond length in going from the ground to the excited state[2] and a decrease in the vibrational frequency. Several assignment schemes were proposed to fit the spectrum, next section.

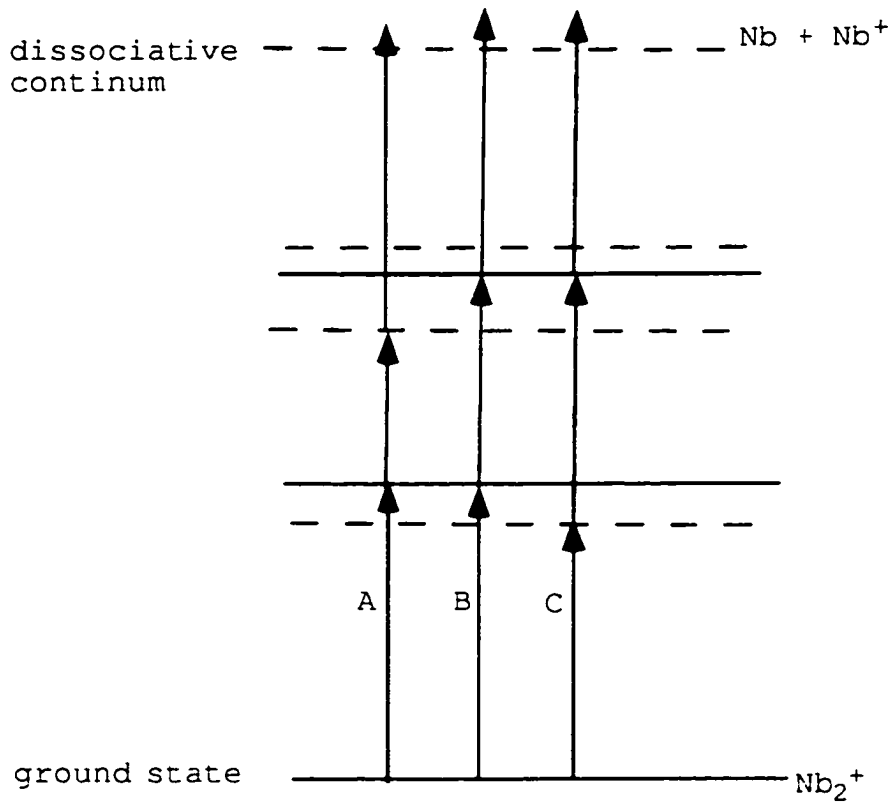

Fig. 5.4 An illustration of three photon dissociation. The dotted lines indicate the presence of virtual states. Dissociation via the virtual states A and C will not be as strong as in B which is in resonance with two real states.

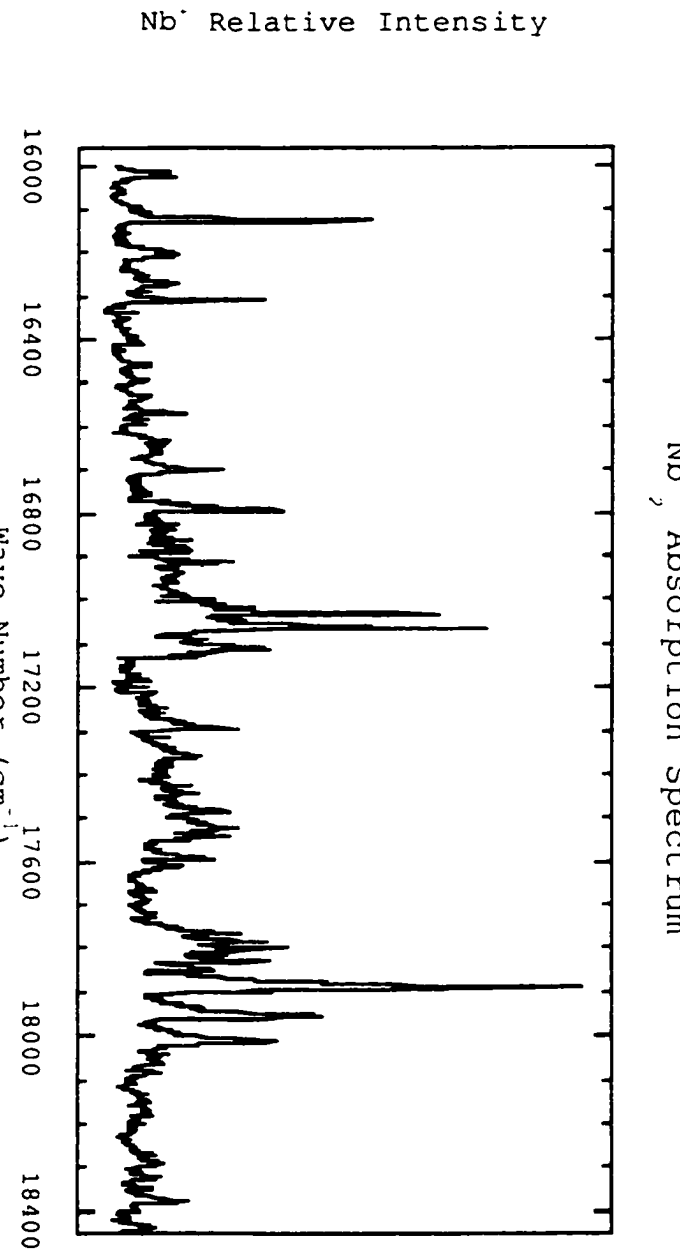

Figure 5.5 Photofragmentation (absorption) spectrum of Nb_2^+.

TABLE 5.1 Table of Peak Frequencies and Intensities

Peak #	Frequency cm^{-1}	Rel.Int. x 10^5	Norm Int.	Peak #	Frequency cm^{-1}	Rel.Int. x 10^5	Norm Int.
1	16027	6.5	17.2	24	17442	8.1	21.5
2	16127	21.8	57.8	25	17484	10.8	28.6
3	16202	6.7	17.8	26	17524	11.5	30.5
4	16273	6.7	17.8	27	17544	10.9	28.9
5	16310	4.4	11.7	28	17584	7.8	20.7
6	16411	3.9	10.3	29	17592	8.7	23.1
7	16457	4.6	12.2	30	17609	7.1	18.8
8	16494	4.5	11.9	31	17768	11.7	31
9	16530	4.7	12.5	32	17783	13.7	36.3
10	16568	7.3	19.4	33	17800	15.3	40.6
11	16576	3.8	10.1	34	17830	14	37.1
12	16632	6	15.9	35	17849	9.6	25.5
13	16702	10.2	27.1	36	17891	37.7	100
14	16794	14.9	39.5	37	17935	8.5	22.5
15	16826	6.6	17.5	38	17955	18.1	48
16	16886	7.7	20.4	39	18013	14.6	38.7
17	16914	11	29.2	40	18043	6	15.9
18	17000	9.6	25.5	41	18065	5.7	15.1
19	17032	26.9	71.4	42	18086	5.4	14.3
20	17065	30.5	80.9	43	18292	5.6	14.9
21	17115	13.9	36.9	44	18323	4.9	13
22	17296	11.4	30.2	45	18375	7.5	19.9
23	17356	8.6	22.8	46	18440	5.1	13.5

V.2.4 DISCUSSION

We begin the discussion by recounting what was known about both the niobium dimer neutral and cation. The niobium dimer neutral is well known as indicated in Table 5.2 which lists ω_e, $\omega_e x_e$, r_e and d_e. Not much is known about Nb_2^+ except that it vibronic peaks are red degraded[5], other information regarding ω_e and the ground state term have been proposed. The photofragmentation spectrum of the niobium dimer cation has eluded many research groups. It was first attempted by Smalley[5], whose studies of gas phase cluster ions, have contributed immensely to the field of photofragmentation and metal cluster ion spectroscopy. Smalley recorded a photofragment spectrum of Nb_2^+ over the region 17800 cm^{-1} to 18250 cm^{-1}, which was classified as having well resolved vibronic bands, with an estimated rotational temperature on the order of 20K. The spectrum was obtained by monitoring the Nb^+ fragment yield as a function of the dissociation laser wavelength during the fragmentation of Nb_2^+. Their studies included a variation of the ion production both with and without the use of an ArF ionization laser to show the reduction in the cluster internal excitation. No assignment was given to that spectrum. However discussions with Phil Brucat[24] alerted us to the difficulties they encountered in attempting to assign the spectrum.

Private communications with Michael Duncan[26] (University of Georgia, Athens), indicated that he also attempted to obtain the photofragmentation spectrum of Nb_2^+,

however his preliminary studies showed an abundance of bands which made him think that it was too congested to resolve and assign.

W. Weltner Jr. et al.[14] obtained an ESR spectrum of an ion he determined to be the niobium dimer cation. His studies were carried out by laser vaporizing a niobium metal rod and trapping the resulting ions in argon matrices. The ESR spectrum they obtained was assigned to the $^2\Sigma$ ground state of Nb_2^+, which was thought to arise from the $5s\sigma_g^2 4d\sigma_g^1 4d\pi_u^4 4d\delta_g^2$ electron configuration. They also calculated that it might have been coupled to an excited $^2\Pi$ state at about 20000 cm^{-1}.

Benoit Simard et al.[15], have done theoretical calculations on the Nb_2^+, V_2^+ and VNb^+ ions. Simard also conducted resonant two photon ionization spectroscopy (R2PI) on Nb_2, VNb and V_2 and has hypothesized that Nb_2^+, V_2^+ and VNb^+ and Nb_2, VNb and V_2 are related in following manner: Vanadium and Niobium both belong to Group 5 having $3d^4,4s^1$ and $4d^4,5s^1$ electron configuration respectively and therefore VNb which is a combination of both V and Nb, is expected to have bond lengths and bond strengths intermediate between V_2 and Nb_2. The same relationship was also expected to hold for the cations of these species. Simard's experimental work had verified this for the neutral species (V-V, V-Nb, Nb-Nb) but had not yet verified the same for the cationic (V_2^+, VNb^+ and Nb_2^+). His calculation was based on the ground state of the ions being a $^4\Sigma$. This state arose from a $5s\sigma_g^1 4d\sigma_g^2 4d\pi_u^4 4d\delta_g^2$ electron configuration.

The ground state configuration could arise either from a $\sigma^1\delta^2$ or a $\sigma^2\delta^1$ electron configuration. If it arose from a $\sigma^1\delta^2$ electron configuration it could give either $^2\Sigma$ or $^4\Sigma$. Simard and Weltner both think that it could arise from a $\sigma^1\delta^2$ electron configuration, however they differ on whether it $^2\Sigma$ or $^4\Sigma$. Since it is also possible for the ground state of Nb_2^+ to arise from a $\sigma^2\delta^1$ electron configuration to give a $^2\Delta$ state. Koopmans' theorem predicts that an electron from the highest occupied δ–orbital would be ejected, giving a cation with ground state symmetry $^2\Delta$. There is the claim however that this theorem does not take into account electronic relaxation effects and makes no allowance for stabilizations due to exchange interactions among the three unpaired electrons.[15] At this point no firm conclusions can be made concerning the symmetry of the ground state.

Armentrout et al[18], has experimentally determined the dissociation energy of Nb_2^+ to be 5.87 eV. Simard et al[15] have also calculated using Density Functional calculations, ω_e' and r_e' for Nb_2^+ to be 470 cm^{-1} and 2.044 A° respectively. A comparison of the spectrum from Smalley et al[5] to ours (Fig. 5.5), indicates that there are several similar features. Their region from 17850 cm^{-1} to 18100 cm^{-1} in general corresponds to the region from 17600 cm^{-1} to 17850 cm^{-1} in our spectrum. There seemed however, to be a wavelength mismatch of about 250 cm^{-1}. A recalibration of our laser using a mercury lamp and a Spex 'Doublemate' monochromator, showed our laser to be off by a minor amount (0.15 nm), therefore

the possibility exists that their laser could have been 'slightly off'. The general comparison of features however does indicate that our beam expansion conditions were at least as cool as Smalley et al ~ 20K as indicated in Ref. 5.

V.2.5 A POSSIBLE ASSIGNMENT ?

Measured frequencies are listed in Table 5.1. A careful study of all the peaks that are at least 15% of the highest peak, reveal six groupings. These groupings are centered around (1) 16,100 cm^{-1}, (2) 16,500 cm^{-1}, (3) 17,000 cm^{-1}, (4) 17,400 cm^{-1}, (5) 18,000 cm^{-1}, and (6) 18,400 cm^{-1} respectively. The groups from 1 through 6 seem to have an alternating intensity, high, low, high, low, high and low, in addition some of the peaks are broader than the others. The peaks were red degraded which hinted at the possible band head positions. This assisted in measuring frequencies and also alerted us to the fact that $r_e' > r_e''$ and $\omega_e' > \omega_e''$. Several assignment schemes were tried based on the differences between these frequencies.

The first assignment that leaps out at you is the one based on the following differences, where P # and ΔP refers peak no. the difference between peaks:

(P # - P #)	ΔP	(P # - P #)	ΔP
1 - 17	= 887 cm^{-1}	18 - 36	= 893 cm^{-1}
2 - 19	= 905 cm^{-1}	20 - 38	= 890 cm^{-1}
3 - 21	= 913 cm^{-1}	21 - 39	= 898 cm^{-1}

These peaks appeared to be a sequence of some sort, however peak intensities did not match. Peak 18 was not very intense and peaks 36, 38 and 39 bore only slight qualitative resemblance to peaks 18, 20 and 21, and none to peaks 1, 2, and 3. There were two other strongly suggestive sequences or progressions prompted by differences of (1) ~ 400 cm^{-1} and (2) ~500 cm^{-1}. The common denominator among them was that they all left several lines unaccounted for and there were slight inconsistencies in the differences. Some differences would gradually decrease then suddenly increase. None of the assignments we tried was satisfactory.

V.2.6 CONCLUSION

That the niobium dimer cation strongly resists probes of its bonding character, can be deduced from the fact that several research groups have attempted to study this ion, none entirely successful. The question that arises is 'Why should the spectra of this ion be so difficult to unquestionably interpret?'. On the whole experimental spectra are difficult to assign even when the identity of the molecular species is known.[28] Since niobium is a 4d transition metal, d-orbital participation in bonding will be of serious importance, because the nd orbital contraction[29] will be less severe in the 4d and 5d than it is in the 3d transition metals, relative to the 5s and 6s orbitals. The d-d bonding in the niobium dimer cation give rise to an abundance of low

lying electronic states which could result in complex electronic spectra. The previous ideas taken together with the possible shortcomings in the theory of bonding of 4d transition metal dimer cations conspire to allow the escape of a more comprehensive understanding of the Nb_2^+ photofragmentation spectrum. The work compiled in this thesis can be viewed as our the addition to the body of knowledge concerning the niobium dimer cation and transition metal cluster ions in general.

Chapter V References

1. John T. Moseley, Photodissociation and Photoionization, edited by K. P. Lawley (Wiley, 1985).

2. S. P. Goss, J. D. Morrison and D. L. Smith J. Chem. Phys.,**75**, 757 and 1820 (1981).

3. Richard N. Dixon, Chem. Soc. Rev., (1994).

4. C. R. Chris Wang, Stuart Pollack, Douglas Cameron and Manfred Kappes, J. Chem. Phys., **93**, 3787 (1990).

5. P. J. Brucat, L. S. Zheng, C. L. Pettiette, S. Yang and R. E. Smalley, J. Chem. Phys., **84**, 3078 (1986).

6. A. Welsford Castleman Jr., and Robert G. Keesee, Chem. Rev., **86**, 589 (1986).

7. Kenneth F. Willey, David L. Robbins, Chen-Sheng Yeh and Michael A. Duncan, Faraday Discuss. **92**, 269 (1991).

8. Martin F. Jarrold and Kathleen M. Creegan, Int. J. Mass Spec. and Ion Processes, **102**, 161 (1990).

9. Martin F. Jarrold and Kathleen M. Creegan, Chem. Phys. Lett., **166**, 116 (1990).

10. Paul C. Engelking, Chem. Rev., **91**, 399 (1991).

11. John M. Hayes, Chem. Rev., **87**, 745 (1987).

12. J. B. Hopkins, P. R. R. Langridge-Smith, M. D. Morse and R. E. Smalley, J. Chem. Phys., **78**, 1627 (1983).

13. Jacqueline C. Pinegar, Jon D. Langenberg, Caleb A. Arrington, Eileen M. Spain and Michael D. Morse, J. Chem. Phys., **102**, 666 (1995).

14. R.J. Van Zee, S. Li and W. Weltner Jr., Chem. Phys. Lett. **217**, 381 (1994).

15. Andrew M James, Pawel Kowalczk, Etienne Langlois, Margot D. Campbell, Ayano Ogawa and Benoit Simard, J. Chem. Phys., **101**, 4485 (1994).

16. Andrew M James, Pawel Kowalczk, Rene Fournier and Benoit Simard J. Chem. Phys., **99**, 8504 (1993).

17. Z. Hu, B. Shen, Q. Zhou, S. Deosaran, J. R. Lombardi and D. M. Lindsay, SPIE Proceedings Vol. **1599**, (1992).

18. David A. Hales, Li Lian, P.B. Armentrout, Int. J. Mass Spec. and Ion Processes, **102**, 269 (1990).

19. S. K. Loh, Li Lian and P.B. Armentrout, J. Chem. Phys., **91**, 6148 (1989).

20. Y. Hamrick, S. Taylor, G. W. Lemire, Z. W. Fu, J, C, Shui and M. D. Morse, J. Chem. Phys., **88**, 4095 (1988).

21. M. Moskovits and W. Limm, Ultramicroscopy **20**, 83 (1986)

22. J. R. Heath, Yuan Liu, S. C. O'Brien, Qing-Ling Zhang, R. F. Curl, F. K. Tittel, and R. E. Smalley, J. Chem. Phys., **83**, 5520 (1985).

23. R. L. Asher, D. Bellert, T. Buthelezi and P. J. Brucat, Chem. Phys. Lett., **224**, 525 and 529 (1994).

24. Private communication with P. J. Brucat, University of Florida, Gainesville.

25. Private communication with M. A. Duncan, University of Georgia, Athens.

26. Benoit Simard, Andrew M. James,, Pawel Kowalczyk, René Fournier and Peter A. Hackett, preprint (High Resolution spectroscopy of small transition metal molecules. Recent experimental and theoretical progress on group 5 diatomics.

27. James C. Weisshaar, J. Chem. Phys., **90**, 1429 (1989).

28. Charles W. Bauschlicher Jr., Stephen R. Langhoff, Chem. Rev. 91, 701, (1991).

29. Scott Taylor, George W. Lemire, Yoon Mi Hamrick, Zhenwen Fu and Michael D. Morse, J. Chem. Phys., **89**, 5517 (1988).

Appendix A1 Spreadsheet set up to calculate Wiley-Mclaren linear TOF arrival times of the niobium dimer cation

z0 (cm)	Z1 (cm)	Z2 (cm)	V1 (V)	V2 (V)	K-ratio	Z3 (cm)	m (amu)	E (V)	T (mus)	T (mus)	T (mus)	ave. T
S	So	d	Vs	-Vd	Ko	D(cm)	M (amu)	Ut	t(w-McL)	t(ffft)		st.dev.T
10	1	5	850	2000	24.53	100.00	185.8	2085.00	3.92	21.53	25.45	
10	2	5	850	2000	12.76	100.00	185.8	2170.00	4.66	21.1	25.76	
10	3	5	850	2000	8.84	100.00	185.8	2255.00	5.24	20.7	25.94	26.08
10	4	5	850	2000	6.88	100.00	185.8	2340.00	5.74	20.32	26.06	0.286
10	5	5	850	2000	5.71	100.00	185.8	2425.00	6.18	19.96	26.14	
10	6	5	850	2000	4.92	100.00	185.8	2510.00	6.58	19.62	26.2	
10	7	5	850	2000	4.36	100.00	185.8	2595.00	6.95	19.3	26.25	
10	8	5	850	2000	3.94	100.00	185.8	2680.00	7.29	18.99	26.28	
10	9	5	850	2000	3.61	100.00	185.8	2765.00	7.62	18.7	26.32	
10	10	5	850	2000	3.35	100.00	185.8	2850.00	7.93	18.42	26.35	

Appendix A2 Spreadsheet set up to calculate Reflectron TOF arrival times for Nb_2^+ and Nb^+.

E(p) eV	phi	Mass AMU	M(f) AMU	U(f)	D (cm)	Vr (V)	Lr (cm)	t(L) (mus)	t ref (mus)	t(tot) (mus)	Y(f) (cm)	av/Y(f) st dev	av (ttot)	Ytot	ave Y(tot)
2050	6	185.8	93.9	1036	11.7	3000	39	8.42	3.42	11.84	1.67	2.037	11.434	5.77	6.137
2150	6	185.8	93.9	1087	11.7	3000	39	8.22	3.5	11.72	1.75	0.246	0.241	5.85	0.23
2250	6	185.8	93.9	1137	11.7	3000	39	8.04	3.58	11.62	1.83			5.93	
2350	6	185.8	93.9	1188	11.7	3000	39	7.87	3.66	11.53	1.92			6.02	
2450	6	185.8	93.9	1238	11.7	3000	39	7.7	3.74	11.44	2			6.1	
2550	6	185.8	93.9	1289	11.7	3000	39	7.55	3.82	11.37	2.08			6.18	
2650	6	185.8	93.9	1339	11.7	3000	39	7.41	3.89	11.3	2.16			6.26	
2750	6	185.8	93.9	1390	11.7	3000	39	7.27	3.96	11.23	2.24			6.34	
2850	6	185.8	93.9	1440	11.7	3000	39	7.14	4.03	11.17	2.32			6.42	
2950	6	185.8	93.9	1491	11.7	3000	39	7.02	4.1	11.12	2.4			6.5	

Appendix B1 Software written in LabVIEW to operate the instrument. This is the main stand alone which control pulses to trigger all the devices.

Figure B1.1 A representation of the graphical user interface which the operator uses to change timing parameters.

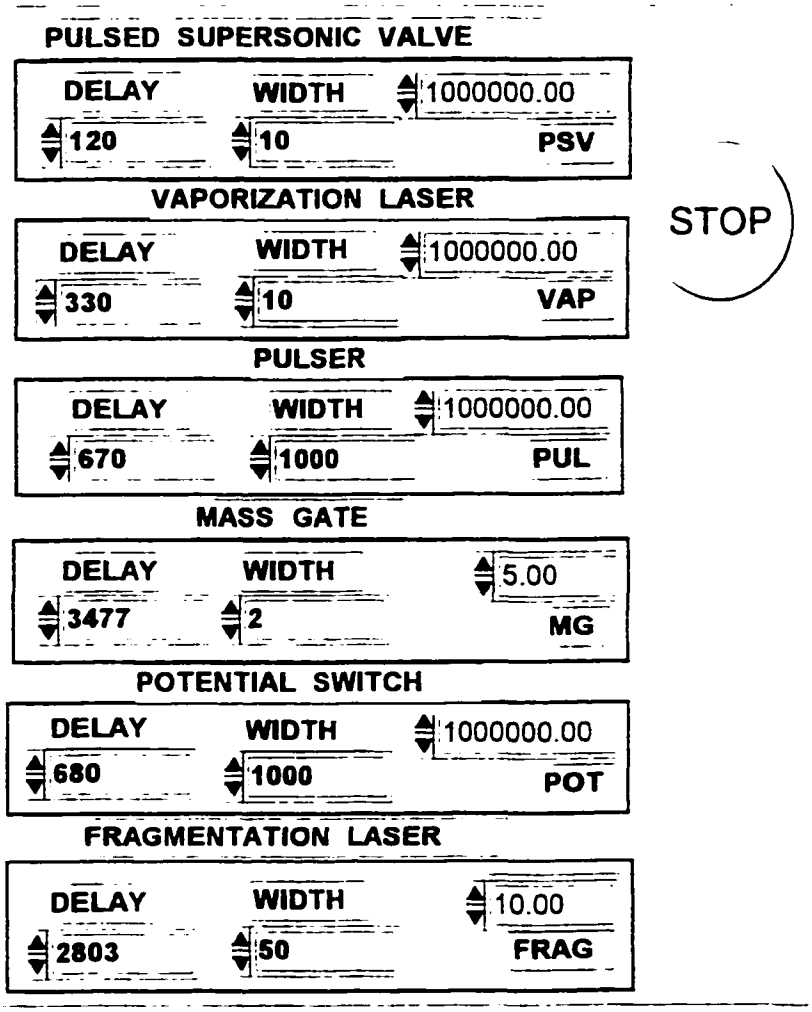

Subsequent frames starting with 0 and ending with give the order of execution of the program (1 to 6 and then 1 to 6 again....).

Frame 0 sets up the Square Wave in a loop to start and stop.

Frame 1 sets up the PSV

Frame 2 sets up the Vaporization laser

Frame 3 sets up the Pulser

Frame 4 sets up the Mass Gate

Frame 5 sets up the Potential Switch

Frame 6 sets up the Fragmentatio laser

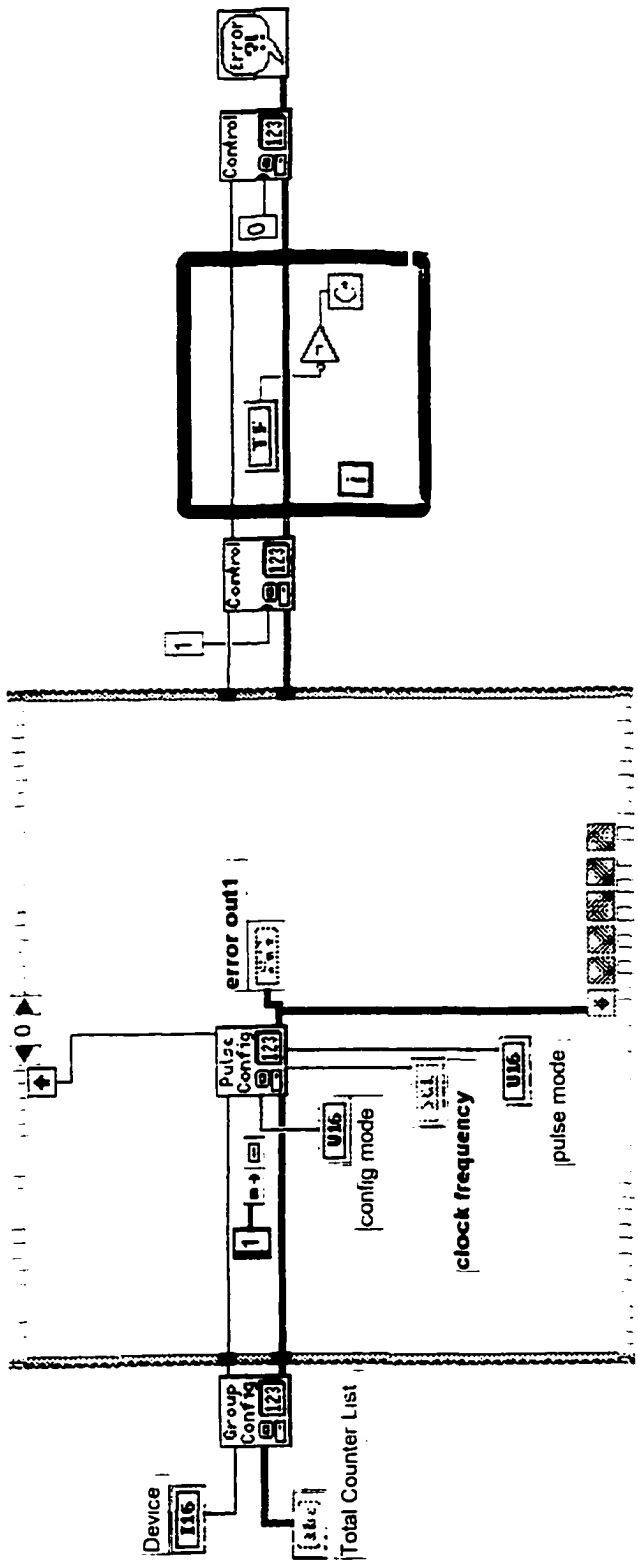

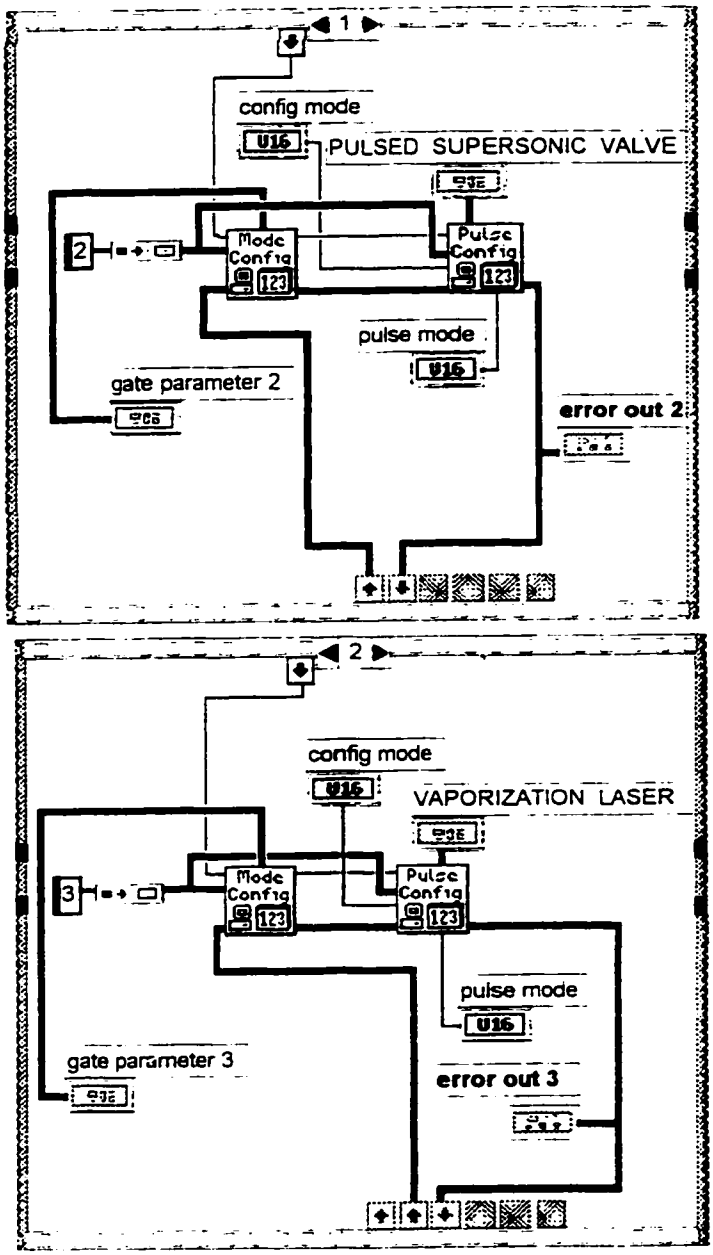

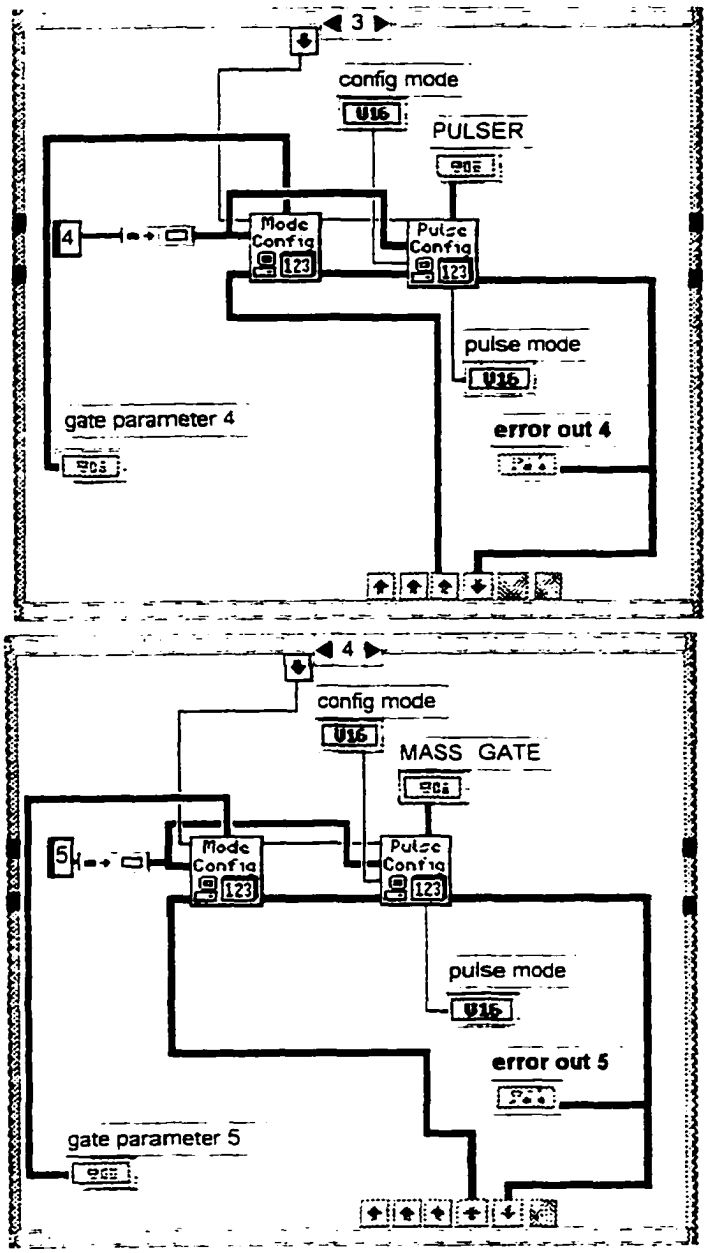

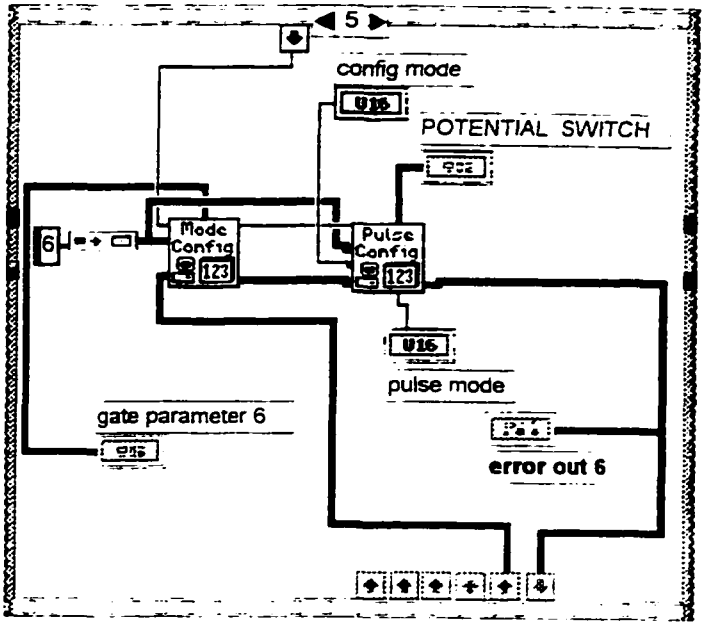

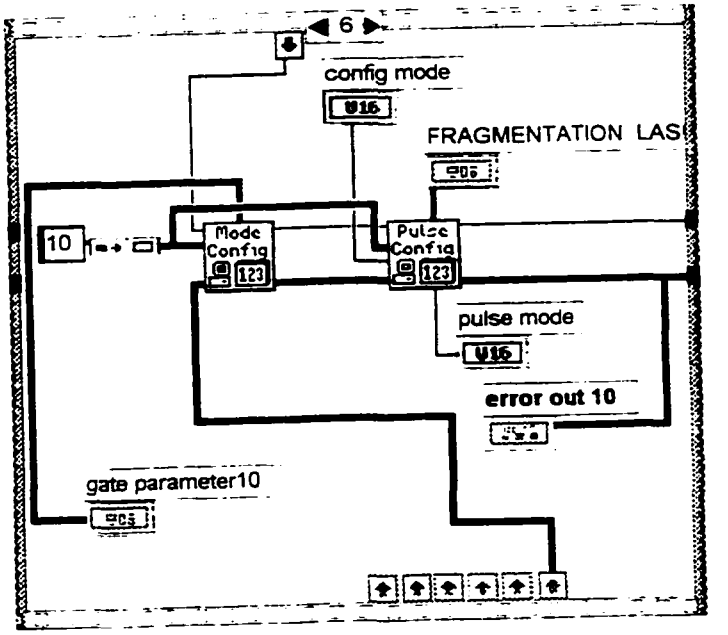

BIBLIOGRAPHY

Chapter I References

1. Jousha Jortner, Ber. Bunsenges. Phys. Chem. **88**, 188, (1984).

2. E. Schumacher, M. Kappes, K. Marti, P. Radi, M. Schär and B. Schmidhalter, Ber. Bunsenges. Phys. Chem. **88**, 220, (1984).

3. V. E. Bondybey, Science, **227**, 125 (1985).

4. E. W. Becker. Z. Phys. D- Atoms Molecules and Clusters, **3**, 101 (1986).

5. W. D. Knight, Walt A. deHeer and Winston Saunders, Z. Phys. D- Atoms Molecules and Clusters, **3**, 109 (1986).

6. Joseph Haggin, C&EN March 2nd 1987.

7. W. Begemann, S. Dreihöfer, G. Ganteför, H. R. Siekmann, K. H. Meiwes-Broer and H. O. Lutz, Springer Ser. Mater. Sci., 230 (1988).

8. J. Mater. Res. vol 4, # 3, 704 (1989).

9. Michael A. Duncan and Dennis H. Rouvray, Sci. Amer. 110 (Dec. 1989).

10. Robert Pool, Science, 248, 1186 (1990).

11. R. Stephen Berry, Sci. Amer., Aug. 1990 (pg. 68).

12. Marvin L. Cohen and Walter D. Knight, Phys. Today, Dec. 1990 (pg. 42).

13. Zhendong Hu, Jian-Guo Dong, John R. Lombardi and D. M. Lindsay, J. Chem. Phys. **101**, 1 (1994).

14. Robert F. Curl and R. E. Smalley, Sci. Amer., 54, Oct. 1991.

15. David J. Wales, Science, 271, 925 (1996).
A. P. Alivisatos, Science, 271, 933 (1996).
Gustavo E. Scuseria, Science, 271, 942 (1996).

Chapter II References

1) For example, Jacox reports that "the argon-matrix shift for most diatomic molecules is less than 2%". See, M. E. Jacox, J. Mol. Spectrosc. **113**, 286 (1985).

2) Metal Clusters, edited by M. Moskovits (Wiley, New York, 1986).

3) D. M. Lindsay, F. Meyer, and W. Harbich, Z. Phys. D **12**, 15 (1989).

4) W. Harbich, F. Fedrigo, F. Meyer, D. M. Lindsay, J. Lignieres, J. C. Rivoal and D. Kreisle, J. Chem. Phys. **93**, 8535 (1990).

5) W. Harbich, F. Fedrigo, J. Buttet, and D. M. Lindsay, Optical Spectroscopy on Size Selected Gold Clusters Deposited in Rare Gas Solids, Z. Phys. D **19**, 157 (1991).

6) W. Harbich, F. Fedrigo, J. Buttet, and D. M. Lindsay, Soft Landing of Monodispersed Small Metal Clusters in Rare Gas Solids, Mater. Res. Soc. Symp. Ser. **206**, 369 (1991).

7) R. Keller, in The Physics And Technology of Ion Sources, edited by I. G. Brown (Wiley, New York, 1989), Chap. 7.

8) K. Besocke, S. Berger, W. O. Hofer and U. Littmark, Radiat. Eff. **66**, 35 (1982).

9) See for example, W. Begemann, Ph.D. thesis, Universität Bielefeld (1988).

10) E. M. Spain and M. D. Morse, Int. J. Mass Spectrosc. Ion Phys. **102**, 183 (1990).

11) K. P. Huber and G. Herzberg, Constants of Diatomic Molecules (Van Nostrand, New York, 1979).

12) D. M. Cox, R. L. Whetten, M. R. Zakin, D. J. Trevor, K. C. Reichmann and A. Kaldor, Advances in Laser Science I, edited by W. C. Stwalley and M. Lapp (AIP Conf. Proc. **146**, 1986), pg. 527; A. Kaldor, D. M. Cox, D. J. Trevor and M. R. Zakin, Z. Phys. D **3**, 195 (1986).

13) C. Cossé, M. Fouassier, T. Mejean, M. Tranquille, D. P. DiLella and M. Moskovits, J. Chem. Phys. **73**, 6076 (1980).

14) A. R. Gee, D. C. O'Shea and H. Z. Cummins, Solid State Commun. **4**, 43 (1965).

15) P. R. R. Langridge-Smith, M.D. Morse, G. P. Hansen, R. E. Smalley and A. J. Mercer, J. Chem. Phys. **80**, 593 (1984).

16) W. Demtröder, Laser Spectroscopy (Springer Verlag, Berlin, 1981).

17) T. A. Ford, H. Huber, W. Klotzbücher, E. P. Kündig, M. Moskovits and G. A. Ozin, J. Chem. Phys. **66**, 524 (1977).

18) D. W. Green and D. M. Gruen, J. Chem. Phys. **57**, 4462 (1972).

19) W. Klotzbücher and G. A. Ozin, Inorg. Chem. **16**, 984 (1977).

20) M. Moskovits and W. Limm, Ultramicroscopy **20**, 83 (1986).

21) R. W. Wood, Phil. Mag. **4**,396 (1902)

22) Wavelengths pertain to measurements in air, whereas energies are given in vacuum wavenumbers.

23) A. R. Gee, D. C. O'Shea and H. Z. Cummins, Solid State Commun. **4**, 43 (1965).

24) R. J. H. Clark, Raman, Resonance Raman and Electronic Raman Spectroscopy in Vibronic Processes in Inorganic

Chemistry, ed. by C. D. Flint, NATO ASI Series (Kluwer Academic Publishers, 1989), pg. 301.

25) M. P. Andrews and G. A. Ozin, J. Phys. Chem. **90**, 2852 (1986).

26) M. C. Manning and W. C. Trogler, J. Amer. Chem. Soc. **105**, 5311 (1983).

27) F. A. Cotton and I. Shim, J. Phys. Chem. **89**, 952 (1985).

28) S. P. Walch and C. W. Bauschlicher, in Comparison of ab initio Quantum Chemistry with Experiment, ed by R. J. Bartlett (Reidel, boston, 1985).

Chapter III References

1) Y. Liu, Q. L. Zhang, F. K. Tittel, R. F. Curl and R. E. Smalley, J. Chem. Phys., **85**, 7434 (1986).

2) D. E. Powers, S. G. Hansen, M. E. Geusic, D. L. Michalopoulos and R. E. Smalley, J. Chem. Phys., **78**, 2286 (1983).

3) P. J. Brucat, L. S. Zheng, C. L. Pettiette, S. Yang and R. E. Smalley, J. Chem. Phys., **84**, 3078 (1986).

4) D. E. Powers, S. G. Hansen, M. E. Geusic, A. C. Puiu, J. B. Hopkins, T. G. Dietz, M. A. Duncan, P. R. R. Langridge-Smith and R. E. Smalley, J. Chem. Phys., **86**, 2556 (1982).

5) Shigeo Maruyama, Lila R. Anderson and Richard E. Smalley, Rev. Sci. Instrum., **61**, 3686 (1990).

6) Paolo Milani and Walt A. deHeer, Rev. Sci. Instrum., **61**, 1835 (1990).

7) Pritha Gangopadhyay and James M. Lisy Rev. Sci. Instrum., **62**, 502 (1991).

8) Winston A. Saunders, Department of Physics, Swiss Federal Institute of Technology - Lausanne, Switzerland.

9) P. K. Carroll and E.T. Kennedy, Contemp. Phys., **22**, 61, (1981).

10) Paul C. Engelking, Chem. Rev., **91**, 399 (1991).

11) Otto F. Hagena, Rev. Sci. Instrum., **63**, 2374 (1992).

12) G.I. Dimov Pribory I Tekhnika Eksperimenta, Nuclear Physics Institute, Academy of Sciences of the USSR, No. 5, pp. 168- 171, (1968).

13) John M. Hayes, Chem. Rev., **87**, 745 (1987).

14) J. M. Pendlebury and K. F. Smith, Contemp. Phys., **28**, 3, (1987).

15) W. C. Wiley and I. H. McLaren, Rev. Sci. Inst., **26**, 1150, (1955).

16) J. A. Syage and J. Steadman, Rev. Sci. Instrum., **61**, 1204 (1990).

17) a) Hellmut Haberland, Hans Kornmeier, Christoph Ludewigt, Andreas Risch and Martin Schmidt, Rev. Sci. Instrum., **62**, 2368 (1991).

b) Hellmut Haberland, Hans Kornmeier, Christoph Ludewigt, Andreas Risch and Martin Schmidt, Rev. Sci. Instrum., **62**, 2621 (1991)

18) D. S. Cornett, M. Peschke, K. LaiHing, P. Y. Cheng, K. F. Willey and M. A. Duncan, Rev. Sci. Instrum., **63**, 2177 (1992).

19) R. T. Laaksonen, D. A. Goetsch, D. W. Owens, D. M. Poirier, F. Stepniak and J. H. Weaver, Rev. Sci. Instrum., **65**, 2267 (1994).

20) W. Begemann, S. Dreihöfer, G. Ganteför, H. R. Siekmann, K. H. Meiwes-Broer and H. O. Lutz, Springer Ser. Mater. Sci., 230 (1988).

21) B. A. Mamyrin, V. I. Karataev, D. V. Shmikk and V. A. Zagulin, Sov. Phys.-JETP.,**37**, 45 (1973).

22 SIMION PC Version 4.0, courtesy D. A. Dahl, Idaho Natl. Lab. Idaho Falls, ID 83415, USA.

Chapter IV References:

1. R.E.Smalley, Laser Chem., Vol. 2, 167 (1983).

2. Y. Liu, Q. L. Zhang, F. K. Tittel, R. F. Curl and R. E. Smalley, J. Chem. Phys., **85**, 7434 (1986).

3. D. E. Powers, S. G. Hansen, M. E. Geusic, D. L. Michalopoulos and R. E. Smalley, J. Chem. Phys., **78**, 2286 (1983).

4. P. J. Brucat, L. S. Zheng, C. L. Pettiette, S. Yang and R. E. Smalley, J. Chem. Phys., **84**, 3078 (1986).

5. D. E. Powers, S. G. Hansen, M. E. Geusic, A. C. Puiu, J. B. Hopkins, T. G. Dietz, M. A. Duncan, P. R. R. Langridge-Smith and R. E. Smalley, J. Chem. Phys., **86**, 2556 (1982).

6. W. C. Wiley and I. H. McLaren, Rev. Sci. Inst., **26**, 1150, (1955).

7. Wieslaw J. Stryjewski, Rev. Sci. Inst., **62**, 1921, (1991).

8. Gary W. Johnson, LabVIEW Graphical Programming :Practical Applications in instrumentation and Control (McGraw-Hill New York, 1994).

9. SIMION PC Version 4.0, courtesy D. A. Dahl, Idaho Natl. Lab. Idaho Falls, ID 83415, USA.

10. HandBook of Chemistry and Physics 78th edition, (CRC Press Inc. Boca Raton,1997).

11. S. C. O'Brien, J. R. Heath, R. F.Curl and R. E. Smalley, J. Chem. Phys., **88**, 220 (1988).

12. M. E. Geusic, M.F. Jarrold, T. J. McIlrath, R. R. Freeman and W. L. Brown, J. Chem. Phys., **86**, 3864 (1987).

13. M. E. Geusic, T. J. McIlrath, M.F. Jarrold, L. A. Bloomfield, R. R. Freeman and W. L. Brown, J. Chem. Phys., **84**, 2421 (1986).

14. M. E. Geusic, M.F. Jarrold, T. J. McIlrath, L. A. Bloomfield, R. R. Freeman and W. L. Brown, Z. Phys. D-Atoms Molecules and Clusters 3, 309-317 (1986).

15. R. Bouyer, P. Roussel, P. Monchicourt, M. Perdrix and P. Pradel, J. Chem. Phys., **100**, 8912 (1994).

Chapter V References

1) John T. Moseley, Photodissociation and Photoionization, edited by K. P. Lawley (Wiley, 1985).

2) S. P. Goss, J. D. Morrison and D. L. Smith J. Chem. Phys.,**75**, 757 and 1820 (1981).

3) Richard N. Dixon, Chem. Soc. Rev., (1994).

4) C. R. Chris Wang, Stuart Pollack, Douglas Cameron and Manfred Kappes, J. Chem. Phys., **93**, 3787 (1990).

5) P. J. Brucat, L. S. Zheng, C. L. Pettiette, S. Yang and R. E. Smalley, J. Chem. Phys., **84**, 3078 (1986).

6) A. Welsford Castleman Jr., and Robert G. Keesee, Chem. Rev., **86**, 589 (1986).

7) Kenneth F. Willey, David L. Robbins, Chen-Sheng Yeh and Michael A. Duncan, Faraday Discuss. **92**, 269 (1991).

8) Martin F. Jarrold and Kathleen M. Creegan, Int. J. Mass Spec. and Ion Processes, **102**, 161 (1990).

9) Martin F. Jarrold and Kathleen M. Creegan, Chem. Phys. Lett., **166**, 116 (1990).

10) Paul C. Engelking, Chem. Rev., **91**, 399 (1991).

11) John M. Hayes, Chem. Rev., **87**, 745 (1987).

12) J. B. Hopkins, P. R. R. Langridge-Smith, M. D. Morse and R. E. Smalley, J. Chem. Phys., **78**, 1627 (1983).

13) Jacqueline C. Pinegar, Jon D. Langenberg, Caleb A. Arrington, Eileen M. Spain and Michael D. Morse, J. Chem. Phys., **102**, 666 (1995).

14) R.J. Van Zee, S. Li and W. Weltner Jr., Chem. Phys. Lett. **217**, 381 (1994).

15) Andrew M James, Pawel Kowalczk, Etienne Langlois, Margot D. Campbell, Ayano Ogawa and Benoit Simard, J. Chem. Phys., **101**, 4485 (1994).

16) Andrew M James, Pawel Kowalczk, Rene Fournier and Benoit Simard J. Chem. Phys., **99**, 8504 (1993).

17) Z. Hu, B. Shen, Q. Zhou, S. Deosaran, J. R. Lombardi and D. M. Lindsay, SPIE Proceedings Vol. **1599**, (1992).

18) David A. Hales, Li Lian, P.B. Armentrout, Int. J. Mass Spec. and Ion Processes, **102**, 269 (1990).

19) S. K. Loh, Li Lian and P.B. Armentrout, J. Chem. Phys., **91**, 6148 (1989).

20) Y. Hamrick, S. Taylor, G. W. Lemire, Z. W. Fu, J, C, Shui and M. D. Morse, J. Chem. Phys., **88**, 4095 (1988).

21) M. Moskovits and W. Limm, Ultramicroscopy **20**, 83 (1986)

22) J. R. Heath, Yuan Liu, S. C. O'Brien, Qing-Ling Zhang, R. F. Curl, F. K. Tittel, and R. E. Smalley, J. Chem. Phys., **83**, 5520 (1985).

23) R. L. Asher, D. Bellert, T. Buthelezi and P. J. Brucat, Chem. Phys. Lett., **224**, 525 and 529 (1994).

24) Private communication with P. J. Brucat, University of Florida, Gainesville.

25) Private communication with M. A. Duncan, University of Georgia, Athens.

26) Benoit Simard, Andrew M. James,, Pawel Kowalczyk, René Fournier and Peter A. Hackett, preprint (High Resolution spectroscopy of small transition metal molecules. Recent experimental and theoretical progress on group 5 diatomics.

27) James C. Weisshaar, J. Chem. Phys., **90**, 1429 (1989).

28) Charles W. Bauschlicher Jr., Stephen R. Langhoff, Chem. Rev. 91, 701, (1991).

29) Scott Taylor, George W. Lemire, Yoon Mi Hamrick, Zhenwen Fu and Michael D. Morse, J. Chem. Phys., **89**, 5517 (1988).

IMAGE EVALUATION TEST TARGET (QA-3)

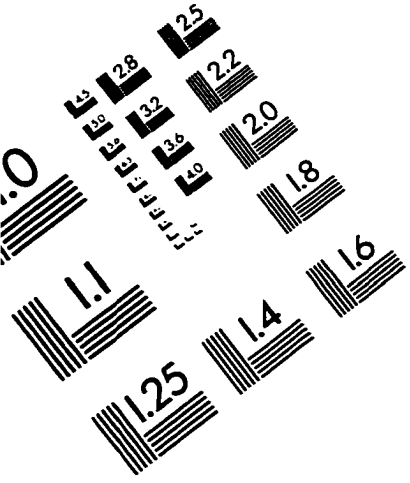

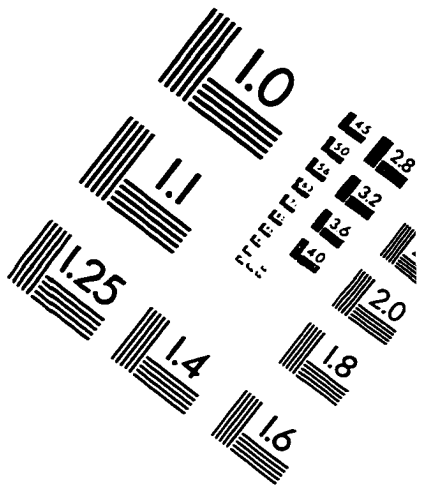

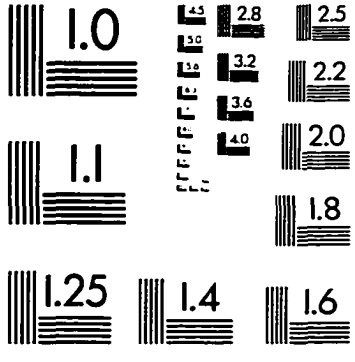

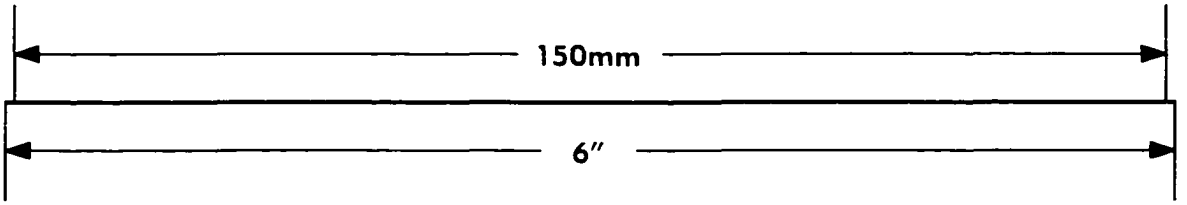

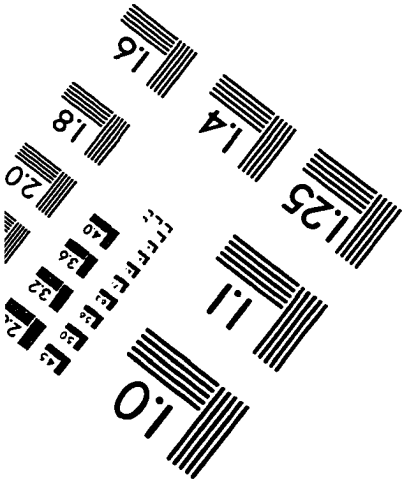

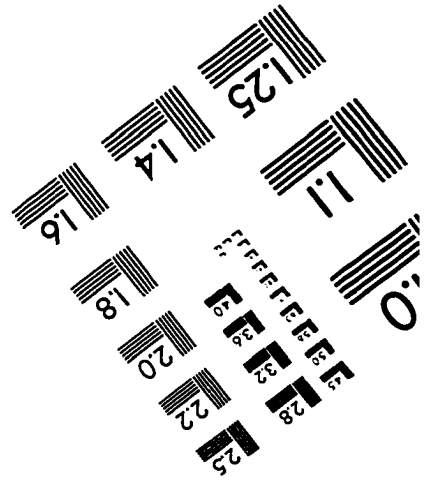

APPLIED IMAGE, Inc
1653 East Main Street
Rochester, NY 14609 USA
Phone: 716/482-0300
Fax: 716/288-5989